PRODUCTION OF DIELECTRIC MATERIALS

A Thesis
Presented to
The Academic Faculty

By

Christopher Blandin

In Partial Fulfillment
of the Requirements for the Degree
Master of Science in Mechanical Engineering

Georgia Institute of Technology
December 2008

PRODUCTION OF DIELECTRIC MATERIALS

Approved by:

Dr. Jonathan Colton, Advisor
School of Mechanical Engineering
Georgia Institute of Technology

Dr. John Schultz
Georgia Tech Research Institute
Georgia Institute of Technology

Dr. Min Zhou
School of Mechanical Engineering
Georgia Institute of Technology

Date Approved: 15 August 2008

"... for want of a nail, the shoe was lost;.."

Benjamin Franklin, Poor Richard's Almanac (1758)

ACKNOWLEDGMENTS

I would like to thank Dr. Jonathan Colton for his experience, guidance, and patience throughout this research. I would also like to praise Dr. John Schultz, not only for serving as my committee member, but for his immense patience and entrusting this project to me. I also thank Dr. Min Zhou for taking the time to serve on my committee.

A large amount of appreciation should be given to my friends and group mates Eric Busillo, Jordan Hamilton, and Taylor Stellman, and also to Tom Forbes and Valli Subbiah. Thank you for listening to all my problems without complaint and freely giving your valued input. I thank my family for their continued support and their confidence in my abilities. Thank you for always keeping me focused and in high spirits.

Thank you to S.T. Lee and Sealed Air Corporation for providing samples of their CelluPlank® polyethylene foam.

Thanks should be given to John Graham and all the co-ops at the Georgia Tech Machine Shop who were responsible for fabricating all the parts necessary for this project. Also, I thank Kyle French and the co-ops at the Georgia Tech Electronics Lab for providing the hardware and electronics coding crucial to this project.

Last, but certainly not least, I would like to express my gratitude to the Mechanical Engineering Graduate Office, especially Glenda Johnson for dearly helping me through all the paperwork necessary to graduate.

TABLE OF CONTENTS

LIST OF TABLES

LIST OF FIGURES

NOMENCLATURE

A_s	Surface area
D	Depth of penetration for energy equations
E	Elastic modulus
Ea(t)	Resistive energy
$F_{friction}$	Friction force
F_{comp}	Compressive force
F_{crush}	Crushing force
Fshear	Shear force
g	Gravity
K(t)	Kinetic energy
L_o	Original length
N	Normal force
P	Contact pressure
r_i	Inner radius
r_o	Outer radius
R	Radius
Re	Resistive forces
V(t)	Potential energy
x	Depth of penetration for force equations
α	Constant forces of crushing and shearing
β	Friction force
Δx	Change in penetration depth
ε	Strain
σ_{comp}	Compressive stress
σ_{crush}	Crushing stress
σ_y	Yield point
τ_{shear}	Shear stress
μ	Coefficient of friction

SUMMARY

Dielectric materials are used as spacers in antennas. The design of the dielectric determines the properties of the antenna. The insertion of high dielectric materials in a specific pattern into a low dielectric matrix material is one means to accomplish this. This thesis studies the means to insert metal cylinders (wire or nails) into polymer foams to produce such a material. Depending on the antenna properties desired, the patterns and number of nails varies tremendously. To decrease the manufacturing time and, therefore, the cost of creating these materials, an automatic machine capable of rapidly inserting wires to a predetermined pattern is developed. This thesis has two parts. In the first part, the ballistic impact of nails into foam is modeled. Experimental observations of the nails impacting the foam are used to verify the model. Penetration equations are developed to express the penetration capability of a nail into foam. All of this allows one to predict the forces required for a nail to be inserted into foam to a desired depth, thereby facilitating manufacture of these dielectric materials. In the second part, a fully automatic nail insertion device is designed, fabricated, and tested with the experimental tests used as control settings.

1. INTRODUCTION

1.1 Motivation

Ceramic-filled artificial dielectrics can be used as substrates for antennas due to their high dielectric constants. High dielectric ceramic substrates effectively reduce the thickness of the antennas but are inherently heavy. These substrates also exhibit isotropic permittivity, which is not necessary for antenna performance. This thesis proposes to insert discrete conductive elements into a light-weight, low-loss, and low-dielectric material, thereby increasing the overall dielectric constant of the substrate, yet retaining its low density. Polymeric foam was chosen as the insulator because of its low dielectric constant and its low density. Conductive metal wires or nails are arranged in a regular pattern in the foam to increase the permittivity of the dielectric in the direction parallel to the aligned nails. Depending on the size of the dielectric sample, the number of nails can be on the order of thousands. Therefore, the purpose of this project is to find a means to fabricate light-weight, low loss substrates. A fully automatic nail gun is designed to quickly and accurately insert the nails in an arbitrary pattern to a desired depth in the foam material. Nails are inserted into the foam in varying three-dimensional patterns. The nail gun is capable of firing the nails to different depths in the foam, and different length nails may need to be introduced in the foam. Pneumatics is used to fire the nails in the foam. The nail gun is mounted on a machining mill for accurate translation and placement of the gun over the foam. However, to achieve the correct control settings required for a pre-determined penetration depth, it is necessary to understand the behavior of the impact between the nails and the foam, which is the main purpose of this thesis.

1.2 Research Objectives

The overall purpose of this research is to develop a system to fabricate low density, low loss antenna substrates. It is essential to understand the mechanics of penetration to properly design the pneumatic system employed to insert the nails in the foam. The objectives are as follows:

1. Develop a comprehensive model describing the mechanisms of the penetration of nails into foam.
2. Quantify the penetration mechanisms into representative force and energy equations.
3. Perform nail-foam impact tests to determine penetration force and energy, and to verify the penetration model.

1.3 Thesis Organization

Chapter 2 presents literature on foam impact and penetration relevant to nail-foam penetration, including the effects taking place during penetration. Chapter 3 of this thesis presents the nail penetration into foam and resulting theoretical equations used for describing the nail-foam penetration. In order to determine the force required to insert a nail to a certain depth in the foam, equations must be derived to quantify the penetration process. To this end, a qualitative analysis of nail-foam penetration is performed using classical mechanics. This analysis allows the total force associated with a specific depth of penetration to be determined. The analysis is further expanded to determine the energy absorbed by the foam. Chapter 4 contains the physical testing executed using the Dynatup® Instron Impact Tester. The experiments were performed to support and verify the theoretical equations. Chapter 5 gives a detailed discussion and analysis of the equations and impact tests, as well as a comparison of all the results. Chapter 6

introduces the final concept design for the nail gun and the actual fabricated gun. Chapter 7 details the conclusions made from this research and future recommendations. It presents an analysis of each chapter and provides correlations between the chapters. It also presents the recommendations for future research and works regarding the analytic equations and the nail gun.

2. LITERATURE REVIEW

Research has been performed to analyze the penetration of projectiles into various materials. The studies reviewed in this section contain analytical and experimental procedures for impact into foam, soil, concrete, and composites. An analysis of these papers contributed to the development of the methodology utilized in investigating the impact of nails into foam.

2.1 Impact and Deformation Studies of Foam

Research previously was performed on the impact response of polyurethane foam by gravity-driven impactors [1]. The tests consisted of impacting rigid, crushable polyurethane foam of density 25.6 kg/m^3 with three steel penetrators of differing geometric shapes: a rectangular block, a cylinder, and a wedge. The tests were performed at velocities between 2 m/s and 4 m/s. Basic principles of continuum mechanics were implemented in order to numerically model the impact process. Experimental data were consistent with the simulated results generated by the two-dimensional numerical model. The significant result discerned from the research is the relationship between the deceleration function and the geometry of the impactor. There was a clear correlation between the geometry of the impactor and the impact response. Through observation of each impactor's deceleration versus time graph, they were able to indicate the effect geometry has on penetration. Figures 1, 2, and 3 show the decelerations of the rectangular block, the cylindrical, and the wedge impactors, respectively. Tables 1, 2, and 3 display the important information corresponding to each impact.

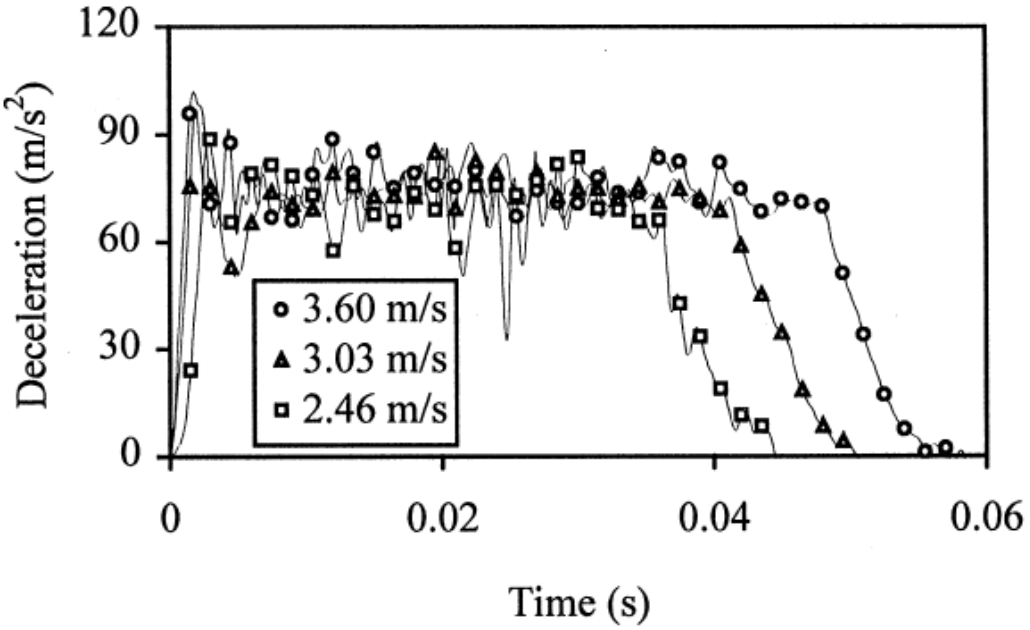

Figure 1: Deceleration of rectangular block impactor with respect to time [1]

Table 1: Impact data of rectangular block and polyurethane foam [1]

Impact velocity (m/s)	2.46	3.03	3.60
Initial deceleration peak (m/s^2)	90.0	97.0	102.0
Occurrence of initial peak (ms)	2.9	2.0	1.8
Deceleration plateau (m/s^2)	72.0	74.0	75.0
Impact duration (ms)	37.0	42.0	48.0
Maximum impactor displacement (cm)	4.6	6.5	8.6

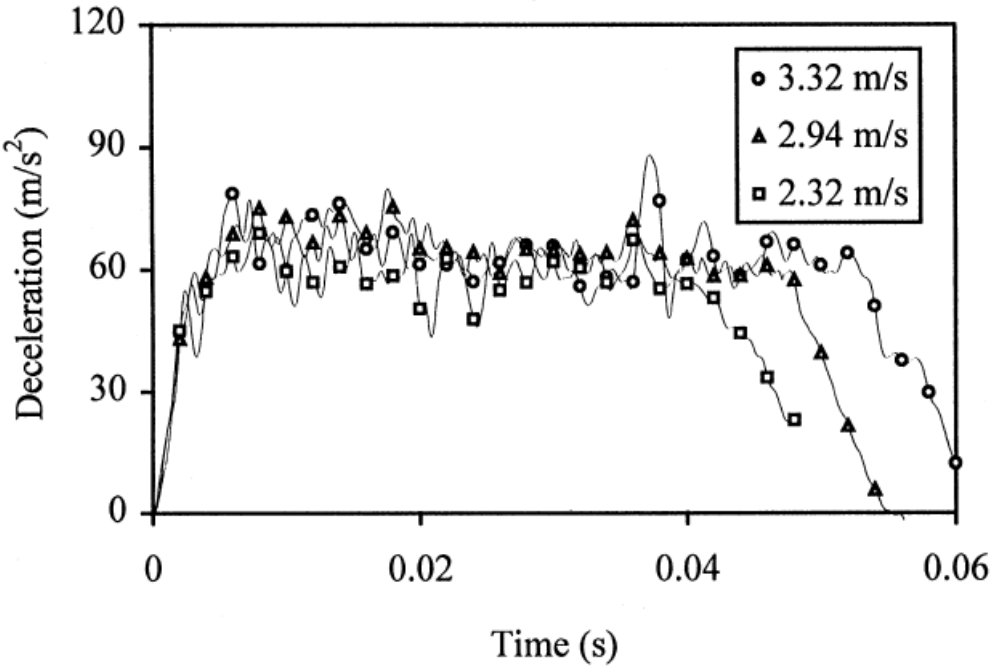

Figure 2: Deceleration of cylindrical impactor with respect to time [1]

Table 2: Impact data of cylindrical impactor and polyurethane foam [1]

Impact velocity (m/s)	2.32	2.94	3.32
Deceleration plateau (m/s^2)	60.0	64.0	65.0
Impact duration (ms)	40.0	47.0	53.0
Maximum impactor displacement (cm)	4.8	7.0	9.0

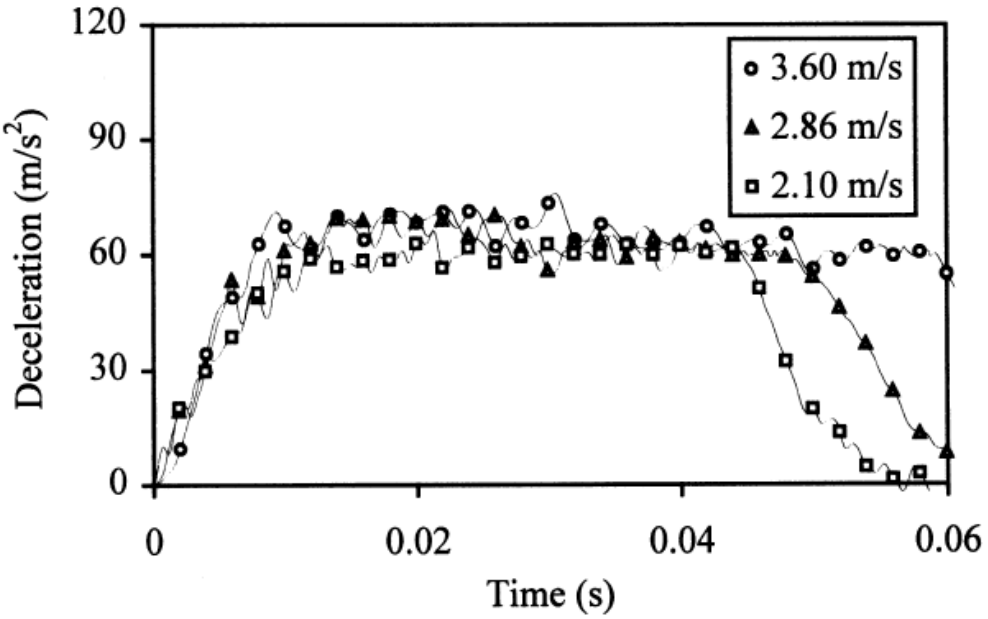

Figure 3: Deceleration of wedge impactor with respect to time [1]

Table 3: Impact data of wedge impactor and polyurethane foam [1]

Impact velocity (m/s)	2.10	2.86	3.60
Deceleration plateau (m/s^2)	61.0	66.0	68.0
Impact duration (ms)	40.0	49.0	59.0
Maximum impactor displacement (cm)	4.6	7.5	11.0

The data reveal several factors concerning the importance of geometry in a penetration process. First, however, it is necessary to understand the type of contact each impactor generates with the foam. The rectangle impacts the foam with the maximum amount of contact area, i.e., the entire flat surface of the block. The cylinder initially forms a line of contact running down the length of the cylinder. As the depth increases, the amount of contact area increases up to one-half of the surface area. The wedge impactor contacts the foam in a manner similar to the cylinder. Instead of a curved surface area, the contact area increases linearly along two adjoined, inclined planes.

Each impactor's deceleration profile is divided into three regimes: the deceleration upon impact, the penetration plateau, and the final unloading phase. There is a sharp peak present in the deceleration as the rectangle initially impacts the polyurethane foam. Shim et al. attribute this increase to the large amount of contact area impacting the foam. This peak is not present in the deceleration profiles of the cylinder and wedge impactors. When compared to the rectangle, the geometry of the cylinder and the wedge impactors cause the foam to crush at a slower rate so have a lower deceleration plateau. This is due to the gradual increase of contact area during the penetration process rather than one abrupt, blunt impact as with the rectangle [1].

Further evidence of the influence of geometry can be seen by the shape of the curve for the first regime between the cylinder and wedge impact geometries. The contact area of the cylinder increases non-linearly as seen in the deceleration profile. The first regime exhibits a nonlinear increase in deceleration for the cylinder while the wedge deceleration increases linearly. This is expected because of the linear increase in contact area that the wedge displays [1].

According to Shim et al., there is a clear relationship between impactor geometry and penetration. Conclusive data illustrate the significant role that the impactor's geometry plays during penetration.

A. Gilchrist et al. studied the deformation of rigid polystyrene, with an approximate density of 35 kg/m^3, when impacted by three striker geometries: a cube, a small cylinder, and a large cylinder. The small cylinder had an overall diameter of 39 mm and the large cylinder had a diameter of 114 mm. The impact response was captured using a high speed camera at 1 ms time periods. Images of the impact can be found below in Figures 4, 5, and 6. A description of their findings follows.

As depicted in Figure 4, when the cube strikes the foam, a crack immediately forms. A 45 degree angled crack propagates from both edges of the cube on the surface of the foam to the impact depth. The crack indicates a boundary line where all foam material lying between cracks is subjected to deformation and all material outside the cracks is negligibly affected by the cube. The images show that the foam shears from the crack walls and deforms under the cube. The results of the force versus distance curve generated by the empirical test were not equivalent to the predicted results. A. Gilchrist et al. attribute this to the neglect of the actual crack growth resulting from the impact.

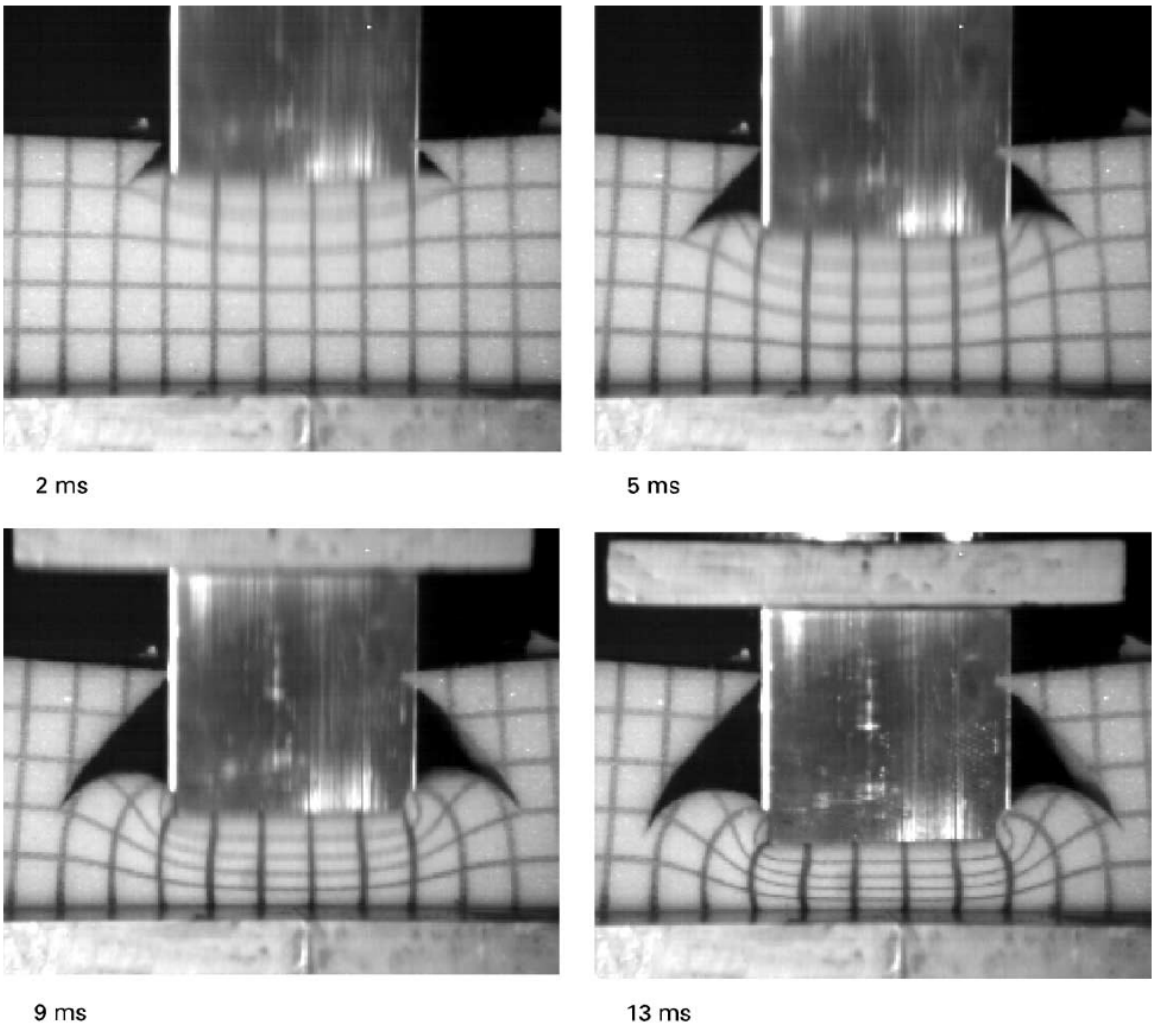

Figure 4: Impact results of cube impactor [2]

Figure 5 shows the deformation of the foam caused by the small cylinder impactor. Similar to the cube impact, a crack develops. Unlike the formation of the crack during cube impact, however, the cylinder crack does not begin at the contact area but away from the cylinder [2]. The cracks grow at angles of 15-20 degrees to the normal of the cylinder with lengths of 10 mm and 20 mm. The force determined from the experiments is 40% higher than the expected values but decreases by half as the penetration depth increases to 20 mm.

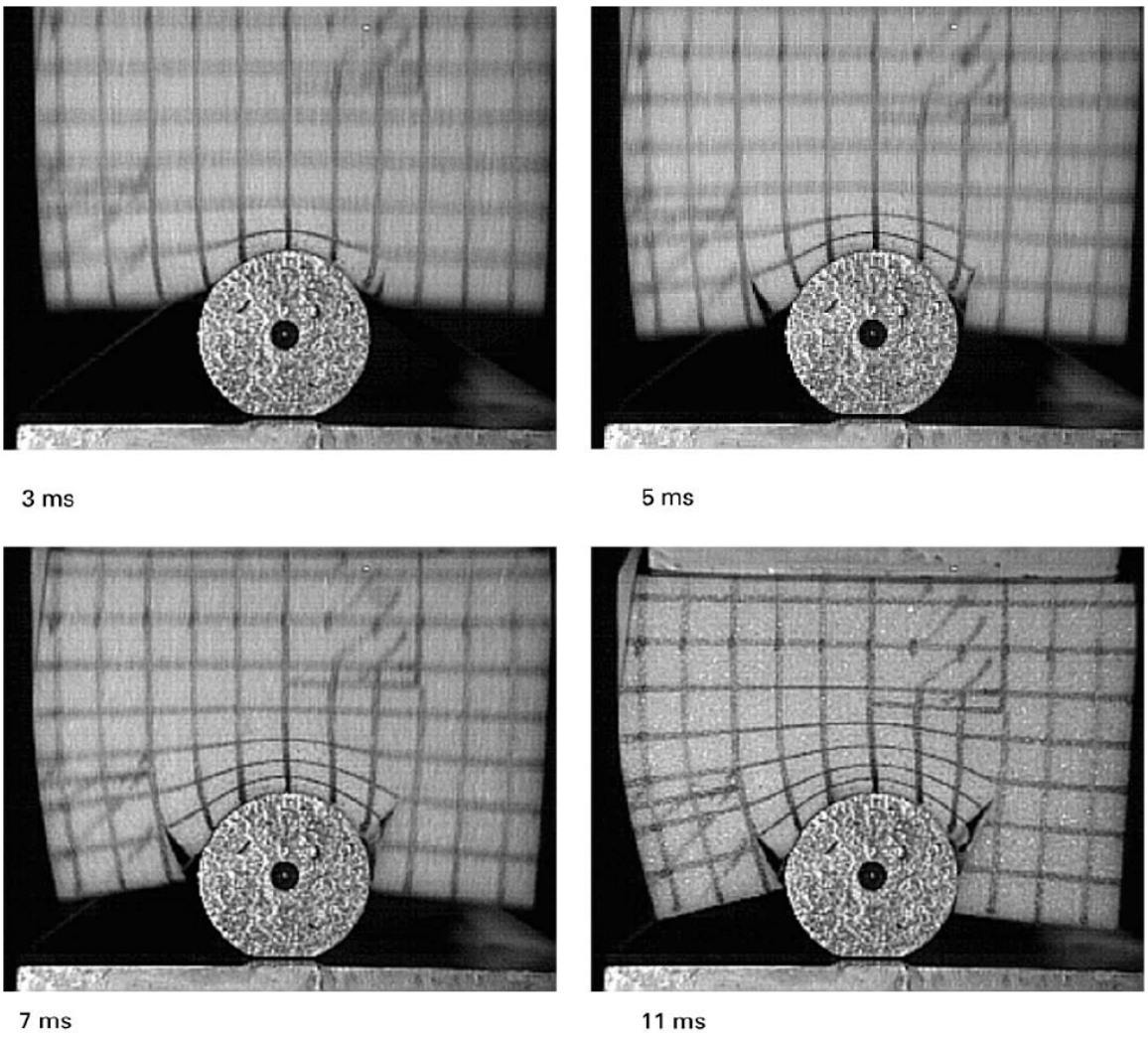

Figure 5: Impact results of small cylinder [2]

The large cylinder impact differs greatly from the small cylinder as shown in Figure 6. 15 mm cracks propagate from the contact area at an angle of 20 degrees. As the penetration increases in depth the crack grows at an accelerated pace until it reaches the bottom surface of the foam. At this point the foam is literally separated into three pieces with the middle section undergoing complete deformation from the cylinder. There is an interesting difference between where the cracks initially form for the small and large cylinder. The small cylinder shows crack growth forming when maximum

contact area was achieved. For the large cylinder, the tensile stresses exceeded the tensile failure stress of the foam at a time before the maximum contact area is reached. This increase in tensile stress is a direct result of the increased surface area of the large cylinder.

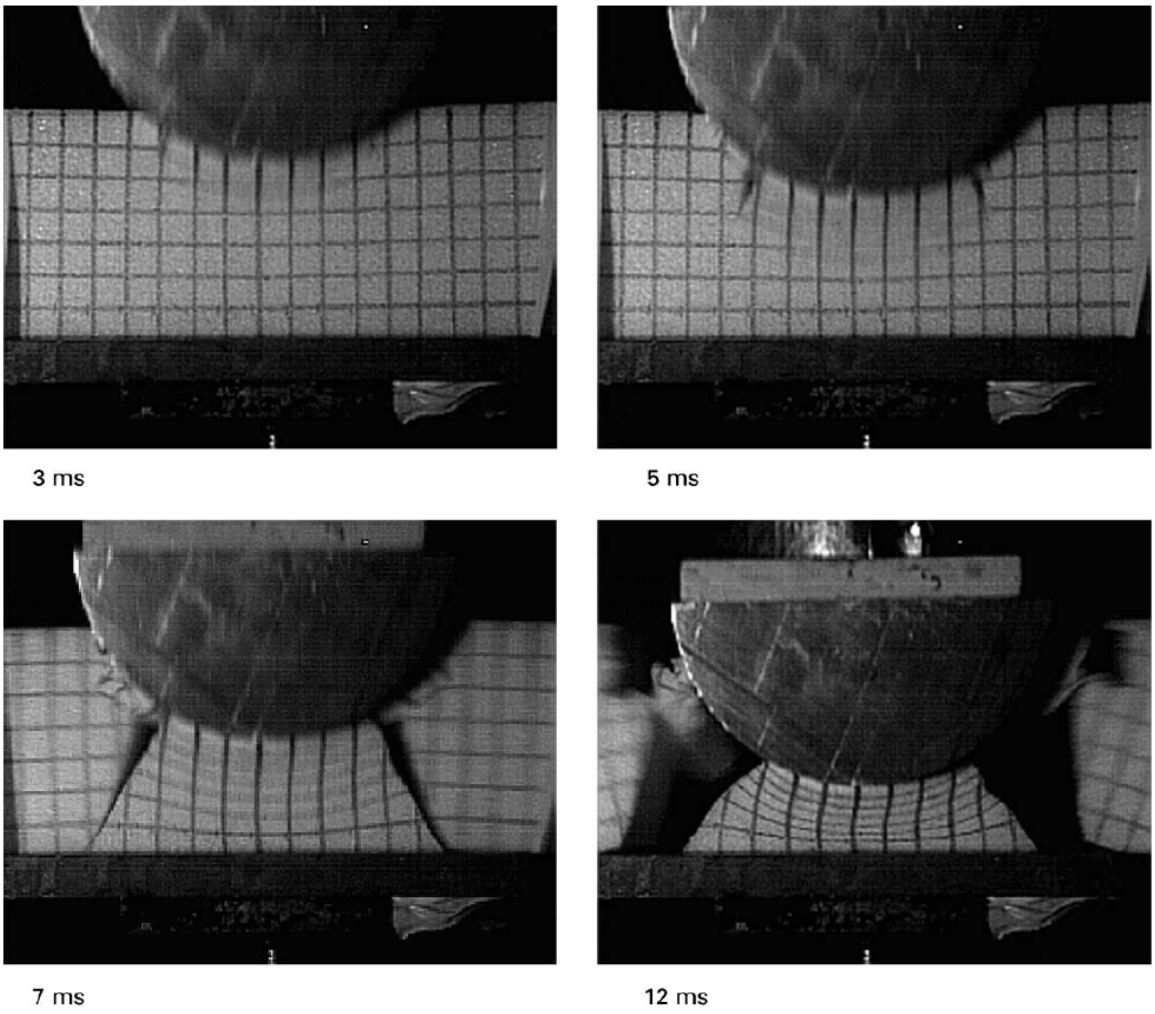

Figure 6: Impact results of large cylinder [2]

2.2 Failure Mechanisms of Foam

The differences in failure mechanisms of high and low density polyurethane foam are discussed in *Fracture Properties of a Rigid Polyurethane Foam* [3]. High density foams (>110 kg/m^3) exhibit a spherical cell morphology. For low-density foams, the foam morphology can be represented by sets of polyhedral cells. Imagining a projectile impacting and penetrating the foam, the failure of the PU cells would be represented by the images shown in Figure 7 (high density) and Figure 8 (low density).

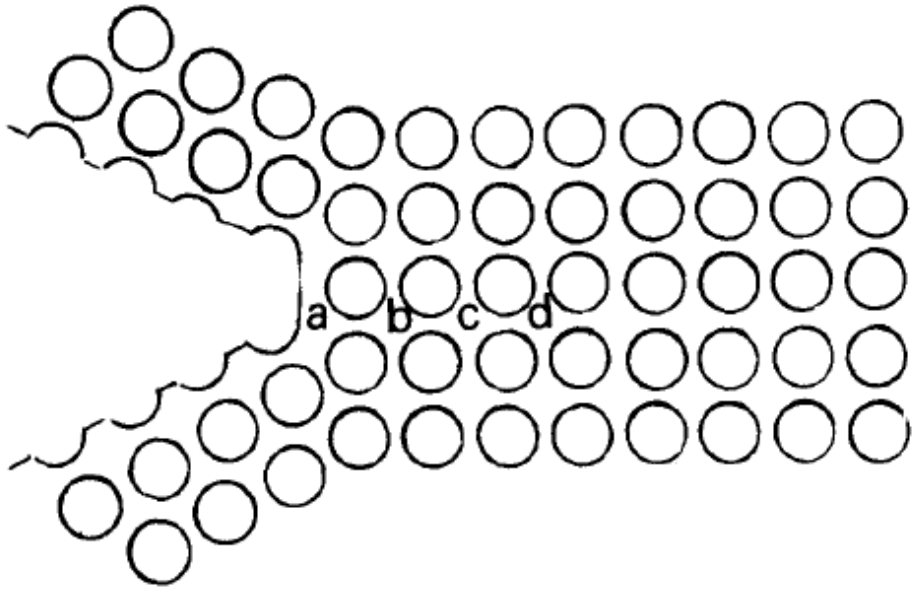

Figure 7: High density cell destruction of foam [3]

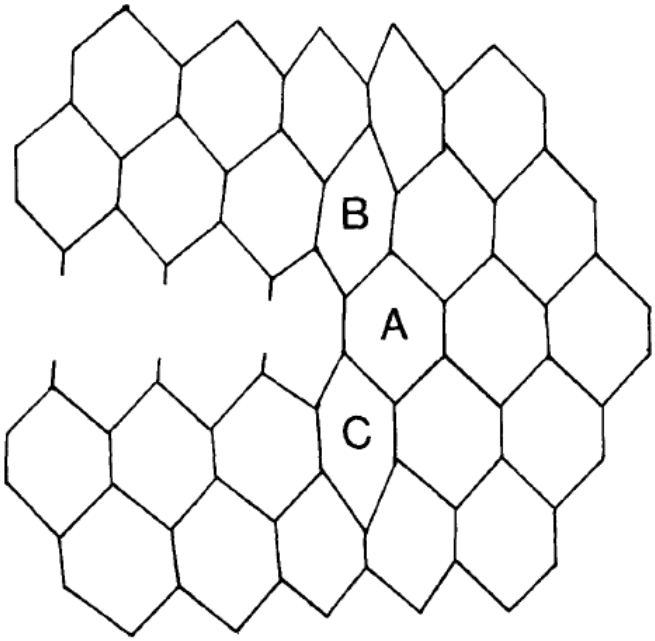

Figure 8: Low density cell failure of foam [3]

Figure 7 shows cell a's wall will fail due to high strain and the same failure mechanisms will continue through cells b, c, and d. According to Figure 8 the cell wall of A would break with continued penetration and cells B and C would deform, thereby increasing the failure strain. McIntyre et al. states that at low densities the foam yields before failure but at higher densities the material fails without yielding. This is observed in the impact of polyurethane and polyethylene for this research project. The polyurethane is of high density, so reaches direct failure when impacted, while the low density polyethylene experiences a failure similar to the low density PU described by McIntyre et al. and yields [3].

Research was performed by M. Ravid and S. R. Bodner on dynamic perforation of viscoplastic plates by rigid projectiles [4]. Their research explains that the penetration of rigid projectiles can be described by five stages of penetration as shown in Figure 9. The

five stages of penetration described by Ravid et al. best represents all foam penetration involving a blunt impactor tip geometry. The viscoplastic targets discussed in their paper experience a high degree of plastic deformation which is similarly experienced by foam, with the exception that polyurethane foam crushes after a certain amount of stress is reached. Ravid et al. associate four methods for which the viscoplastic plates could fail. Two of these mechanisms could apply to the failures experienced in foam, hence will be the focus of this review.

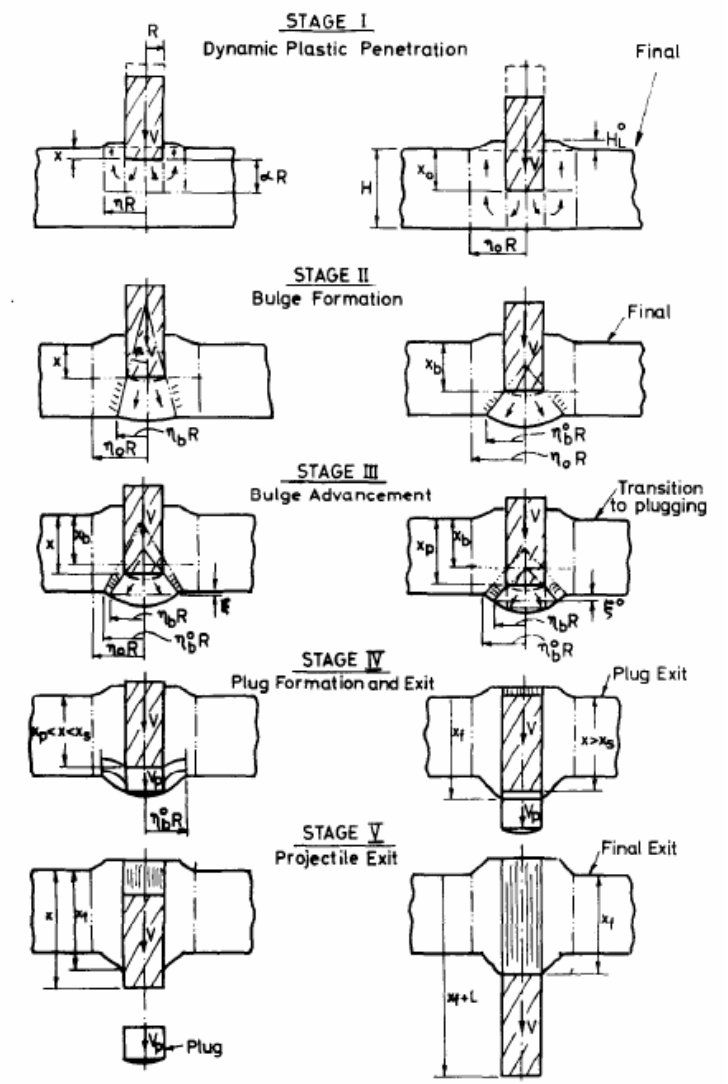

Figure 9: Failure mechanisms stages of foam [4]

Brittle failure in shear occurs when the material rupture condition is reached along surface A23. Surface A23 can be seen in Figure 10, which shows the penetration during stages 2 and 3.

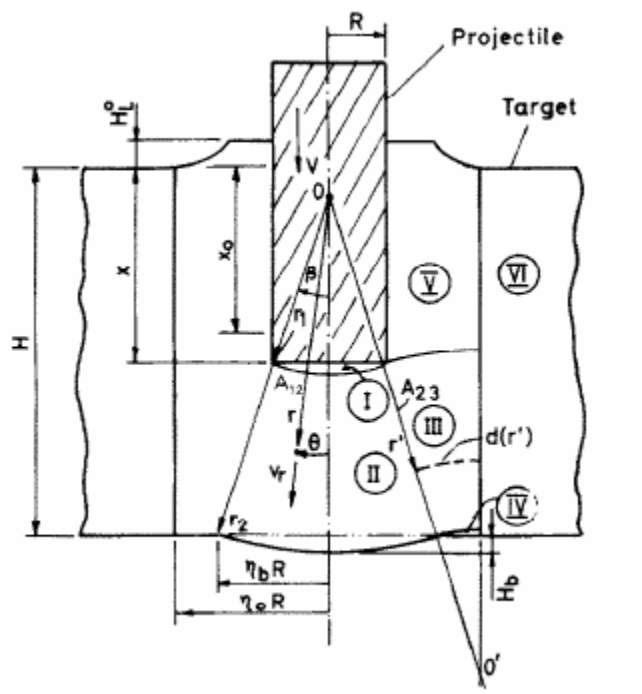

Figure 10: Stages 2 and 3 plug formation of foam penetration [4]

Plug formation and exit is the second noteworthy failure mechanism presented by Ravid et al. [4]. Figure 11 helps to understand this failure process. Zone I material travels in tandem with the projectile after impact at a velocity equal to the projectile's. The penetration induces shear stresses in Zone II, which restrict the target material deformation. Zone III is absent of shear because the target material is already fractured at this location [4]. According to Ravid et al., the projectile is resisted during penetration by the "work rates of inertial forces of zones I-III, the shear work rate in zone II, and by friction along the lateral surface of the projectile" [4]. Ravid et al. further state, "the

bulge [of the target material] will continue to advance until the ultimate shear strain is realized in zone II. The plug will then detach and exit with the projectile" [4]. Applying the conclusions drawn from this journal with the penetration of foam, reveal the penetration mechanisms involve inertial forces, shearing forces, and friction. The failure mechanisms listed in this article are applied to the penetration equations developed for the penetration into foam and are discussed further in Chapter 3.

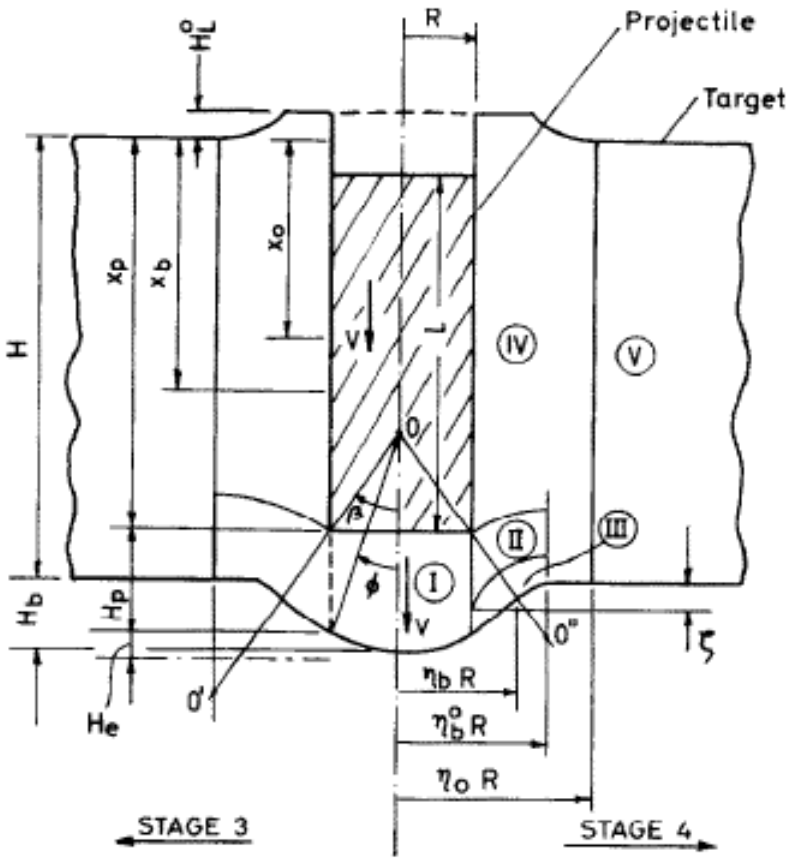

Figure 11: Final stage of foam plug displacement [4]

2.3 Impact Behavior

When impact occurs and penetration begins, it is important to fully realize the behavior of the impact so as to understand all the mechanics of penetration. S.C. Sharma et al. describe the impact behavior associated with composite sandwiches. The important aspect of their study is the behavior of the polyurethane foam core during impact. Figure 12 shows the impact of a composite sandwich with section B representing the PU foam.

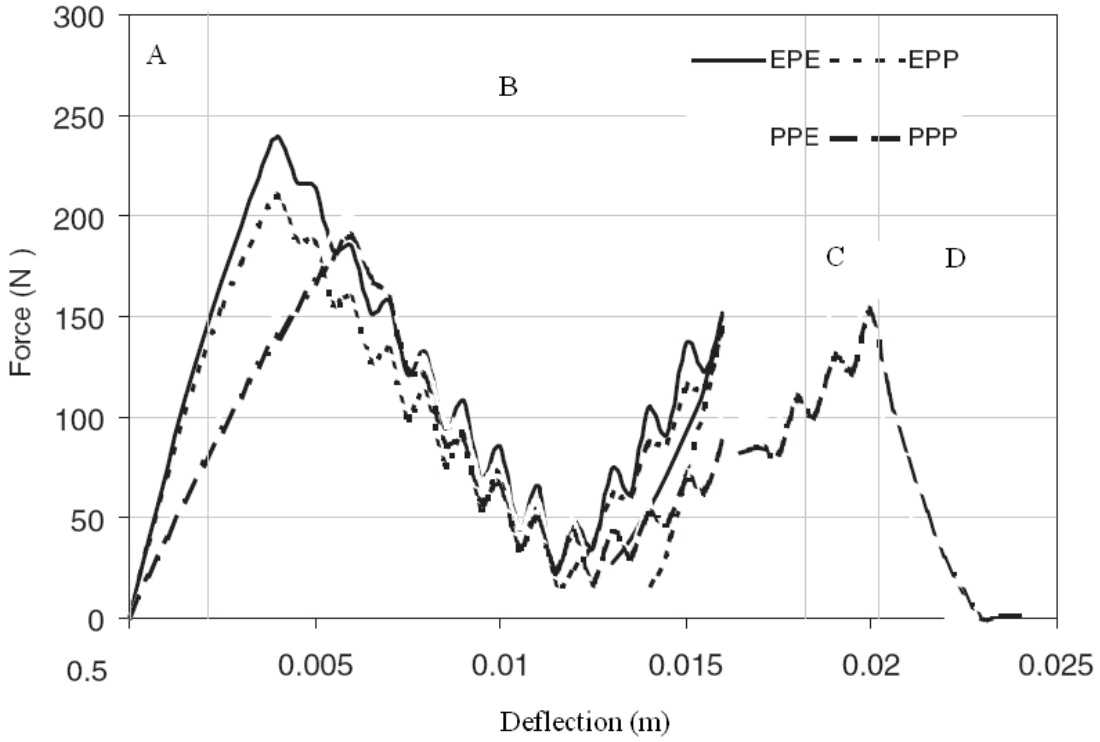

Figure 12: Impact profile for composite with foam core [5]

According to Sharma, region B of Figure 12 shows a bilinear behavior, meaning the presence of valleys and humps are present during penetration. The valleys represent the reduction of stiffness due to crushing while the humps represent the further resistance of crushing by the foam [5]. Sharma further explains both crushing and shearing forces are present during impact and penetration. The foam being compressed by the projectile

is also constrained by surrounding cells. These areas must become sheared for continuous penetration. A friction is known to be present and increase as the contact between projectile and foam becomes greater. Therefore, the forces known to be present during penetration are crushing, shearing, and friction.

2.4 Literature Review Summation

The literature presented in this chapter provided insight into the mechanics of penetration with respect to failure mechanisms, resistive forces, and impact geometry. This information was used to develop penetration and numerical models. Two different failure mechanisms for impact in viscoplastic plates can be found to correlate strongly with similar responses in foam. Indications of the mechanisms (compression, shear, friction) that resist penetration are apparent. The literature also shows penetration occurs more easily with sharp tip geometries as compared to large, blunt geometries due to the effective area in contact. The following chapter, Chapter 3, details the mechanics of the nail-foam penetration and the theoretical equations derived for penetration. The information obtained from the literature review is used to develop the theoretical equations found in Chapter 3.

3. ANALYTIC PENETRATION EQUATIONS

An analytic penetration equation into foam was developed by observing the penetration of nails into polyurethane foam. The purpose of the penetration equation is to determine the force or energy required for a penetration process. Penetration can be described by a reference coordinate system placed either on the nail or the foam. The penetration from the nail's viewpoint consisted of two aspects: compression and friction. The penetration from the foam's point of view comprised three mechanisms: crushing, shearing, and friction. These elements were considered, and specific equations were developed to represent the aforementioned behaviors mathematically. The summation of these equations generated the penetration equation. Data from empirical testing was used to determine the accuracy of the penetration equation and is further discussed in Chapter 4. Empirical Impact Testing.

3.1 Stages of Penetration

There are two viewpoints from which to observe the penetration process: either placing the reference coordinate system on the nail or on the foam. First, the forces opposing the nail's penetration by the foam can be considered. Second, the forces applied by the nail to the foam to attain a specific depth can be determined. This chapter will explore both viewpoints and determine the equations required to calculate these forces. It should be noted that when the penetration is complete, these opposing forces should balance each other in equilibrium.

The penetration equation, which describes the energy created during penetration, can be found from both the perspectives of the foam and nail. If the coordinate system is placed on the nail, the equation can be determined from the compression force and

friction force applied against the nail. If the coordinate system is placed on the foam, the equation can be considered the summation of three stages of penetration: crushing, shearing, and friction. Each stage has an energy equation associated with it, which will be developed in turn. In this thesis the energy equations will focus on the perspective of the foam against the nail.

3.1.1 Penetrator Perspective

If the reference coordinate system is placed on the nail, then the penetration is described as the compression force applied by the foam on the nail and the friction present between the nail and the foam.

Compression

The nail initially strikes the foam with a sudden impact force and then continues to penetrate through the foam. As the nail penetrates, the contact area between the nail and foam eventually becomes equivalent to the surface area of the projectile's penetrating face (face normal to penetration). A force acts on the nail in a direction opposite to penetration. This force operates as a compressive force on the nail. The effective nail area compressed depends upon the area in contact with the foam at any time, t. This process can be viewed as a simple compression.

The equations describing the compression force acting on the nail are presented in Equation 1. The compression force acting on the projectile is described in Equation 1, where σ_{comp} is the compressive stress and A_{comp} is the area being compressed. The compressive stress involved with Equation 1 is described in Equation 2 (Hooke's law),

where E_{comp} is the compressive modulus of the nail and $(\frac{\Delta x}{L_o})$ is the strain induced in the nail. Δx is the length the nail is compressed, and L_o is the original length of the nail.

$$F_{comp} = \sigma_{comp} \cdot A_{comp} \quad (1)$$

$$\sigma_{comp} = E_{comp} \cdot (\frac{\Delta x}{L_o}) \quad (2)$$

Equation 2 will only hold true if the stress on the nail remains in the linear-elastic region of the stress-strain curve. Compared to the foam, the nail has a much higher density and Young's modulus. It is assumed there will be little deformation of the steel nail due to its greater density and stiffness. Table 4 shows the calculated results obtained from Equations 1 and 2, proving the nail deforms very little and behaves according to Hooke's law.

Table 4: Calculations of steel nail compression

F_{comp}	A_{comp}	σ_{comp}	E_{comp}	ε	Δx	L_o
10.49 N	0.9E-06 m^2	11.4 MPa	207 GPa	5.53E-05	1.4E-06 m	0.0254 m

It can be seen the strain on the nail is extremely small. The compressive stress on the nail does not exceed the yield strength of the nail (σ_y >100 MPa), and remains in the linear elastic region [11]. The surface area was calculated for the tip of the nail, which is

the area being compressed. A very small amount of strain is present and the deformation of the nail is 0.0014 mm.

Friction

The frictional force on the nail is equivalent to the frictional force acting on the foam. They are equal in magnitude but opposite in direction. The main factor influencing the friction force is the depth of penetration. Friction increases linearly with penetration depth. This also can be seen in the friction equations, Equations 3 and 4. The friction force is a product of the normal force, N, and the coefficient of friction between the nail and foam, μ. The normal force is a product of the contact pressure exerted between the nail and foam, P, and the area of contact between the two nail and foam, $A_{friction}(x)$.

$$F_{friction} = \mu \cdot N \tag{3}$$

$$N = P \cdot A_{friction}(x) \tag{4}$$

3.1.2 Target Foam Perspective

The stages of penetration in the foam are a combination of crushing, shearing, and friction. These are considered to be the forces acting on the foam by the nail and are necessary for penetration to occur.

Crushing

The nail initially impacts the foam with an abrupt, dynamic load and then begins to penetrate through the foam. The material under the nail is crushed as the nail penetrates. The effective material area crushed depends on the area in contact with the penetrator at any time, t. This process can be viewed as a simple compression. A typical compressive stress-strain curve is displayed in Figure 13.

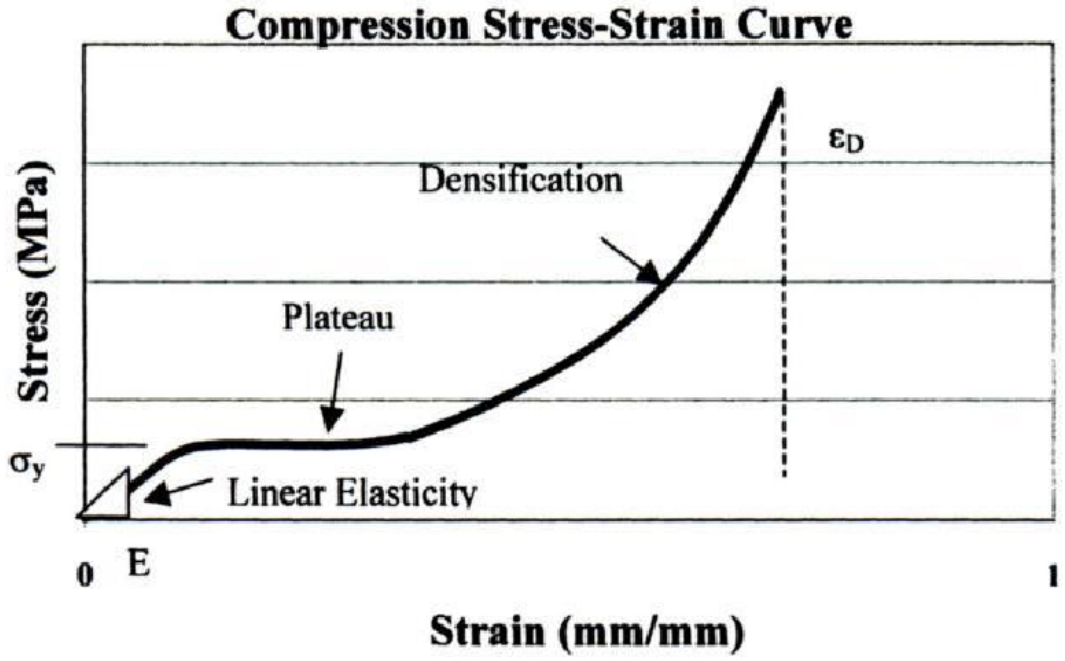

Figure 13: Compressive stress strain curve showing fracture point [6]

As the foam is compressed, the compressive stress value eventually reaches the yield point (σ_y) after which the material will no longer recover elastically, but deforms plastically. Compression does not display a necking region and if the stress reaches a

high enough level, the ultimate strength of the material could be reached (located at ε_D). At this point the material fractures and is crushed beneath the penetrator.

The compressive strength of a material is defined as the amount of stress required to crush the material. To this end, the measure of the foam's ability to resist crushing is equivalent to its compressive strength. Once an object reaches this value, it will crush. It is known from observation that foam is crushed throughout penetration. Therefore, the compressive stress present in the foam during penetration is always equal to the compressive strength of the foam. The crushing force component, then, remains constant throughout penetration. From the perspective of the foam, the equation for crushing is shown in Equation 5. σ_{crush} is the compressive strength of the foam and A_{crush} is the contact area between the foam and projectile. The compressive strength of the foam is a constant, so, only A_{crush} will affect the resistive penetration force. The resistive compressive force increases proportionally with the contact area. A greater area means a higher compressive force is necessary to penetrate while a smaller area means a lesser force is required to penetrate the foam.

$$F_{crush} = \sigma_{crush} \cdot A_{crush} \tag{5}$$

Figure 14 best explains the area being crushed by the projectile. Figure 14 shows a cross-sectional view of the contact between the nail and the foam. The area is equal to the surface area of the penetrator's face (wedge) that is in contact with the foam during penetration [2]. The area in contact is initially a finite area representing the tip of the wedge. This area increases as the nail penetrates the foam. Figure 14 (a)-(d) depicts the

penetration at different stages. This means the area in the force equation is equal to the surface area of the nail tip once the tip is fully penetrated. This is shown in the figure where the area being crushed equals the surface area of the nail tip.

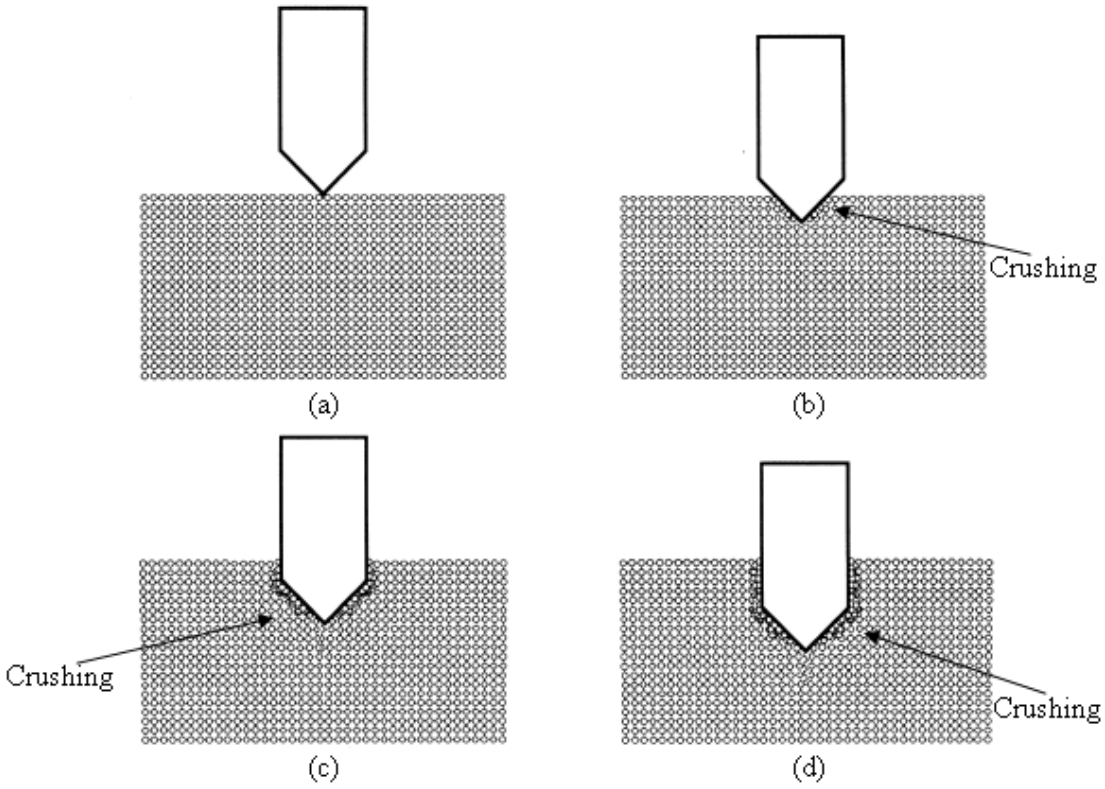

Figure 14: Cross-sectional view of nail projectile penetrating foam [2]

Shearing and Friction

After initial impact and penetration commences, the foam in contact along the walls of the projectile shears. A shearing stress is present along the sidewall-foam and tip-foam interface and causes a deformation of the foam in a direction normal to the projectile's sidewall. The shear diagram below illustrates shear in the foam.

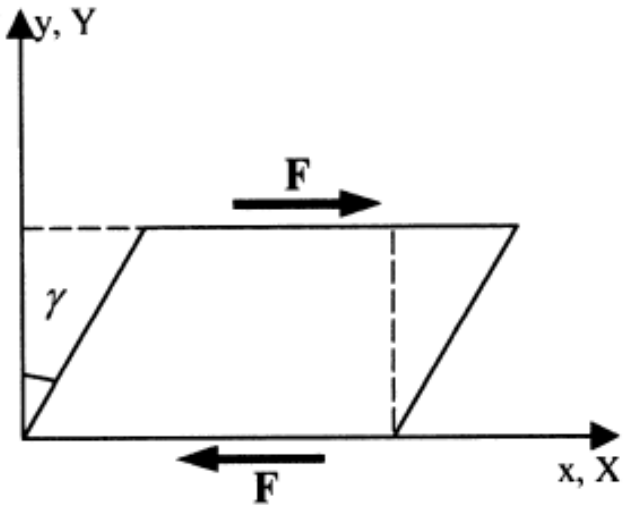

Figure 15: Simple shear diagram [1]

The nail penetrates through the foam with an applied force, F. The surface area tangent to the force is the area being sheared. The deformation of the foam continues until the shear strength of the material is reached and the foam can no longer remain attached to the fixed wall and is sheared. The shear force acting on the foam can not exceed the shear strength of the material at any point during penetration. Therefore, the resulting shear force is a constant value, similar to the crushing force throughout penetration.

Friction is present along the materials' entire interface as the penetrator moves through the foam. The foam shears during penetration and when the nail slides along the recently sheared path a friction force is induced. This friction force depends on the normal force and the surface area of contact between the parts.

To understand the different phases that the penetrator undergoes, it is important to observe the penetration process at instantaneous intervals. In order to better elucidate

where and how shearing occurs in penetration, a two dimensional diagram of the penetration at an arbitrary time interval was created (Figure 16).

The nail initially penetrates through the foam with an applied force. This action induces a shearing stress at each point the nail tip contacts the foam. The material shears when the shear strength of the material is reached. As the nail moves further along during penetration, the region of the nail above the tip slides along the recently sheared walls. The sliding action results in frictional resistance to the penetration. As the depth of penetration increases, so does the amount of material sheared as well as the total material undergoing friction.

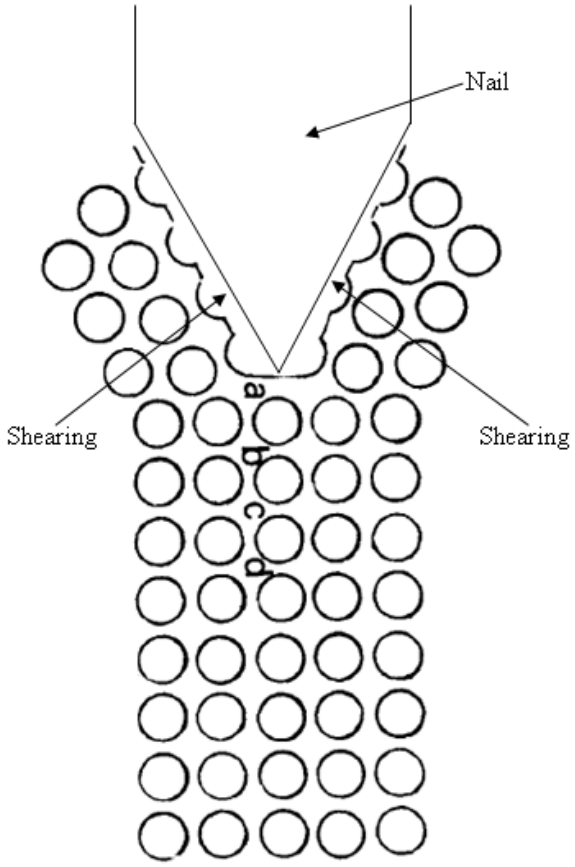

Figure 16: Shearing of foam at arbitrary time interval [3]

Equation 6 describes the shearing force, F_{shear}, where τ_{shear} is the shear strength of the foam and A_{shear} is the amount of area sheared. The area sheared is equal to the surface area of the nail's tip in contact with the foam at any time during penetration, so is dependent on depth. Once the nail tip is completely penetrated, the shear area will equal the surface area of the tip.

$$F_{shear} = \tau_{shear} \cdot A_{shear} \tag{6}$$

Equation 7 describes the frictional force during penetration, where μ is the friction coefficient between the penetrator and foam and N is the normal force. As stated before, the frictional force increases with penetration depth. The coefficient of friction is constant; therefore, penetration depth affects only the normal force component. The normal force depends on the contact area, which is a function of depth, so N is a function of penetration depth as well. The equation for N is shown in Equation 8. The normal force was determined by characterizing the interaction between the nail and foam as a shrink-fit problem.

$$F_{friction} = \mu \cdot N \tag{7}$$

$$N = P \cdot A_{friction}(x) \tag{8}$$

$$\delta = \frac{RP}{E_o}\left(\frac{r_o^{\,2} + R^2}{r_o^{\,2} - R^2} + \nu_o\right) + \frac{RP}{E_i}\left(\frac{R^2 + r_i^{\,2}}{R^2 - r_i^{\,2}} - \nu_i\right) \tag{9}$$

Equation 9 represents the shrink-fit interference equation [7]. This equation is used to calculate the normal force component in the friction force equation. δ represents the interference between the projectile and the foam and is the total deformation undergone between the parts. E_o and E_i are the elastic moduli of the foam and nail, respectively. υ_o and υ_i are the Poisson's ratio of the foam and nail, respectively.

A contact pressure, P, is exerted between the parts as they push against each other. This pressure is related to the normal force component by the surface area in contact amid the parts. Solving for P provides the value of the contact pressure and, when multiplied by the surface area, the normal force component can be found. Figure 17 indicates the critical lengths that the variables r_o, R, and r_i represent.

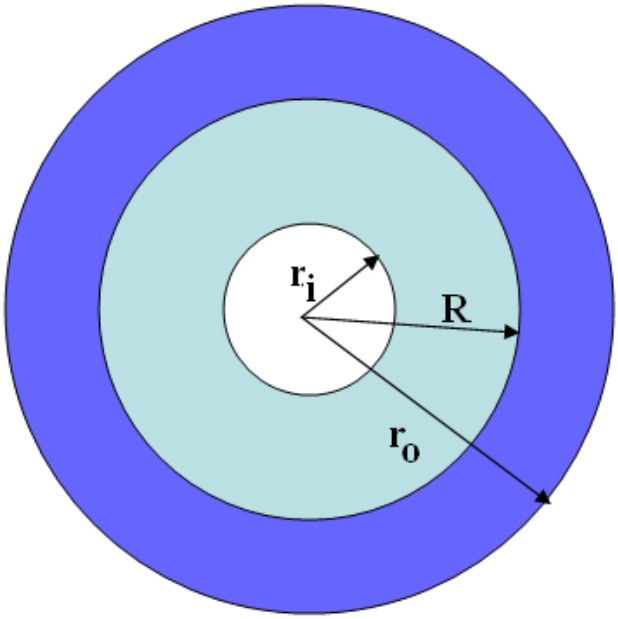

Figure 17: Front view of general press fit problem [7]

The interaction between the nail and foam does not precisely represent the definition of a shrink fit problem, but, with some assumptions, it is an acceptable model. According to Figure 17, R is the radius of the inner member, r_o is the radius of the outer member, and r_i is the inside radius of the inner member. In order to apply the shrink fit equation, the projectile (inner member) must be modeled as a solid body and not a hollow cylinder. This assumption removes the variable r_i from Equation 9. It should also be assumed the interference between the two parts is very small. This is due to the fact the nail creates its own hole as it penetrates rather than press fitting into a pre-existing hole. The interference is not zero, though, because the foam still compresses the nail along the nail's side walls, which creates the pressure between the parts in contact. Also, it is assumed the strain present in the foam is greatest around, and does not propagate far from, the interface of the two parts, so is negligible outside this location. From these conclusions, the difference in R and r_o is assumed to be extremely small, but not zero. The following section labeled Interference explains how an acceptable difference was determined.

Interference

The interference was calculated using the modified shrink-fit equation, Equation 10, and solving for the outer radius, r_o [7]. The variables in Equation 10 represent the same variables found in Equation 9. To accomplish this task, the unknown contact pressure had to be solved empirically. First, a test was performed to determine the amount of friction present when a nail is inserted into foam a distance of 9.55 mm (depth of penetration related to impact tests). The frictional force was found empirically by

removing the already penetrated nail and recording the force to do so. The coefficient of friction was determined by placing a nail on the surface of a piece of foam, and tilting the foam until the nail slides off the foam. The tangent of the angle of tilt is equal to the coefficient of friction. The coefficient of friction was measured to be 0.27 for the polyurethane and 0.33 for the polyethylene. From the frictional forces and friction the normal force was able to be determined. Dividing the normal force by the surface area of the nail yielded the expected contact pressure between the nail and foam.

$$\delta_o = \frac{RP}{E_o}\left(\frac{r_o + R}{r_o - R} + \nu\right) \tag{10}$$

Substituting all known values into Equation 10 resulted in one equation with one unknown, r_o. From here, the outside radius of the member was solved. The outside radius was found to be 0.3680 mm. The radius of the nail is 0.3607 mm, which means the outside radius was calculated as a 2.16% increase of R, the inner member radius. With the outside radius successfully determined, the shrink fit equation can be applied to solve for the normal force component necessary to calculate friction force. The calculations for the interference can be found in the Appendix of this thesis.

3.2 Total Penetration Force

Either reference coordinate system shows the existing forces in the system remain constant except for friction, which is a function of depth, f(x). The penetration of the nail into foam is the main focus of the equations, so continued analyses performed in this research use the equations for crushing, shearing, and friction. The total force acting on

the system during penetration is equivalent to the summation of the three aforementioned components and can be seen in Equations 11 and 12.

$$F_{total} = F_{crush} + F_{shear} + F_{friction} \tag{11}$$

$$F_{total} = \sigma_{crush} \cdot A_{crush} + \tau_{shear} \cdot A_{shear} + \mu \cdot P \cdot A_{friction}(x) \tag{12}$$

Equation 12 is a linear function for penetration force of the generalized form $y = \alpha + \beta x$, where α is a constant force (crushing and shearing) at any point during penetration, and βx is a variable force (friction). This signifies that penetration forces increase linearly with depth.

Force Calculations

Using the above equations, subsequent calculations were made to determine the forces due to crushing, shearing, and friction for all foams. Table 5 shows the variables and calculated results of the force equations for all foams. A table of the material properties is given in Chapter 4.

Table 5: Calculated penetration forces for PU and PE foams

	PU	Plank900	Plank600	Plank400
F_{crush}	6.684 N	0.5369 N	0.240 N	0.171 N
A_{crush}	0.9E-06 m^2	0.9E-06 m^2	0.9E-06 m^2	0.9E-06 m^2
σ_{comp}	7296000 Pa	586054 Pa	262000 Pa	186158 Pa
F_{shear}	3.802 N	0.634 N	0.407 N	0.300N
A_{shear}	0.9E-06 m^2	0.9E-06 m^2	0.9E-06 m^2	0.9E-06 m^2
τ_{shear}	4150000 Pa	691819 Pa	443884 Pa	327914 Pa
$F_{friction}$	31.4 N	2.5 N	1.2 N	0.9 N
μ	0.27	0.33	0.33	0.33
F_{total}	41.89 N	3.67 N	1.84 N	1.37 N

The polyurethane had a crushing force and a shear force equal to 6.68 N and 3.80 N, respectively. The friction force was calculated using the shrink-fit equation and equals 31.4 N. The total penetration force is equal to the summation of the three components of penetration and equals 41.89 N. The surface area being sheared is equal to the surface area being crushed. The foam is sheared along the surface area of the nail's tip, and the remaining foam becomes crushed underneath the same area [4-5].

The polyethylene show much lower forces than the polyurethane. This is expected because the polyurethane has a much higher density and modulus of elasticity than the polyethylene. The Plank 900 show forces of 0.534 N for crushing and 0.634 N for shearing. The frictional force is 2.5 N. The total force equals 3.67 N. The Plank 600 show forces of 0.240 N for crushing and 0.407 N for shearing. The frictional force is 1.2 N. The total force equals 1.84 N. The Plank 400 show forces of 0.171 N for crushing and 0.300 N for shearing. The frictional force is 0.9 N. The total force equals 1.37 N. From the calculated results, it known the shearing forces are greater than the compressive forces for the polyethylene. This is because the foam fails in shear at a stress higher than

in compression. The crushing and shearing contact areas are both equal to the surface area of the nail tip (wedge tip geometry). As the nail penetrates, the area along the tip is sheared. As penetration continues, the remaining material along the tip is crushed [4-5].

The penetration forces calculated in this chapter will be compared in Chapter 6: Discussion and Analysis with the penetration forces determined through the experimental impact tests (Chapter 5).

3.3 Penetration Energy Equations

The law of conservation of energy states the energy in a system can neither be created nor destroyed. This can be seen in the simplified energy equation $\Delta W = \Delta PE + \Delta KE = 0$. The change in energy is equivalent to the change in potential energy plus the change in kinetic energy, so $\Delta PE = \Delta KE = constant$. In reality other forms of energy are present and become apparent when observing the penetration of the nail into foam.

The total energy of the system is composed of the kinetic energy K(t), potential energy V(t), and the energy absorbed by the foam Ea(t) and is shown below in Equation 13 [8].

$$E(t) = K(t) + V(t) + Ea(t) = Const \tag{13}$$

During impact the potential energy is lost and Ea(t) = 0, so the constant is equal to the kinetic energy at time 0, K(0) [8]. This yields Equations 14 and 15:

$$E(t) = K(t) + Ea(t) = K(0) \tag{14}$$

$$Ea(t) = K(0) - K(t) \tag{15}$$

The energy absorbed by the system is equivalent to the amount of energy present due to the forces resisting penetration, so $Ea(t) = \mathrm{Re}\cdot x$, where Re is the force resisting penetration. Equation 16 expands $\mathrm{Re}\cdot x$ to show the energy absorbed by the foam consists of a constant resistance, α, overcome at any point and a friction force, β, which increases directly with penetration depth [9-10]. Equation 16 was derived from the theoretical force equations developed previously in this chapter. The total penetration force equation is integrated with respect to depth (dx) from 0 to D (final depth). Equation 17 shows the energy absorbed during penetration is a quadratic function with respect to depth.

$$\mathrm{Re}\cdot x = \int_0^D (\alpha + \beta x)dx = \alpha D + \frac{1}{2}\beta D^2 \tag{16}$$

As stated earlier, the resistive forces are the crushing, shearing, and friction forces. The compressive strength and shear strength values are constant at any point of penetration, so represent α, while the friction force changes with depth and represents βx. Equation 17 then yields:

$$Ea(t) = \alpha D + \frac{1}{2}\beta D^2 \tag{17}$$

Equation 18 is the completed total energy equation for penetration formulated by the Dynatup® Impact software which can be solved quadratically for penetration depth.

$$E(t) = K(t) + V(t) + \alpha D + \frac{1}{2}\beta D^2 = Const \tag{18}$$

Energy Calculations

Equation 17 was solved to find the energy for a penetration of a single nail to a depth of 9.55 mm. The 9.55 mm depth is the average depth of penetration for the impact tests discussed in Chapter 4. The variables α (crushing and shearing force) and βx (friction force) used in the energy calculations were solved in section 3.2 and can be found in Table 5. Table 6 shows the calculated energies for the polyurethane and polyethylene foams using the energy equation.

Table 6: Calculated penetration energies for PU and PE foams

	Depth	Crushing (J)	Shearing (J)	Friction (J)	Total Energy (J)
PU	9.55 mm	0.06383	0.03631	0.14994	0.25008
Plank 900	9.55 mm	0.00513	0.00605	0.01194	0.02312
Plank 600	9.55 mm	0.00229	0.00389	0.00573	0.01191
Plank 400	9.55 mm	0.00163	0.00287	0.00430	0.00880

The energy associated with the polyurethane crushing and shearing forces calculated in section 3.2 equaled 0.100 J. The frictional energy was calculated using the friction force determined in section 3.2. The frictional energy was found to equal 0.150 J. The total energy, therefore, equals 0.250 J. The friction force dominates the penetration forces. Likewise, the frictional energy dominates the total energy in the penetration. This is similarly seen for the polyethylene total penetration energies.

The Plank 900 has a total energy of 0.023 J. Most of this energy is contributed by the friction (0.012 J). The Plank 600 has a total energy of 0.012 J. The crushing and shear components contribute about 0.006 J combined, while the frictional energy also

equals 0.006 J. The Plank 400 has a total energy of 0.009 J. The crushing, shearing, and frictional energies equal around 0.002 J, 0.003 J, and 0.004 J, respectively.

According to the calculated energies, the frictional force contributes the most energy to the total penetration energy. This is true because the frictional energy is quadratic in the energy equation and should be the largest energy component. The polyurethane exhibits the largest energy of the foams, while the energy for the polyethylene decreases from the Plank 900 to the Plank 400. As expected, this follows the exact pattern of the penetration forces calculated in the preceding section.

The energy calculated from the analytic equations will be compared in Chapter 5: Discussion and Analysis with the energies obtained through the experimental impact tests (Chapter 4).

3.4 Chapter Discussion

Crushing, shearing, and friction forces act on the foam during nail penetration. Subsequent equations were developed based on the principles of classical mechanics. The equations for crushing and shearing incorporated the known variables of compressive strength and shear strength for the foam material, respectively. The frictional force is a function of the depth of penetration, so the friction increases linearly with depth due to the increased contact area. Therefore, the summation of the forces equals the total penetration force and is a linear function of the generalized form $y = \alpha + \beta x$, where α represents the constant crushing and shearing forces and βx represents the friction force. The energy present in the penetration is found by calculating the area under the Force-Depth curve. Integrating the force equation with respect to depth yields a quadratic function of the generalized form $y = \alpha x + \frac{1}{2}\beta x^2$. The total energy of the

system is conserved and is equal to the summation of the potential, kinetic, and penetration energies. The energies calculated from the penetration equations can be compared to the energies found by the empirical impact tests discussed in Chapter 4. Equivalent energy values indicate the equations are valid for describing foam penetration, and can be applied to the setting the nails gun's parameters. The impact tests performed to find the force and energy required for a nail to penetrate foam to a certain depth can be found in the following chapter, Chapter 4. .

4. EMPIRICAL IMPACT TESTS

Two types of foam were selected as the material for the antenna spacer: polyurethane (PU) and polyethylene (PE). Subsequent insertion of nails into foam through impact testing was performed on each individual material using the Instron Dynatup® 8200 Impact tester. The impact tests were performed to determine the load necessary to penetrate nails into foam a certain depth. The results of the impact tests will be a control for which to determine the validity of the analytic equations. The materials and their respective physical properties are as follows:

Polyurethane foam:

The polyurethane foam was supplied by General Plastics Manufacturing Company and is part of their 6700 aircraft foam product line (General Plastics Manufacturing Company, Tacoma, WA). The foam chosen was the FR-6718 foam. The FR-6718 foam is a rigid, closed cell, polyurethane foam of density 288 kg/m^3. FR-6718 has the properties listed in Table 7.

Table 7: Polyurethane foam properties [12]

Physical Properties	Metric
Density	288 kg/m^3
Compressive strength @75˚F	7296 kPa
Compressive modulus @75˚F	213208 kPa
Tensile strength	4838 kPa
Tensile modulus	237100 kPa
Shear strength	4150 kPa
Shear modulus	57506 kPa
Closed cell content (%)	97.4
Poisson's Ratio	~0.3

Polyethylene foam:

The polyethylene foam was supplied from Sealed Air (Sealed Air Corporation, Elmwood Park, NJ). Three types of polyethylene foam were used for the antenna spacer tests: CelluPlank® 400, CelluPlank® 600, and CelluPlank® 900. Table 8 shows the physical properties associated with the three polyethylene foams.

Table 8: Polyethylene foam properties [13]

	CelluPlank®		
Physical Properties	**400**	**600**	**900**
Compressive strength	186158 Pa	262000 Pa	586054 Pa
Tensile strength	565370 Pa	765318 Pa	1192793 Pa
Density range	60.9-70.5 kg/m^3	92.9-102.5 kg/m^3	144.2-157.0 kg/m^3
Cell Size	0.8 mm	0.7 mm	0.6 mm

4.1 Impact Drop-test

Figure 18 is the Instron Dynatup® 8200 series floor model impact test machine (Instron Corporation, Norwood, MA) . This impact tester was used for the impact experiments. A basic explanation of the functionality of the impact tester is as follows: a specimen is placed in the target area and clamped between two pneumatically controlled steel plates. The impact striker is set to a desired height above the specimen. The mass of the impactor is 3.67 N. The drop-test utilizes only gravity as the source of energy in the experiment. The height that the impactor begins its free-fall descent towards the target determines the energy of the test. During its drop, the impactor passes through a gate which triggers the data acquisition system connected to a computer to begin recording. Data is recorded from the initial impact to the end of the test when the impactor reaches the pneumatic safety bumpers.

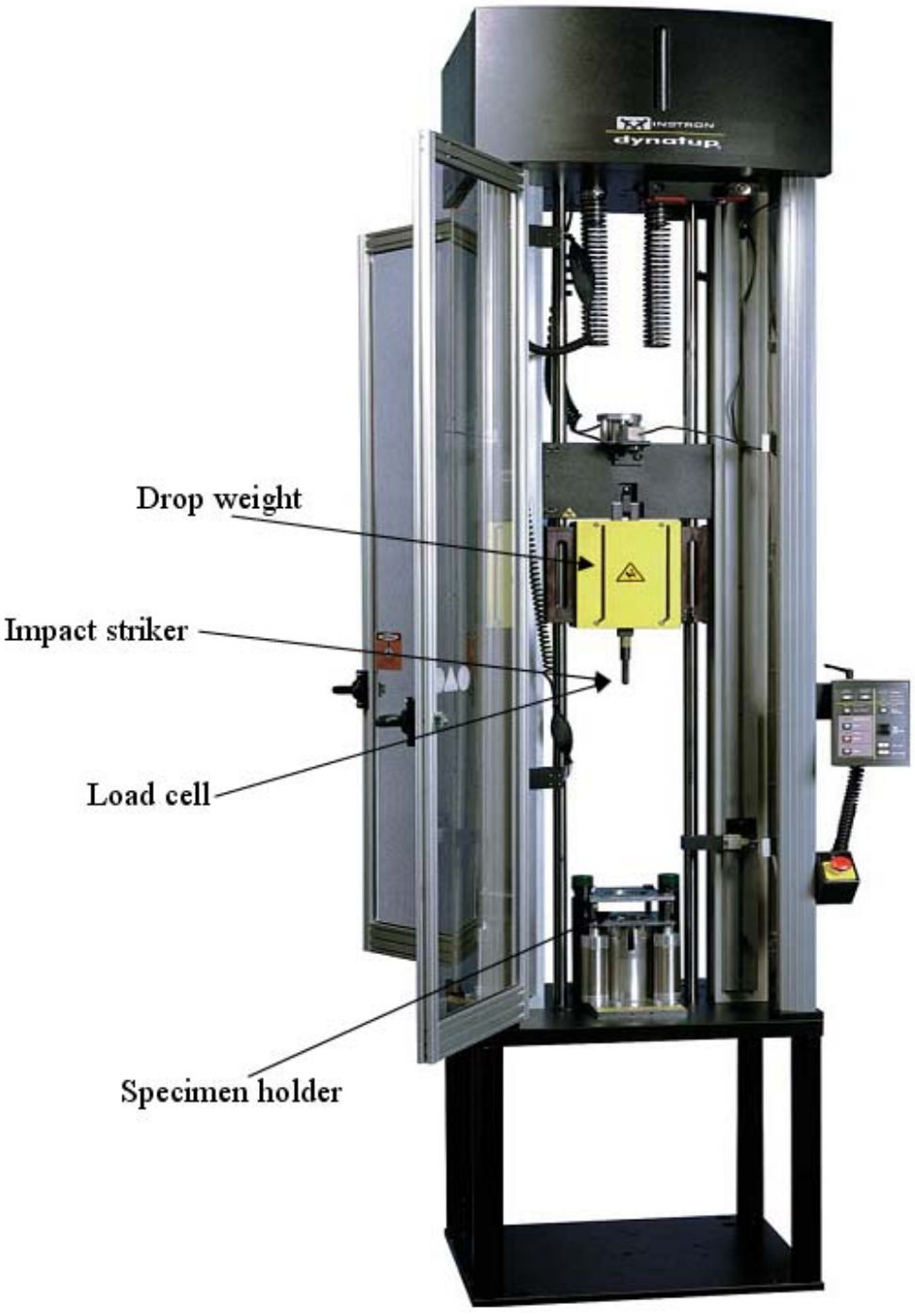

Figure 18: Instron Dynatup® Impact Test Machine [14]

4.2 Impact of Nails

To obtain data on the force required for nails to penetrate foam, a flat impact striker (Figure 19) was used to hammer the nails into the foam. It was determined through experimentation that the sensitivity of the Dynatup® impact tester was not great enough to measure the small force produced by a single nail penetrating the foam, so a greater number of nails was used. It was believed that increasing the number of nails would equally increase the measured penetration force by the same factor. To ensure this was true, multiple tests were conducted varying the numbers of nails driven into the foam specimen. Four trials were conducted on each type of foam. Each trial for the polyurethane foam consisted of 10 tests of 4, 6, 20, or 30 nails. The trials for the polyethylene foam consisted of 10 tests of 12, 18, 25, or 30 nails each.

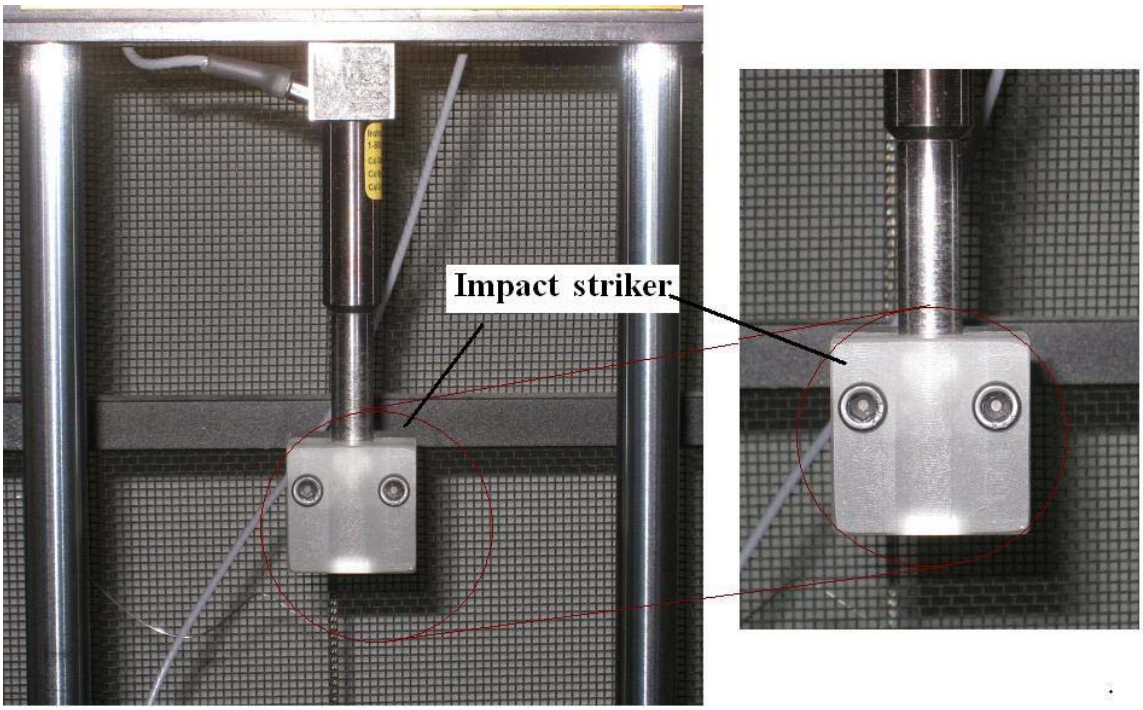

Figure 19: Impact striker attached to Instron load cell

The nails were placed in a holding apparatus that was placed over the foam in the impact machine and can be seen in Figure 20. The impactor was raised to a height of 1.02 meters before being dropped onto the bed of nails. The average velocity of the trials was 3.32 m/s. The results of the impact tests are discussed in the following sections.

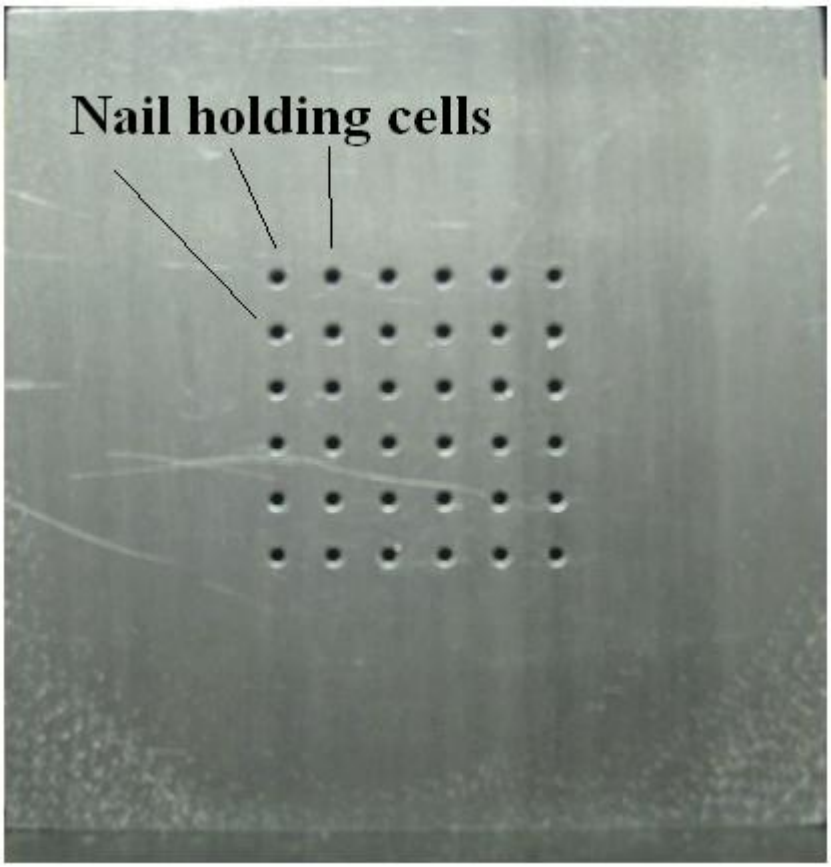

Figure 20: Nail holding apparatus

4.3 Polyurethane Impact Trials

4.3.1 Polyurethane 4 Nails Trial

The polyurethane-nail impact tests consisted of the four trials mentioned in Section 4.2. The first trial discussed is the 4 nail impact tests. The data taken from the

impact test are displayed as a graph of Force (kN) versus Time (ms). Figure 21 shows the results gathered and output by the computer's data acquisition unit.

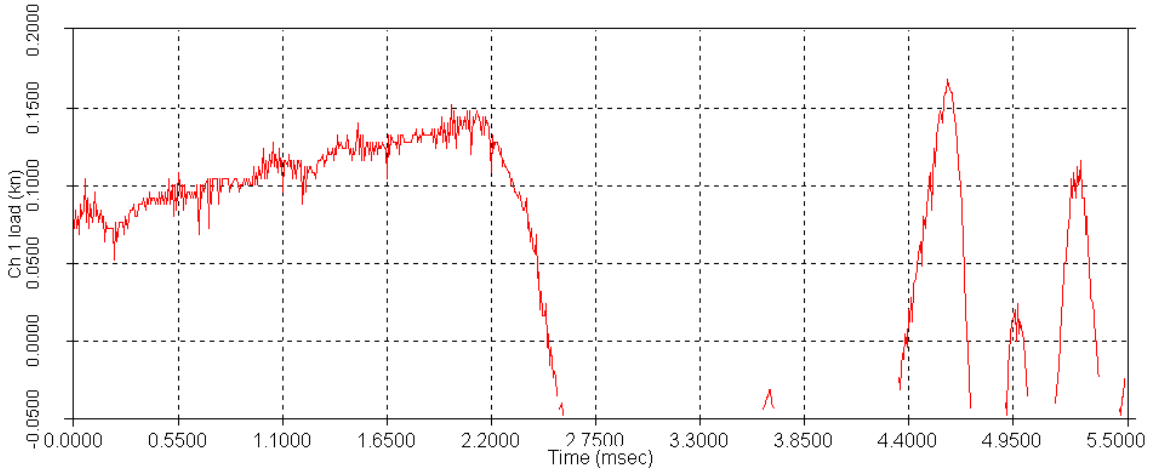

Figure 21: Force curve for 4 Nails trial

A problem arises in determining which forces displayed by the computer are critical to the penetration and which forces are irrelevant. To determine if the point of penetration is present in the data requires Figure 21 to be compared to the results of an impact test with no penetration present. To fabricate this 'empty' test, the impact striker was released in the exact manner as in the actual nail trial, but with no target to impact. Figure 22 shows the data obtained from the 'empty' test.

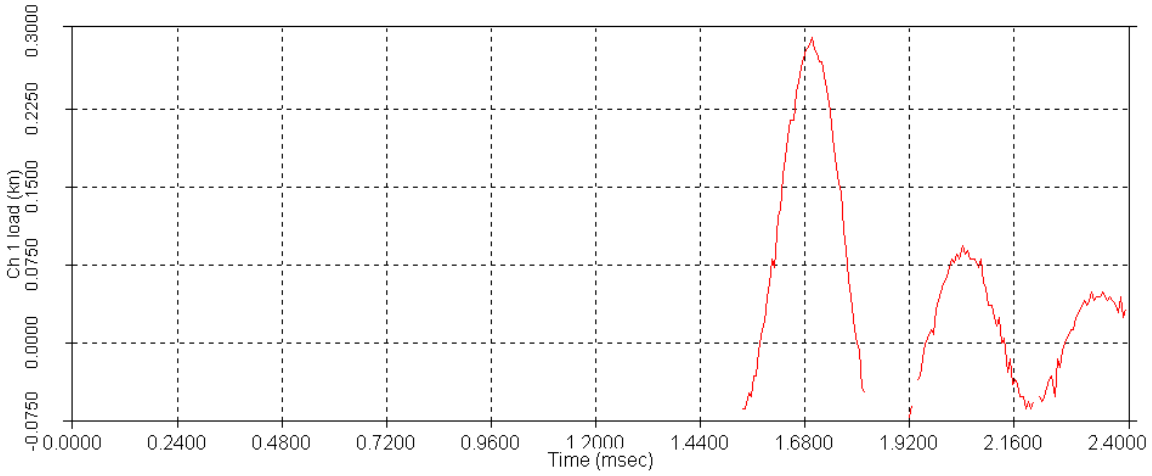

Figure 22: 'Empty' test results

Subtracting Figure 22 from Figure 21 reveals where the penetration exists and can be seen in Figure 23. It is clear the waves present at the end of the 4 Nails trial 1 are identical to the waves present in Figure 22. The only event in common between the tests that would cause these forces is the pneumatic action of the bumpers absorbing the energy of the impactor. Eliminating this bumper force shows the resulting penetration forces versus time in Figure 23.

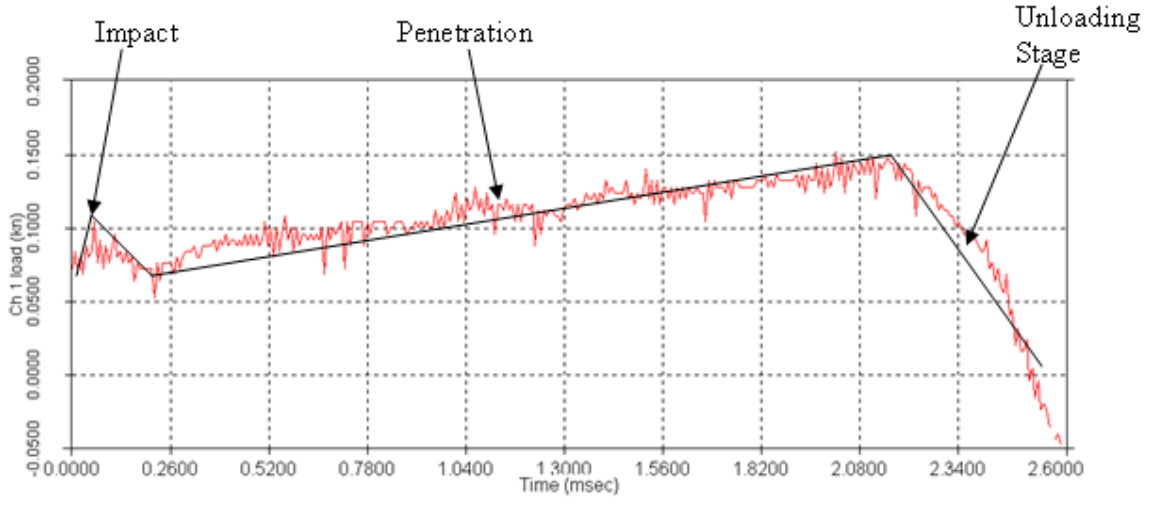

Figure 23: Penetration curve for 4 Nails trial impact test

The curve can be divided into three phases: impact, penetration, and unloading. The first wave starting at 0.00 ms represents the impact phase of the penetration, with the peak measuring the maximum load at impact. The load value at this point is approximately 96.43 N. This sudden amount of load is associated with the impact of the foam. The time it takes to reach 96.43 N is the initial impact time. The hammer strikes the nails with a force large enough to push the nail into the foam, or to begin penetration. This impulse is from time 0.00 ms to the zenith point of the first wave. The impact phase illustrates the force required to initialize penetration is equal to the maximum load at this point, or 96.43 N.

After the impact phase the penetration phase can be observed with a starting point at the impact phase end point and ending at an approximate time of 2.11 ms. The start of the penetration phase produces a load smaller than the impact force, but eventually the total force becomes greater by the end of the penetration. During this phase the force gradually increases to a maximum of 150.78 N. The maximum force corresponds to a depth of 9.47 mm. This depth was measured after the experiment was performed. When compared to the penetration equations, this increase in force seems logical. As the time increases, so does the penetration depth. As a result of the increasing depth, the frictional force should become larger. Friction is affected by the total distance traveled because the surface area in contact rises.

The final phase represents the decline in impact force as the penetration process ends. According to Figure 23, the un-loading time is from about 2.11 ms to roughly 2.60 ms. This short time accounts for the abrupt end of contact between the nail and the striker. During this stage the nail does not have the required force necessary to overcome

the resistance of the polyurethane foam. After the final phase the load eventually experiences massive oscillations. These wave forms present in the graph are due to the rebound of the impactor as it bounces off the pneumatic safety bumpers. The loads during this time have no bearing on the actual impact results.

When the load reaches zero, marking the end of penetration, the final distance traveled by the impactor is recorded to be 8.26 mm. In fact, the final depth of the nails measured using calipers after the penetration test to be 9.47 mm. Apparently there is some discrepancy in the data which can easily be understood by observing the conservation of linear momentum.

The impactor has a mass (m1) much larger than the nails (m2), (m1>>m2). When a collision occurs between these objects the nails move along the same path as the impactor. The impactor can only travel a certain distance (8.26 mm) until it reaches the pneumatic bumpers and contact is lost with the nails. After contact, the nails still contain some momentum from the impact and will continue to penetrate without an applied external force until its kinetic energy returns to zero. The impactor no longer records data associated with the nail and foam when contact is lost. This explains why there is a 1.20 mm difference in recorded deflection and final depth.

According to Figure 23 the penetration ends around a time of 2.11 ms. The area under the load deflection curve equals the measured energy of the test. Figure 24 shows at 2.60 ms the total energy of the system is 0.616 J. From Figure 24 it can be seen the energy increases quadratically with time. The energy is computed by calculating the area under the load curve. The energy slope slightly lessens between the times of maximum load to the end of contact. This is due to the work done on the system diminishing as the

force reduces. After the impact ends, contact is lost, and the energy dissipates before the impactor strikes the bumpers.

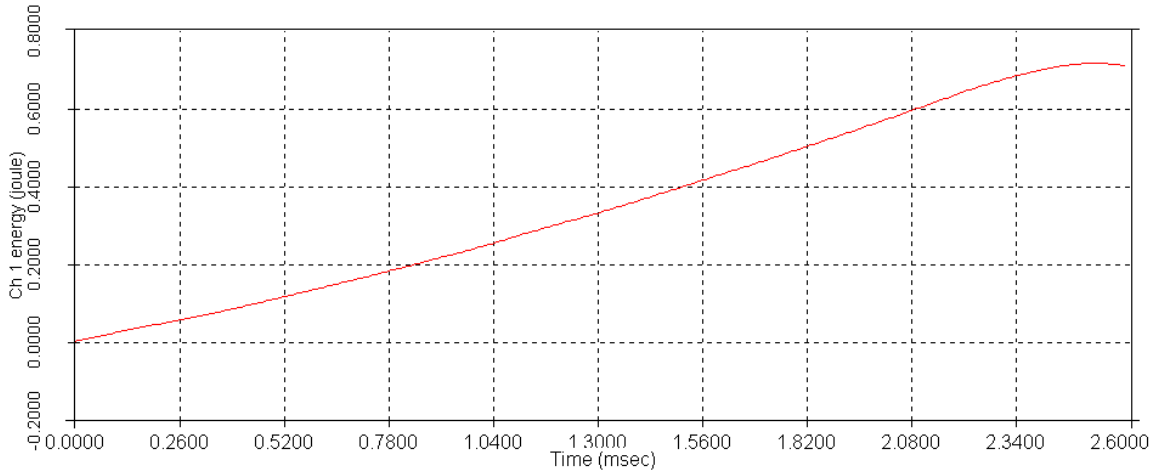

Figure 24: Energy-time curve for 4 Nails impact test

Figure 25 represents the velocity profile for the impact and shows that the velocity at the start of the experiment is 3.33 m/sec. The velocity remains fairly constant during the penetration. The velocity profile is a measure of the speed of the impact striker. The lowest point before the slope rises is where the striker ceases contact with the nail. Here, the nail's velocity profile changes from the profile of the striker seen below. After contact is removed there is no force present to drive the nail, only its momentum. Due to inertial forces the nail's momentum eventually dissipates and its velocity goes to zero. As the data acquisition unit (DAQ) receives information from the load cell, it can not show the velocity profile for the nail after contact is broken. The rise of the impactor's velocity slope indicates when it begins to strike the bumper.

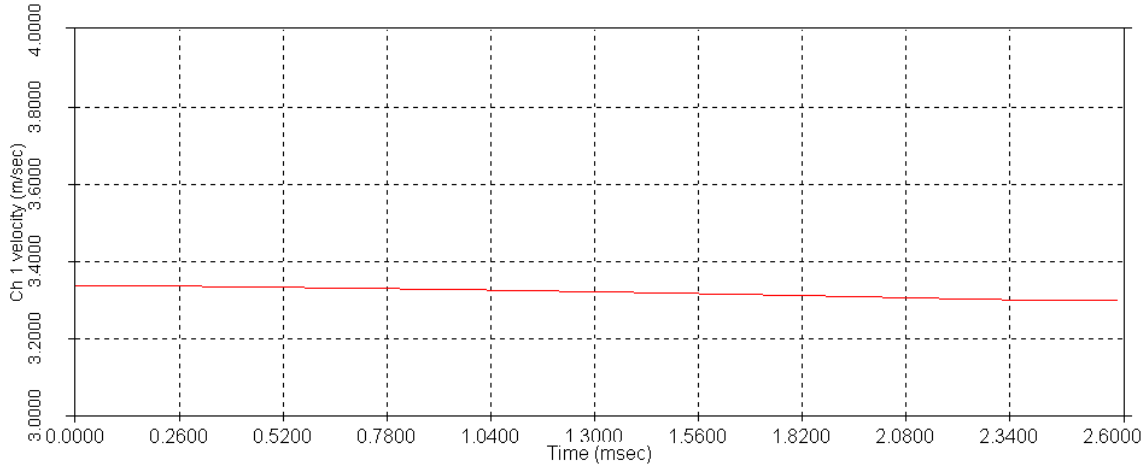

Figure 25: Velocity profile for 4 Nails trial impact test

4.3.2 Polyurethane 6 Nails Trial

A graph of the results for the 6 Nails trial can be seen in Figure 26. Similar to the 4 Nails trials, the graph can be divided into three primary phases. The penetration can be seen without the bumper impact in Figure 27.

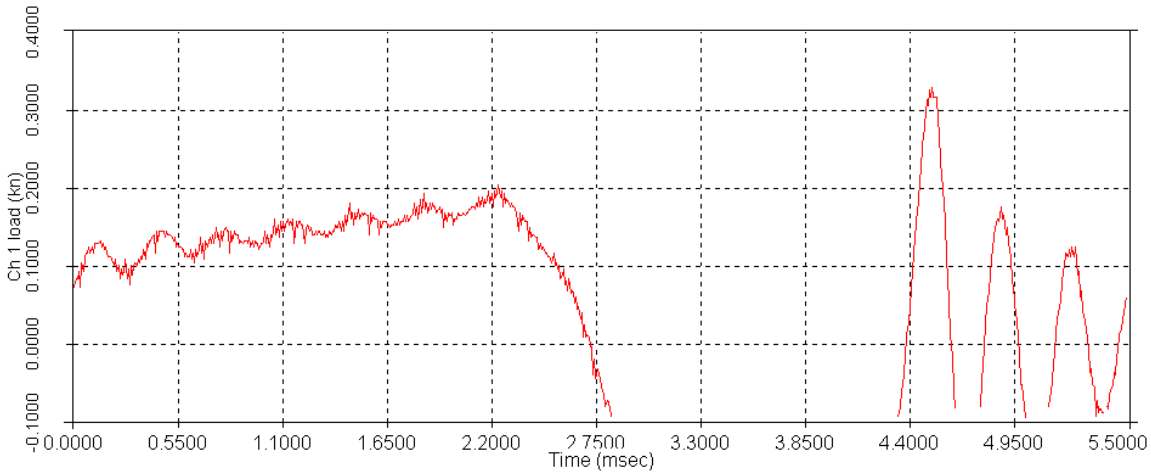

Figure 26: Load-time profile for 6 Nails trial

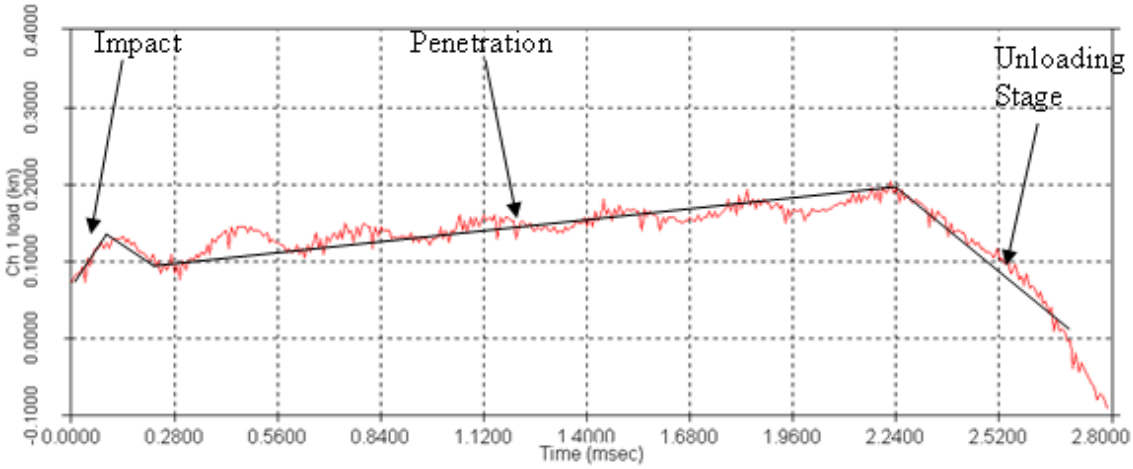

Figure 27: Load-time profile for 6 Nails trial neglecting bumpers

Figure 27 shows the 6 Nails test experiences a similar output for the impact phase as the 4 Nails test. The impact phase yields a maximum load of 129 N at an approximate time of 0.08 milliseconds. This represents an impact load equivalent in respects to the load found in the 4 Nails trials. It is important to realize adding an additional two nails to the impact test should deliver a higher force, comparatively.

The penetration phase indicates a load increase with respect to time. So, as the time is recorded from the beginning to the end of the second stage, roughly from 0.08 ms to 2.24 ms, the load becomes larger. The maximum load for the penetration phase is also the maximum load for the entire impact test. The maximum load is located at the end of the second stage and has a value of 195.72 N. According to what is known of the forces involved in penetration, the maximum load should be greater than the initial impact load. The resulting depth of penetration was measured to be 9.62 mm.

Again, the final phase is related to the loss of momentum when the penetrator reaches the pneumatic bumpers and contact is lost between the impactor and nails.

Evidence of the bumper's effect can be seen in Figure 26 as the large waves present immediately after the final phase.

The energy-time curve for the penetration can be seen in Figure 28. The total energy was found to be 0.98 J. Figure 29 shows the velocity decreased from 3.33 m/s to 3.29 m/s during the penetration.

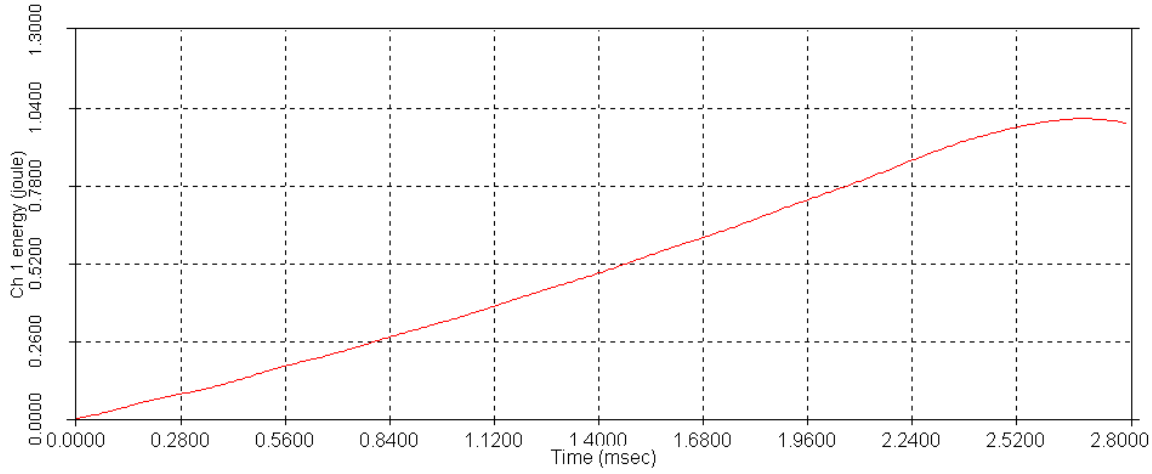

Figure 28: Energy-time curve for 6 Nails impact test

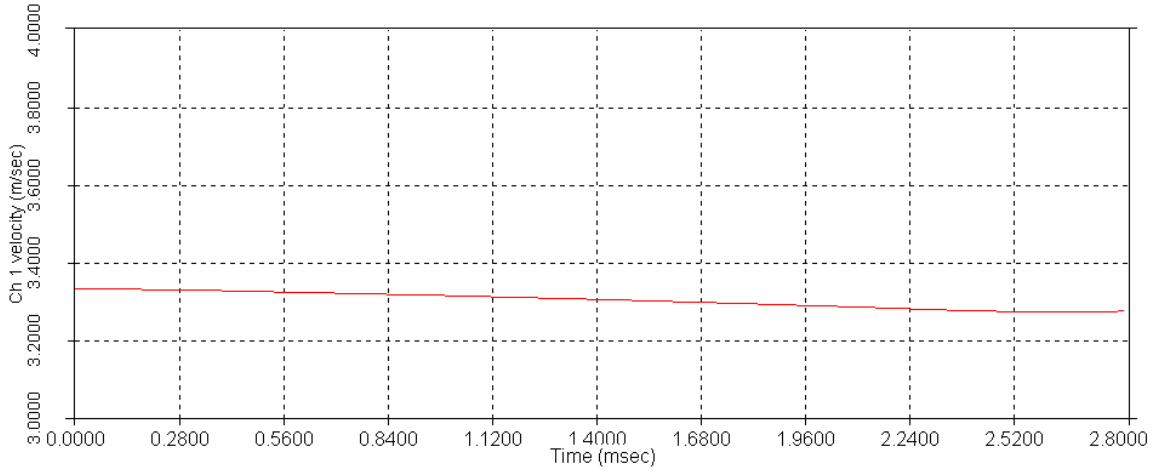

Figure 29: Velocity-time curve for 6 Nails impact test

The same penetration phases discussed in the 4 Nails and 6 Nails are present in all polyurethane foam nail trials, so do not require further discussion. Only the results of the

phases will continue to be discussed. A table of results for the 6 Nails can be found in section 4.3.5 Polyurethane Results Discussion.

4.3.3 Polyurethane 20 Nails Trial

The polyurethane 20 Nails trial run 1 data can be seen to represent a similar profile as the 4 and 6 Nails trials. The impact load registers as 175.00 N. It is interesting to note in Figure 30 that the load decreases after a maximum value of around 640.54 N as expected, but then experiences a spike near the end. The spike is when the impactor reaches the bumpers. It is not easily recognized compared to the previous polyurethane tests because the load reached when impacting 20 Nails is much larger. The bumper is impacted with a high force and then acts as a shock absorber. The first impact wave registered from the rebound brakes is more evident in the earlier nail trials because the higher loads experienced during penetration with 20 Nails camouflage the bumpers' effect. Without the spike its appearance may not have been observed. Figure 30 shows the load results with the known bumper rebounding. Figure 31 shows the results with only the first bumper collision force remaining. From these figures it can be seen that the penetration ends around 2.70 ms. After this time the impactor reaches the bumper. The load impacting the nails has achieved a much higher value than the impact of the bumpers. This was not true for the previous polyurethane trials. The final depth of nail penetration due to the maximum load was 9.55 mm.

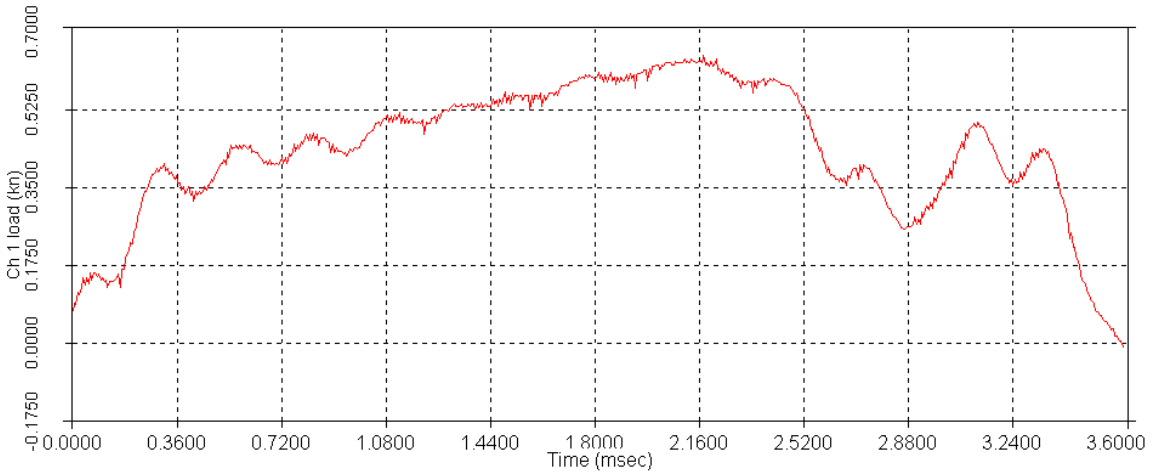

Figure 30: Load profile for 20 Nails versus time

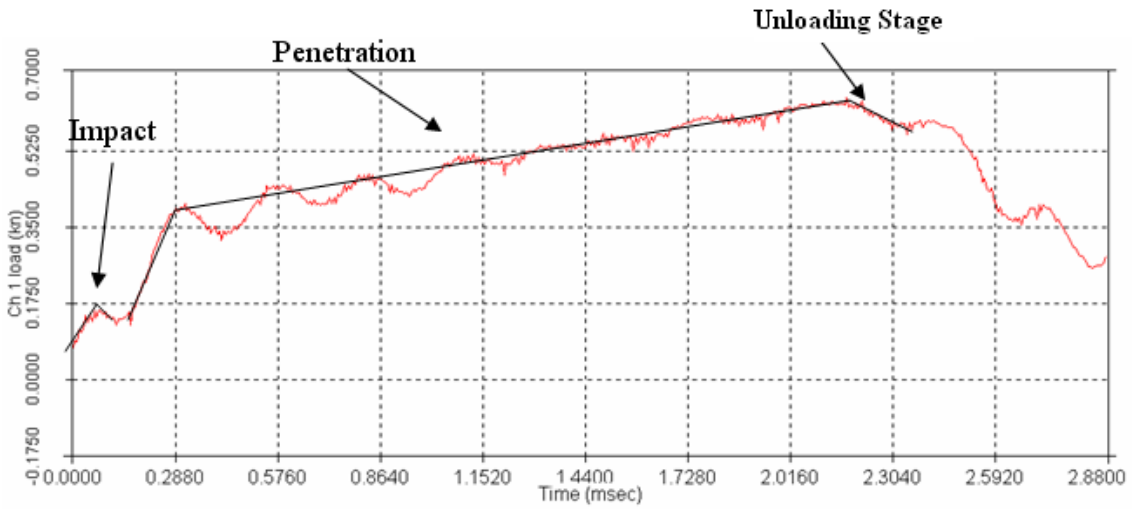

Figure 31: Load profile for 20 Nails versus time excluding bumper rebounding

Figure 32 shows that the penetration energy reaching 4.10 J at 2.70 ms and then the slope starts to decrease. The time at 4.10 J matches the data from the load-time graph marking the end of penetration. The energy obtained from impacting the nails is larger than the energy from the pneumatic bumpers. When the impact striker reaches the bumpers the energy curve begins to experience a decreased slope. This marks the

presence of the bumper impact at the spike. The bumpers absorb the shock and the energy levels will continue to increase but the slope will continue to lessen.

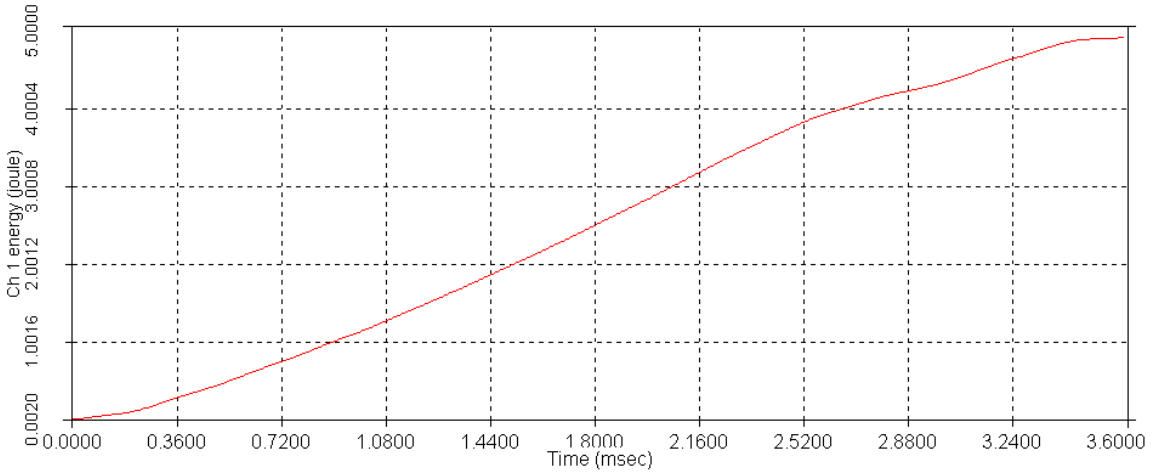

Figure 32: Energy-time curve for 20 Nails trial

Figures 33 below shows the velocity-time curve obtained from the 20 Nails trial. The velocity-time graph shows, for the same reason as the energy curve, the velocity slope decreasing and then gradually increasing. The time at the intersection point between this negative and positive slope corresponds to when the penetration finalizes and the safety bumpers are activated.

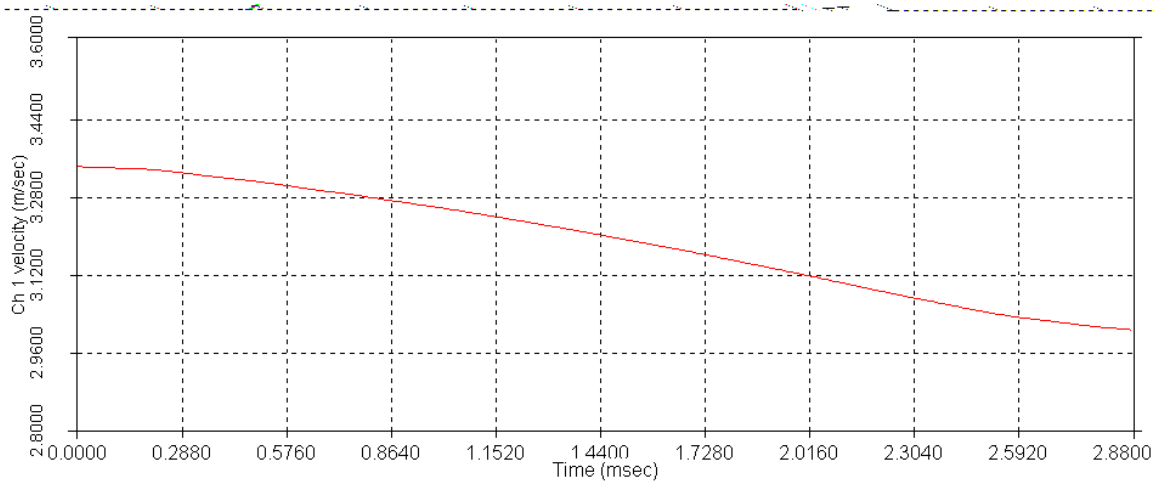

Figure 33: Velocity-time curve for 20 Nails trial

4.3.4 Polyurethane 30 Nails Trial

The polyurethane tests involving 30 Nails are similar to the previous nail trials. The same profiles exist for the recorded data. The marked difference in the trials is a larger load is initiated upon impact of the 30 Nails than the smaller nail quantities. The increase of total energy throughout the experiment is attributed to the larger force. Overall, the final depth was measured around the same value as the other experiments. The graphs for the 30 Nails trial can be found in the Appendix. A table of results can be found in the following section, 4.3.5 Polyurethane Results Discussion.

4.3.5 Polyurethane Results Discussion

The penetration curves of all the polyurethane tests contain series of small sinusoidal waves. These waves are due to the interactions of the impactor, the foam, and the structural dynamics of the Instron drop test machine. The first peak on the graph is where the material fails under the dynamically applied load. The load drops as the impactor momentarily loses contact with the nails after the initial impact. Contact is re-established at the next wave cycle and the load wave increases and penetration continues [8]. The period of the oscillations is a structural effect due to the natural frequency of the system and is a property of the impact tester. This was determined by performing multiple impact tests while varying the foam, nail quantities, and energy of the system. The frequency of the waves did not alter during the experiments and was concluded to be the frequency at which the Instron impact tester vibrates during the impact tests. The natural frequency of the impact tester can be computed as the inverse of the wave's time period and is equal to 3000 Hz.

The three phases of the impact curve must be analyzed to calculate the force required for the nail to penetrate to a desired depth. The impact force will always be

equal to the maximum peak of the first wave. The penetration force is equivalent to the maximum load present at the end of the penetration phase.

An explanation was previously given for why the impact curve is a series of sinusoidal waves. Many points located on these waves are considered extraneous because only continuous contact between the impactor and nails causes penetration of the foam. The best way to eliminate any extraneous forces present in the waves is to average the forces. The impact force is known to be a correct value because contact is continuous to that point. However, the impact force has no bearing on the actual penetration forces, so can be ignored [8]. The maximum force marking the end of penetration is accurate because it is the final point of contact between the impactor and nails. Curve fitting through the penetration phase results in a linear trend for penetration and can be seen in the PU load curves throughout Chapter 4. The start point for the penetration phase is located after the initial impact and ends at the final penetration time, t_f. The penetration phase represents the point when the resistive forces begin to take effect and are measured. Linear interpolation of the penetration phase will determine the force corresponding to any time during penetration.

The polyurethane penetration phases show that the penetration force increases with time and depth. The crushing and shearing forces are constant throughout penetration. Therefore, the increase in force can only be associated with friction. This is due to the frictional force being directly linearly related to penetration depth.

The results of the impact tests can be seen in Table 9. As expected the force present in the polyurethane foam tests increases as the quantity of nails increase. In fact, this increase in nails correlates to a direct increase in force by the same factor. Dividing

the final force by the number of nails yields the average force per single nail. The final penetration force found for each trial run, when divided by their respective nail quantities, show similar force per nail values. The mean penetration load per nail for all trials ranges from 31.32 N to 34.55 N. Each trial has a range for penetration forces calculated for a 95% confidence interval. This confidence interval shows the force to drive a single nail into polyurethane foam has a 95% probability of falling inside the determined penetration force range [15]. Table 9 shows that the force ranges for the different nail trials overlap. This shows that the penetration force increases directly with the quantity of nails. The range of standard deviations for all trials goes from approximately 1 N to 3 N, which is relatively low when compared to the high loads experienced (mean 31.32 N – 34.55 N) during penetration.

Table 9: Polyurethane impact test data

Polyurethane Trials	4 Nails	6 Nails	20 Nails	30 Nails
Quantity of tests	10	10	10	10
Mean Resistive Energy	0.645 J	1.023 J	4.638 J	5.371 J
Resistive Energy Standard Deviation	0.049 J	0.039 J	0.195 J	0.139 J
Resistive Energy Range (95% C.I.)	0.533 J - 0.757 J	0.934 J - 1.112 J	4.193 J - 5.083 J	5.054 J - 5.688 J
Mean Penetration Force/Nail	32.00 N	32.21 N	31.32 N	34.55 N
Penetration Force Standard Deviation	3.07 N	2.04 N	0.96 N	2.56 N
Penetration Force Range (95% C.I.)	25.00 N - 38.99 N	27.56 N - 36.86 N	29.13 N - 33.51 N	28.71 N - 40.39 N
Impact Velocity	3.32 m/s	3.32 m/s	3.32 m/s	3.32 m/s
Average Penetration Time	2.64 ms	2.77 ms	2.70 ms	2.73 ms
Average Depth of Penetration	9.47 mm	9.60 mm	9.55 mm	9.55 mm

The penetration energy is quadratic and a function of depth. The standard deviation shows the resistive energy for each trial remains consistently low throughout testing.

4.4 Polyethylene Impact Trials

The polyethylene trials consisted of three varying PE foams: 900 CelluPlank®, 600 CelluPlank®, and 400 CelluPlank®. The polyethylene impact tests set-up differed from the polyurethane tests. With regards to the polyurethane tests, the foam was dense enough for the force to be calculated with at least four nails being impacted. The polyethylene foam, however, was much less dense and, as a result, the impact force generated from striking four nails was not high enough to be recorded. This meant more nails had to be impacted for data to be obtained. Therefore, the polyethylene nail trials were run with batches of 12 nails, 18 nails, 25 nails, and 30 nails for the 900 and 600 Plank foams. The 400 Plank foam was tested with batches of 18 nails, 25 nails, and 30 nails. The phases describing the PU foam penetration are the same for the PE foams, including the effects taking place during penetration.

4.4.1 900 Plank 12 Nails Trial

Figure 34 below shows the recorded data from run 1 displayed as Force (kN) versus Time (msec). This graph displays a curve similar to the polyurethane foam trials. The graph of the polyethylene tests also can be divided into the three different phases: impact, penetration, and final. However, there are some key differences apparent between the PE foams' respective impact tests.

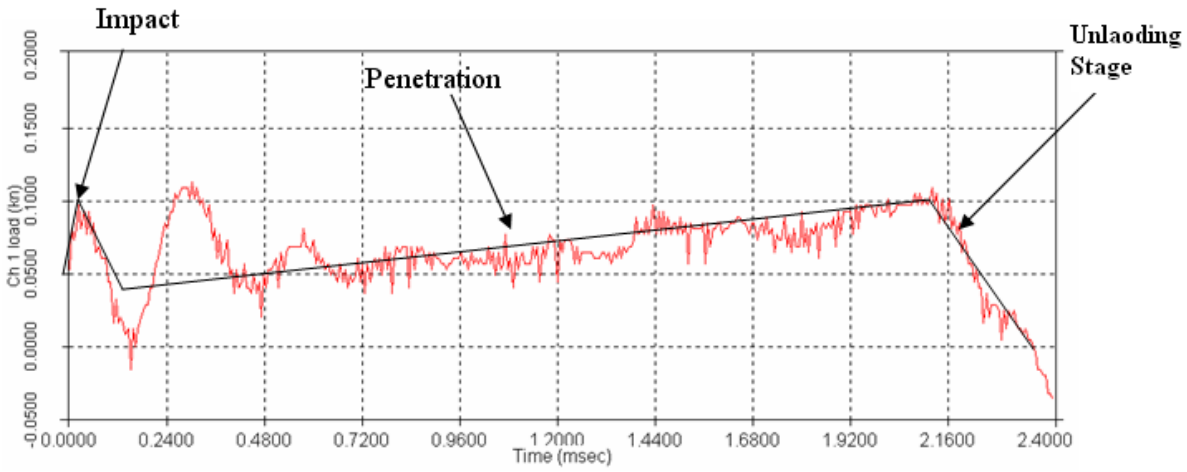

Figure 34: Load-time curve for PE Plank 900 12 Nails trial

The impact striker impacts the nails until the peak of the first curve. The time when the maximum load is reached marks the end of the impact phase. The maximum load reached during this phase is 100.0 N. The impact is very fast and sudden which explains why it displays the largest difference in force.

The penetration phase begins when the force drops from its maximum force at impact to a time of 2.16 ms. The maximum load reached during penetration is 106.76 N. The penetration phase for the polyethylene is similar to the polyurethane foam tests. The amplitude for the polyethylene penetration waves is much larger on average than the polyurethane. As the only difference between the two phases is the material, it can be concluded the wave profiles are attributed to the material properties of the target foam. The polyethylene has a much smaller density and compressive strength than the polyurethane accounting for the lower initial impact force. The high amplitude waves can result from the density of the polyethylene. A lesser density could mean there is less interference to prevent the slight rebounding occurring with the striker and nail. As the

nail penetrates the foam, the foam acts as a natural damper which is the reason that the wave amplitudes lessen throughout the penetration. The depth of penetration measured with calipers after the experiment ended was 9.44 mm.

Figure 35 shows the energy present in the system increases from 0.00 J to 0.49 J at an equivalent time when the penetration ends.

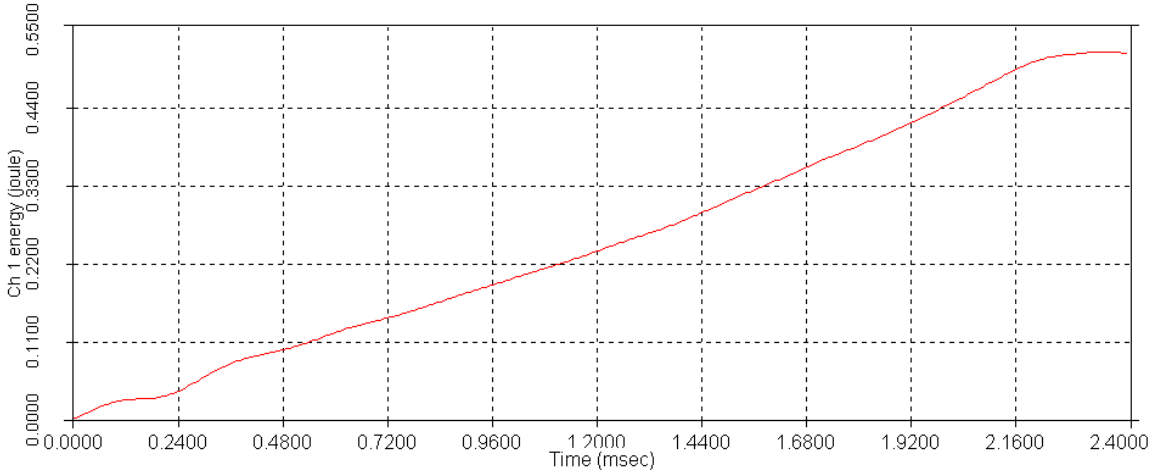

Figure 35: Energy-times curve for PE Plank 900 12 Nails trial

Figure 36 shows the initial impact velocity was 3.33 m/s. The velocity continues to decrease as the nails move through the foam to a value of 3.31 m/s when the impact striker hits the bumpers and no longer remains in contact with the nails. The velocity slow down is 0.02 m/s when contact is lost between the impactor and nails and the velocity is no longer measureable.

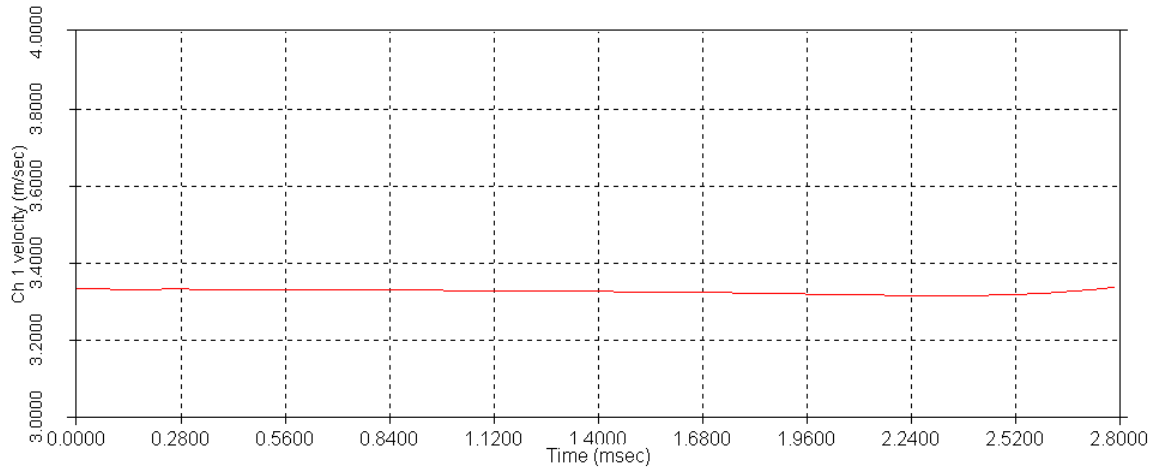

Figure 36: Velocity-time curve for PE 900 Plank 12 Nails trial

The 900 Plank nail trials exhibit similar curves to each other, so only the results of the tests need be discussed, not the penetration phases.

4.4.2 900 Plank 18 Nails Trial

The 18 nails impact test displays a distinct load increase from the 12 nail trial as shown in Figure 37. Figure 37 shows the load-time curve when the rebound loads are negated. The impact load is around 120.10 N and the maximum penetration load is around 142.34 N. The time to maximum load is around 2.02 ms with the total penetration time around 2.37 ms. The final depth of penetration recorded was 9.44 mm.

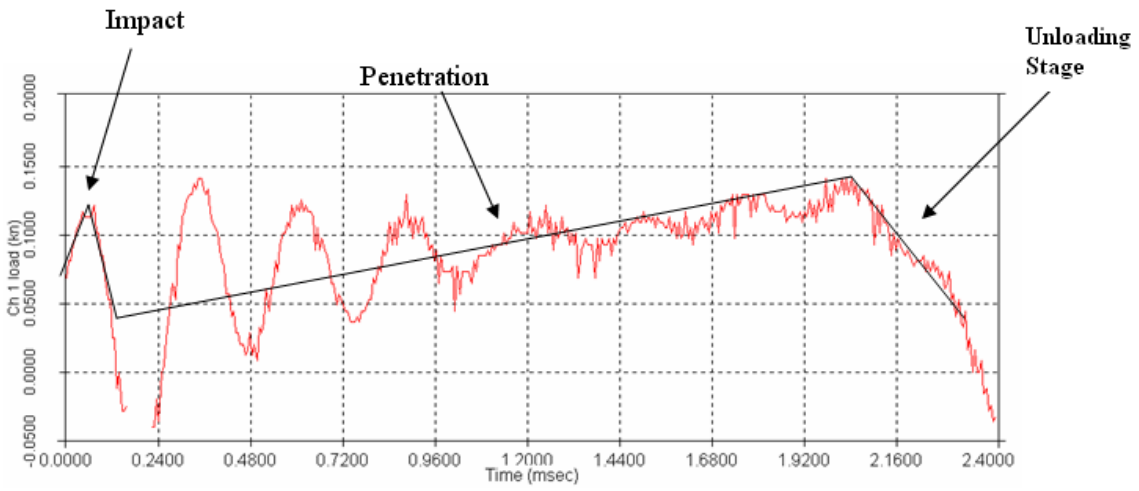

Figure 37: Load-time curve for PE Plank 900 18 Nails trial

The energy curves for the 18 Nails trials show a similar profile as those of the 12 Nails impact tests. The energy is of course higher for the 18 Nails than the 12 Nails trials which can be seen in Figure 38 below. The total energy is 0.66 J and is found at a time of 2.37 ms. The curve starts to level off indicating the end of penetration.

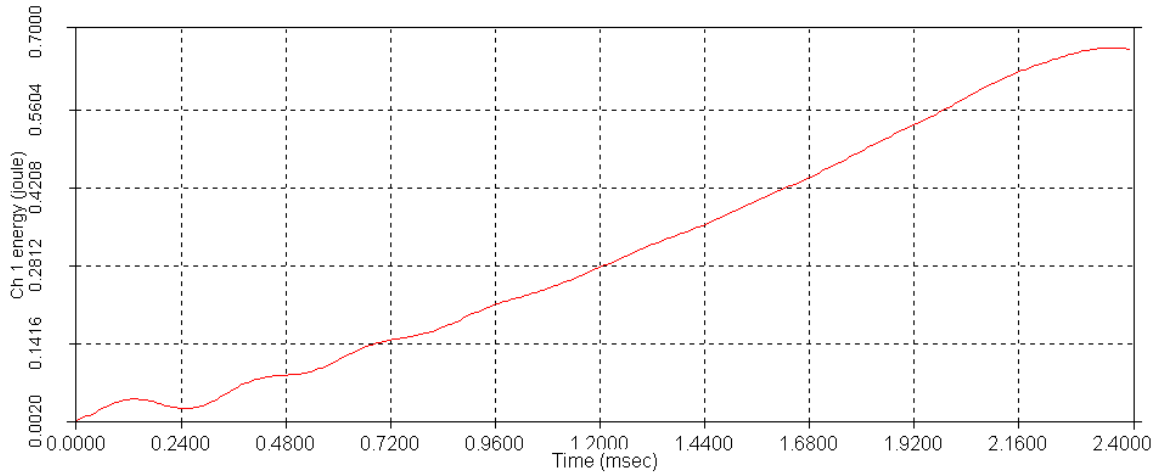

Figure 38: Energy-time curve for PE Plank 900 18 Nails trial

The velocity-time curve shown in Figure 39 shows the initial velocity to be 3.33 m/s and the final velocity to be 3.31 m/s.

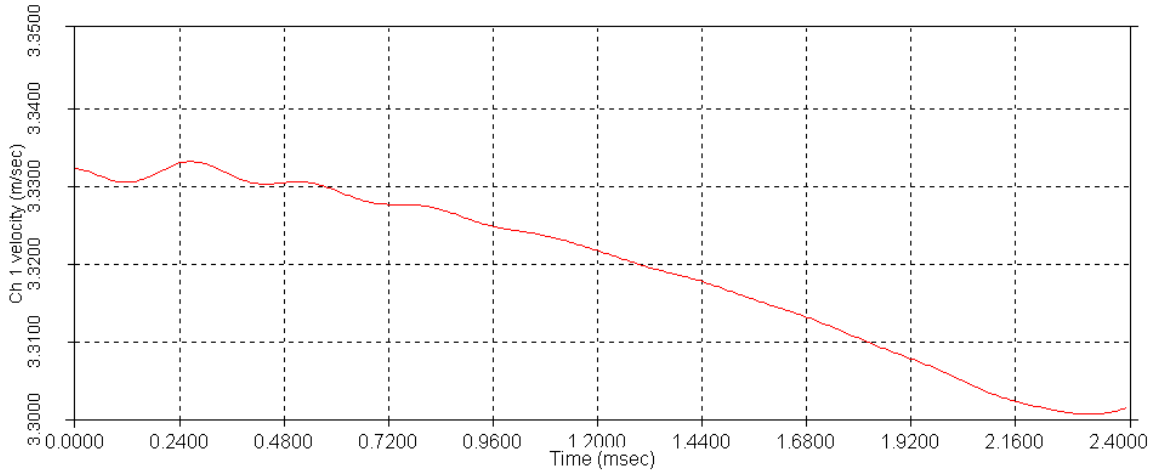

Figure 39: Velocity-time curve for PE Plank 900 18 Nails trial

4.4.3 900 Plank 25 Nails Trial

Figure 40 shows the load-time curve for the 25 Nails impact. The nails are impacted by a load of 184.00 N and the penetration load rises to 184.83 N. The total time of penetration is 2.40 ms and the final depth of penetration is 9.45 mm. Figure 41 shows the total energy of the penetration. The total energy of the system is approximately 0.98 J. Figure 42 shows the velocity impacts at 3.33 m/s and ends at 3.28 m/s. Both the energy and velocity curves have a slight decrease in slope to signify when the penetration phase begins to end.

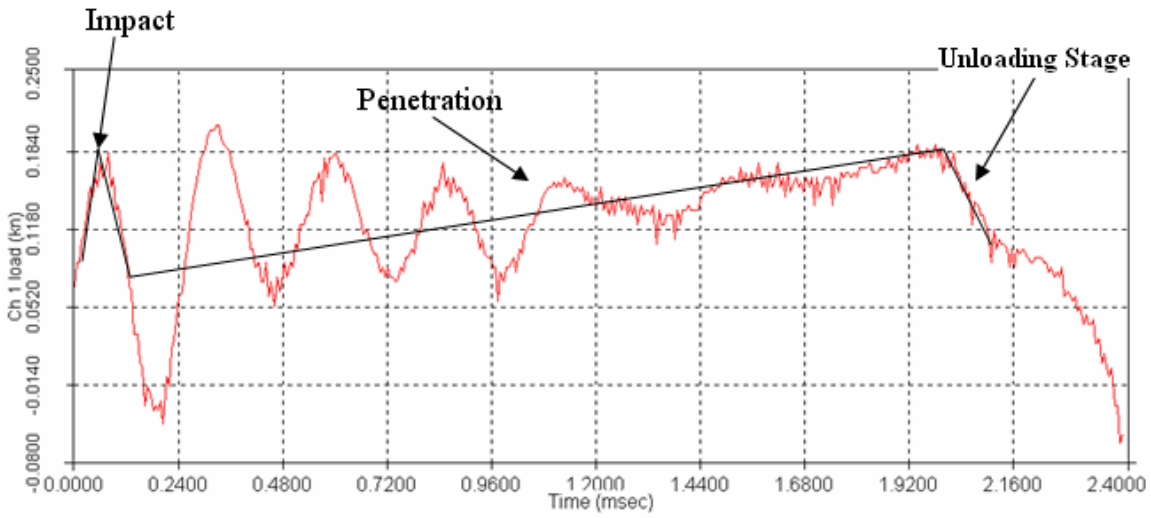

Figure 40: Load-time curve for 900 Plank 25 Nails trial

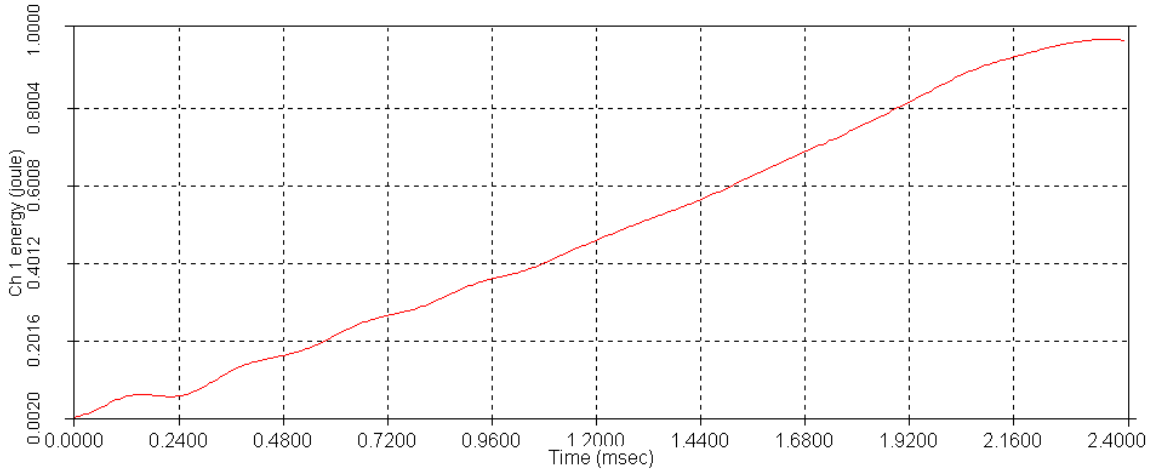

Figure 41: Energy-time curve for 900 Plank 25 Nails trial

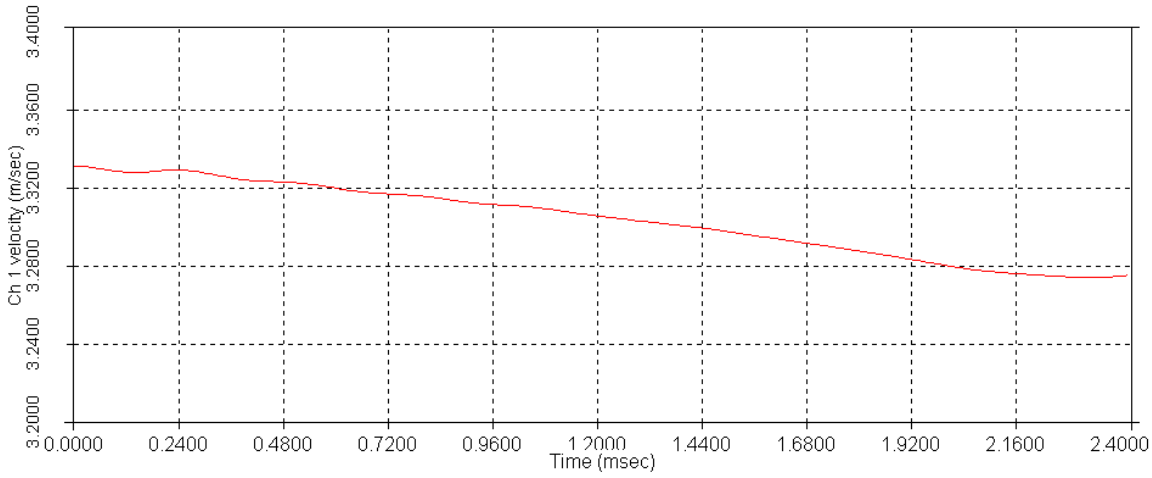

Figure 42: Velocity-time curve for 900 Plank 25 Nails trial

4.4.4 900 Plank 30 Nails Trial

The 900 Plank 30 Nails tests show similar results to the previous 900 Plank Nail trials. The obvious difference in the trials is that a larger load is initiated upon impact of the 30 Nails than the smaller nail quantities. The increase in total energy throughout the experiment is attributed to the larger force. The graphs for the 30 Nails trial can be found in the Appendix.

4.4.5 600 Plank 12 Nails Trial

The 600 Plank load-time curve displayed in Figure 43 below shows a notable difference in its profile from the 900 Plank nails trial. The load increases to the point of impact, but the force decreases on average instead of increasing though the rest of the penetration. The impact load is about 77.84 N and the total penetration time is about 2.77 ms. Throughout the penetration phase the load remains fixed around the same value. The maximum load peaked on the last wave is around 69.5 N. Figure 43 displays the penetration without the impact of the pneumatic bumpers. The final depth was recorded to be 9.56 mm.

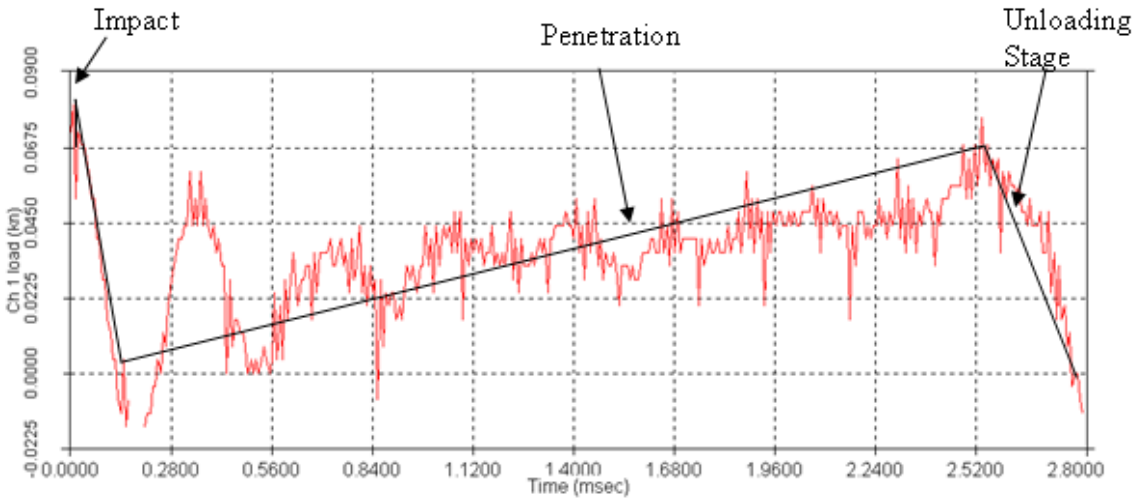

Figure 43: Load-time curve for 600 Plank 12 Nails trial

The energy-time curve in Figure 44 shows an increase in energy during the penetration. The total energy is very small, approximately 0.26 J by the end of penetration.

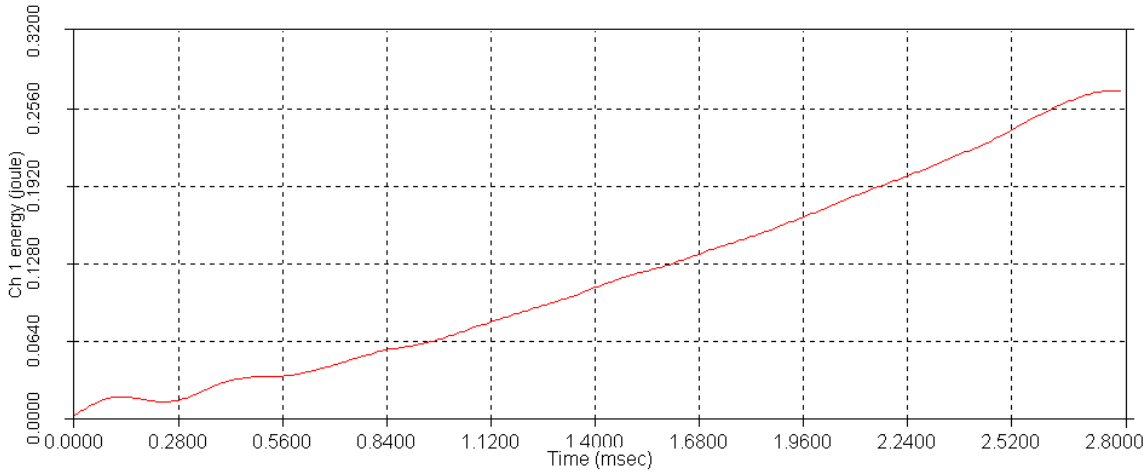

Figure 44: Energy-time curve for 600 Plank 12 Nails trial

The velocity profile is shown below in Figures 45. The velocity profiles for the previous trials decrease slightly whereas this velocity shows relatively no change. The energy provided by the impactor is so great compared to the energy absorbed by the

foam, the velocity remains fairly constant [8]. The velocity remained approximately 3.34 m/s until it starts to increase when the bumpers are impacted.

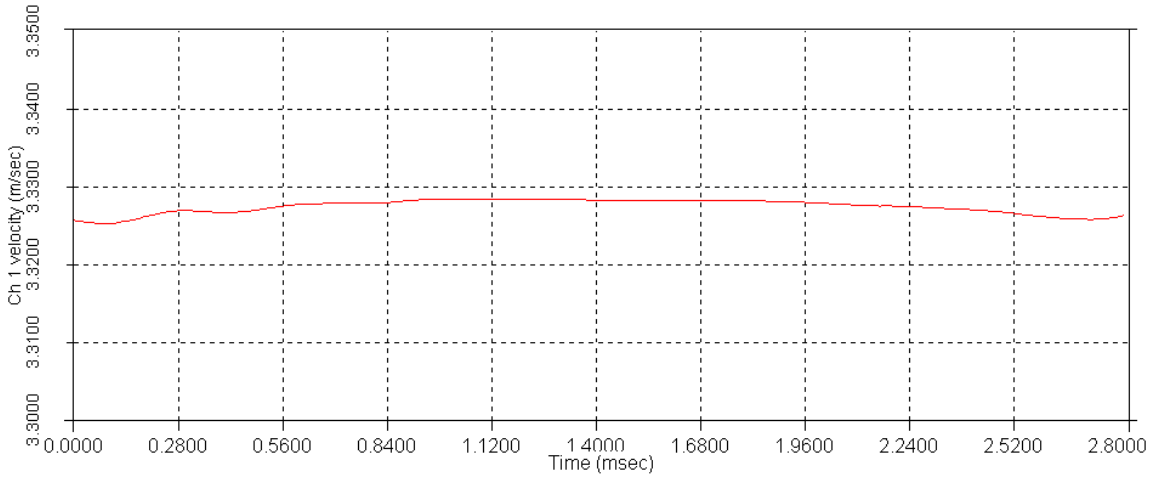

Figure 45: Velocity-time curve for 600 Plank 12 Nails trial

The load-time profiles for the remaining 600 Plank trials are nearly identical except that the forces increase with nail quantities.

4.4.6 600 Plank 18 Nails Trial

Figure 46 shows the maximum load at impact to be 124.55 N. The force decreases after impact and remains fairly constant during penetration. The total penetration time is 2.77 ms and the peak of the final wave displays a maximum load of 117.07 N. The final depth of penetration was measured to be 9.55 mm.

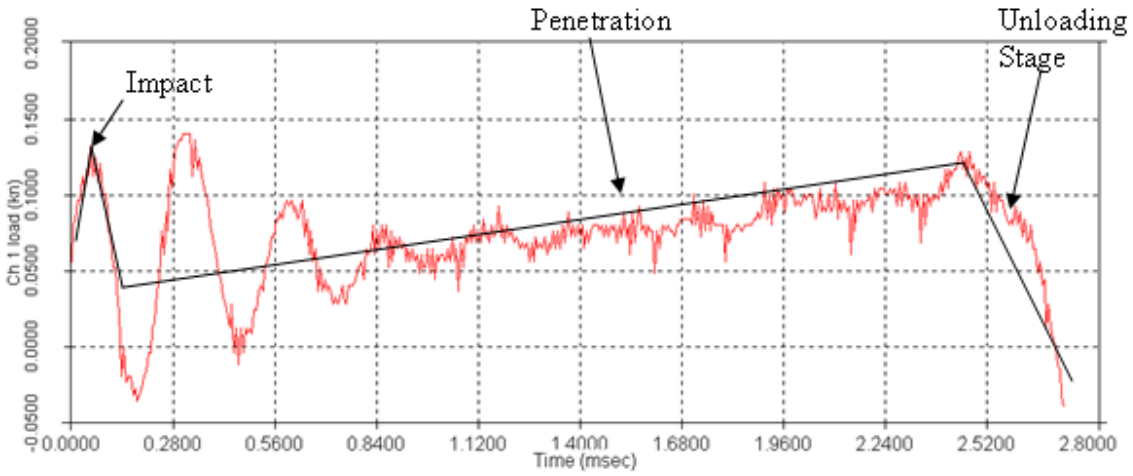

Figure 46: Load-time curve for 600 Plank 18 Nails trial

Figure 47 shows the energy-time curve for 600 Plank 18 Nails trial. The total energy of the system is 0.63 J at 2.77 ms. The velocity curve shown in Figure 48 has an initial velocity of 3.33 m/s and the final velocity of 3.31 m/s.

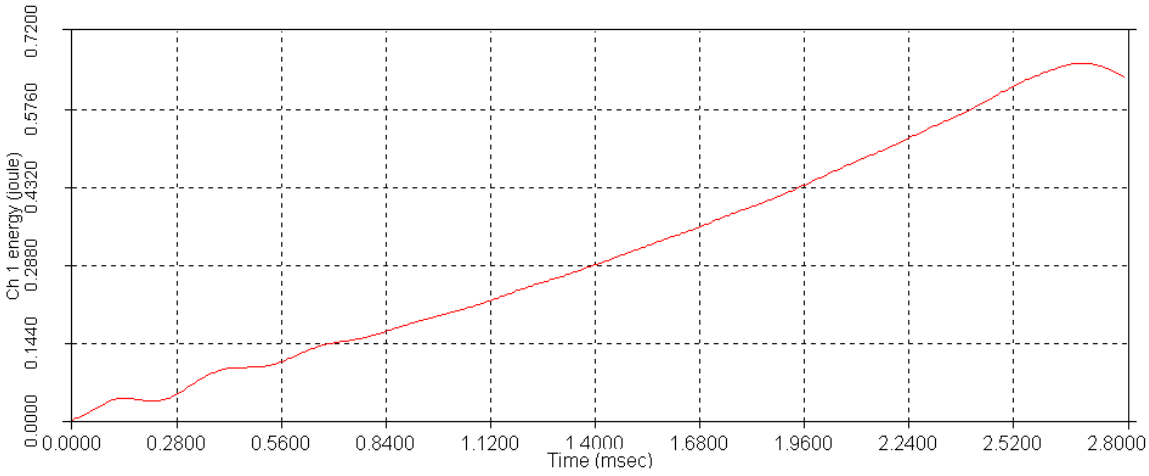

Figure 47: Energy-time curve for 600 Plank 18 Nails trial

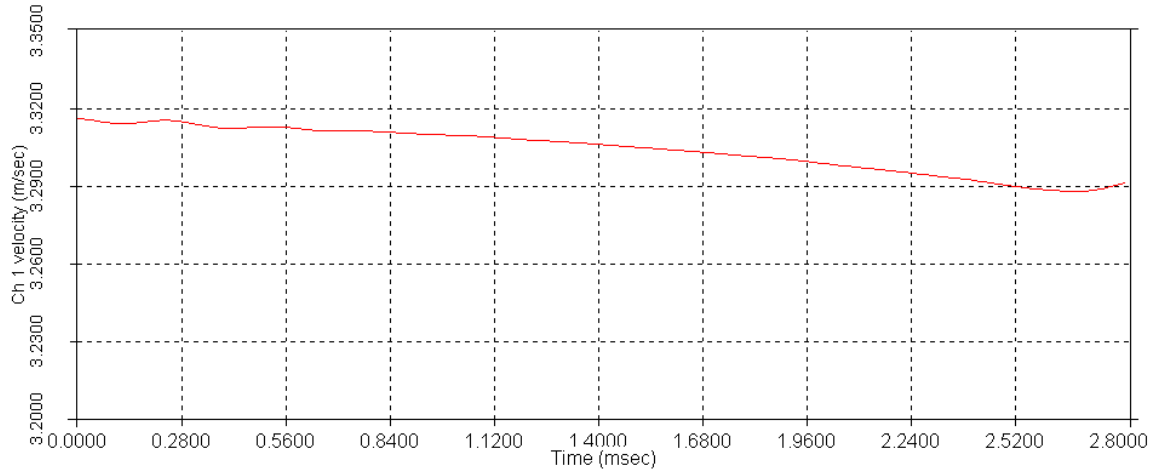

Figure 47: Velocity-time curve for 600 Plank 18 Nails trial

4.4.7 600 Plank 25 Nails Trial

It can be seen from Figure 49 that the 25 Nails trial follows the same pattern as the previous 600 Plank trials. The nails are first impacted with a load of 151.43 N which decreases to a somewhat level load value. The maximum load of the final wave is about 150.42 N. The total time of penetration is 2.77 ms. The nail penetrated to a final depth of 9.55 mm.

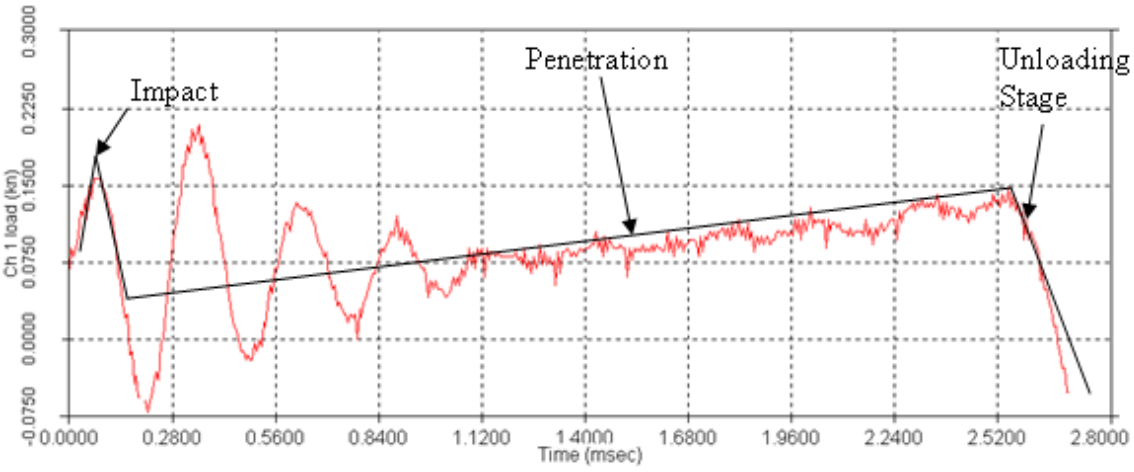

Figure 48: Load-time curve for 600 Plank 25 Nails trial

The total energy reached by the end of penetration is 0.77 J and can be seen below in Figure 50. The curve begins to experience a decrease in slope marking the end of penetration.

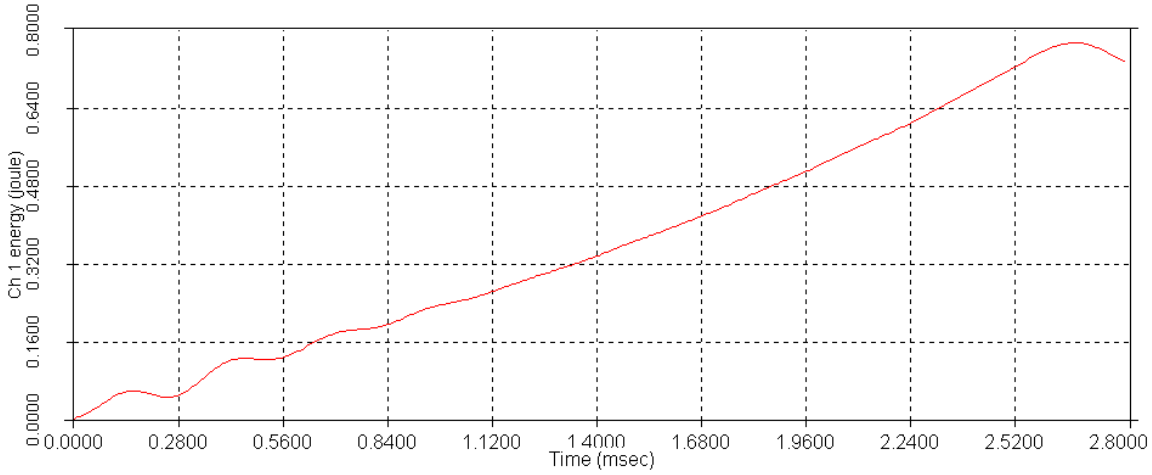

Figure 49: Energy-time curve for 600 Plank 25 Nails trial

Figure 51 shows the velocity of the impactor at impact is 3.33 m/s and loses contact at 3.29 m/s. Once again the change in slope specifies when the end of penetration.

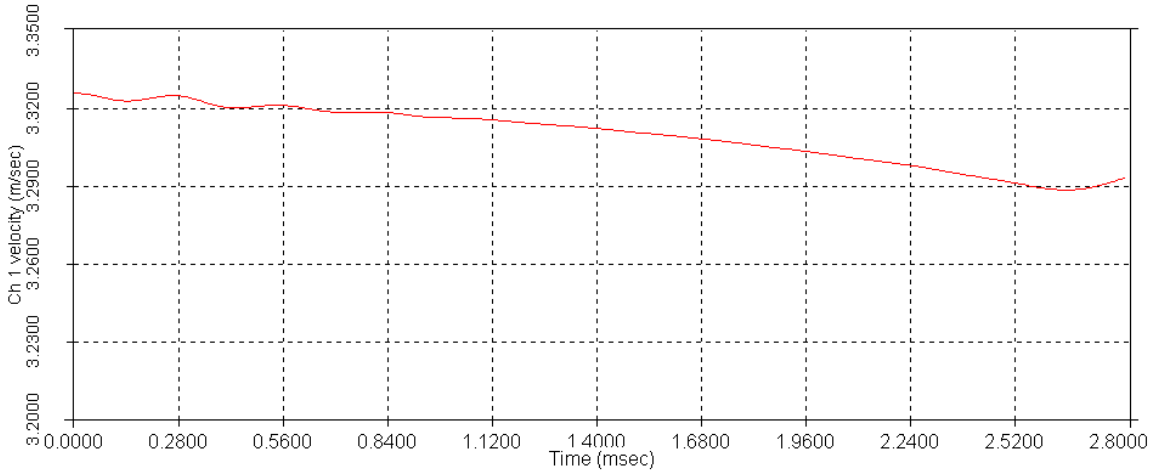

Figure 50: Velocity-time curve for 600 Plank 25 Nails trial

4.4.8 600 Plank 30 Nails Trial

The load curve below in Figure 52 shows an impact load of about 160.00 N and the final peak of the penetration phase reaching a load of 190.30 N. The time of penetration is 2.77 ms. The final depth was measured to be 9.55 mm.

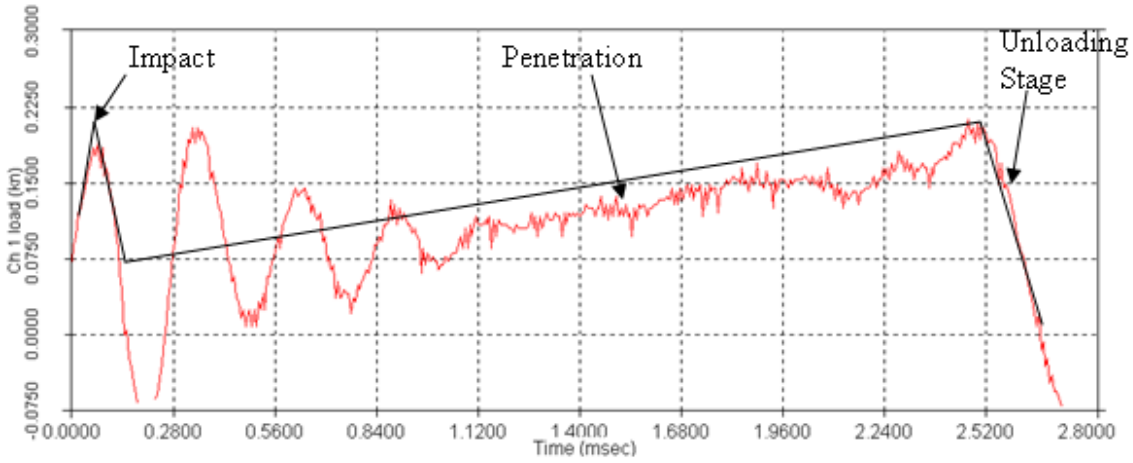

Figure 51: Load-time curve for 600 Plank 30 Nails trial

Figure 53 below represents the total energy present throughout the penetration. The energy curve stays linear during the penetration from 0.00 J to about 0.97 J. Figure 54 shows the velocity decreasing linearly from an impact velocity of 3.33 m/s to 3.31 m/s at loss of contact.

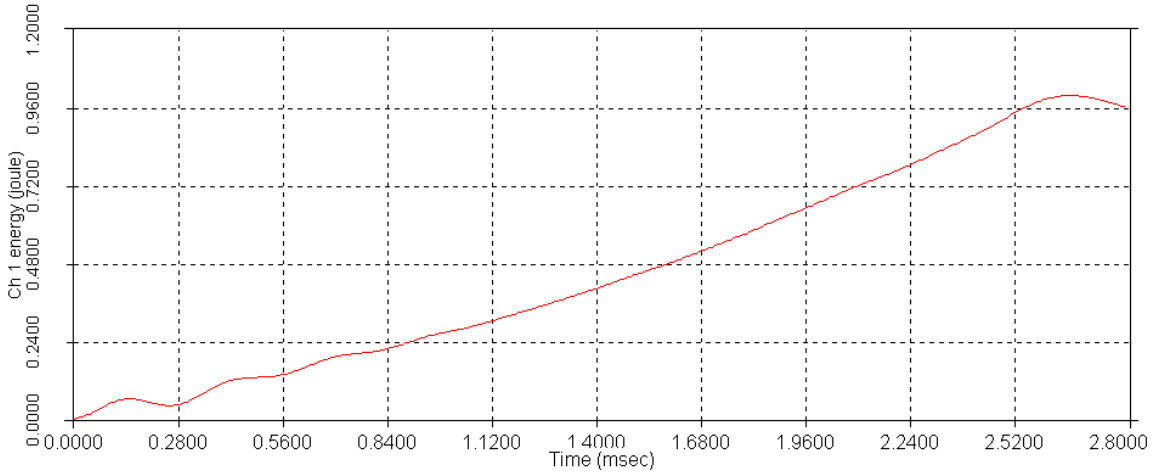

Figure 52: Energy-time curve for 600 Plank 30 Nails trial

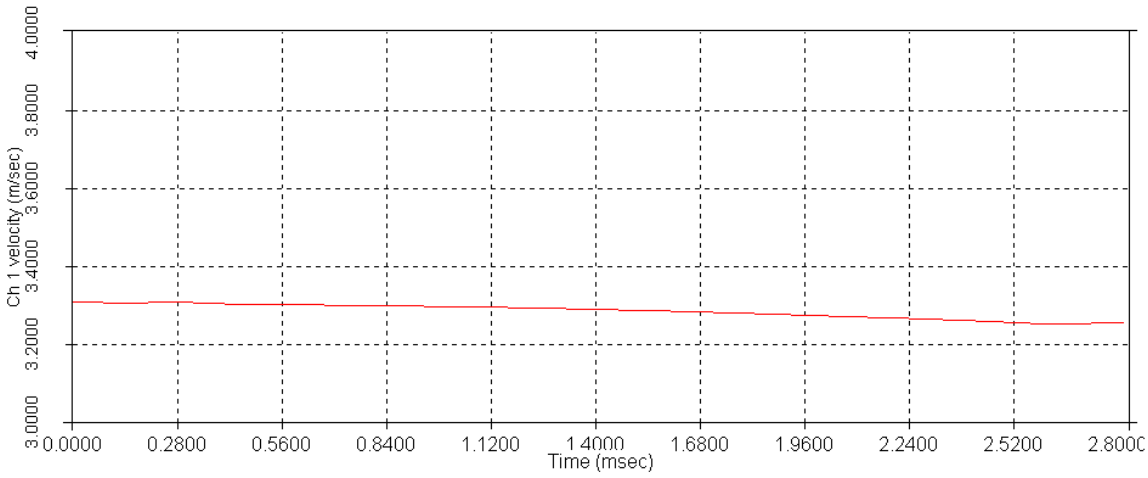

Figure 53: Velocity-time curve for 600 Plank 30 Nails trial

4.4.9 400 Plank 18 Nails Trial

Figure 55 indicates the 400 Plank 18 Nails is impacted with an approximate load of 108.98 N. The load wave decreases during penetration and the peak of the final wave reaches 100.00 N. The final penetration depth was measured to be 9.48 mm. The total time of penetration was 2.70 ms. Figure 56 shows the total energy reached during the penetration was 0.43 J. This total energy corresponds to a final time of 2.70 ms and a final depth of 9.48 mm. The velocity curve shown in Figure 57 shows the velocity stays reasonably constant around 3.33 m/s.

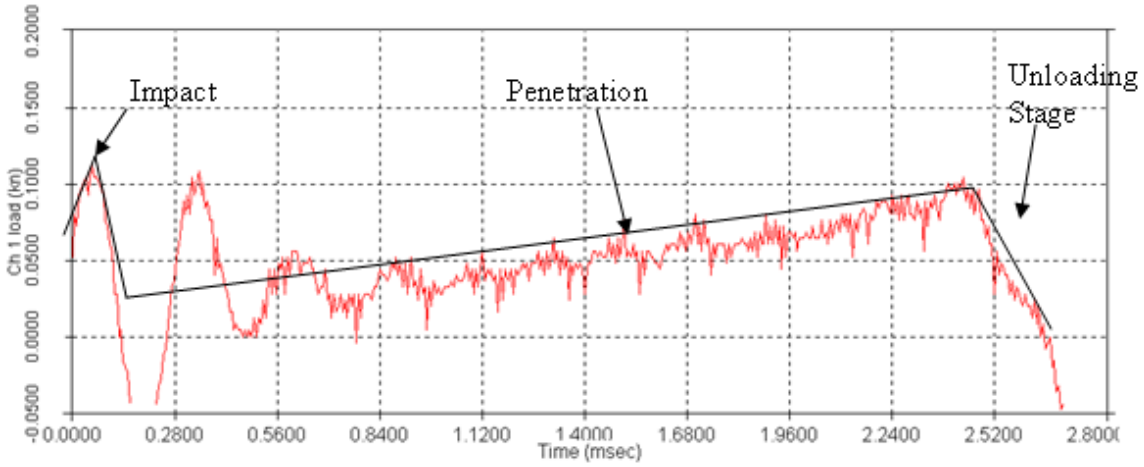

Figure 54: Load-time curve for 400 Plank 18 Nails trial

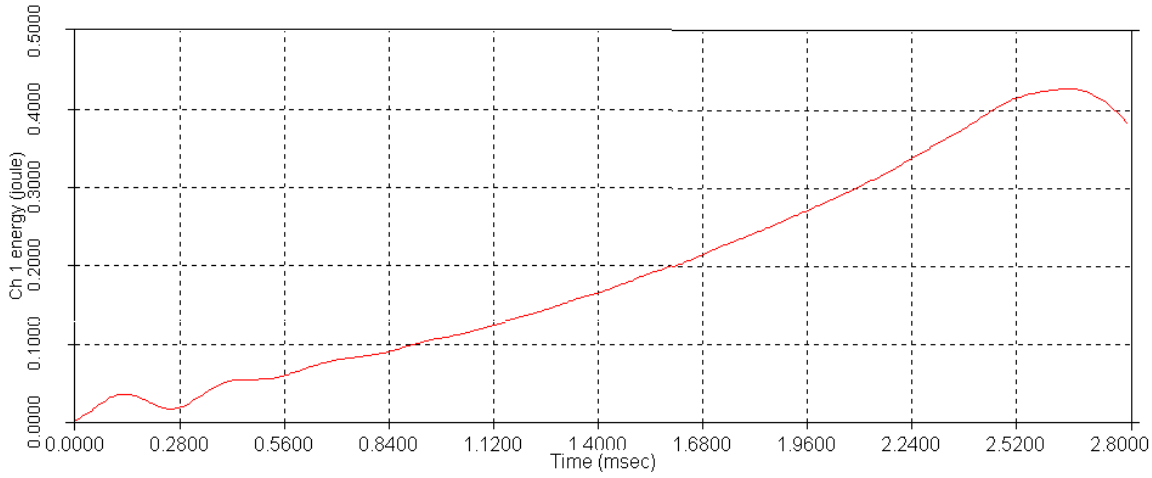

Figure 55: Energy-time curve for 400 Plank 18 nails trial

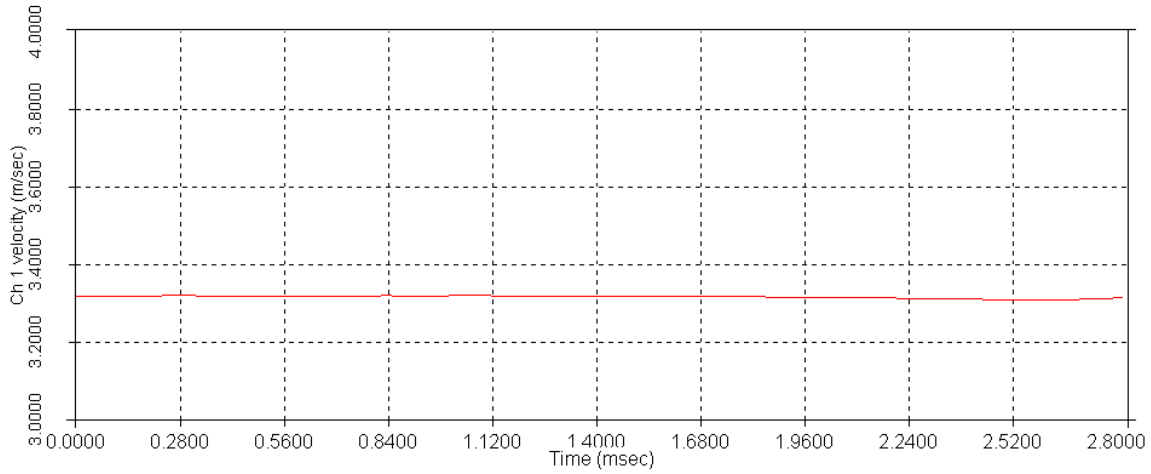

Figure 56: Velocity-time curve for 400 Plank 18 Nails trial

4.4.10 400 Plank 25 Nails Trial

Figure 58 displays an impact force of 146.79 N. The load wave also decreases during penetration until the maximum load of 100.00 N at the final wave before the penetration ends. The total time of penetration was about 2.70 ms. The depth of the nail was recorded after the test to be 9.54 mm. Figure 59 shows the total energy reached during the penetration was 0.54 J. The velocity curve shown in Figure 60 shows the velocity slowly decreases from 3.33 m/s to 3.32 m/s.

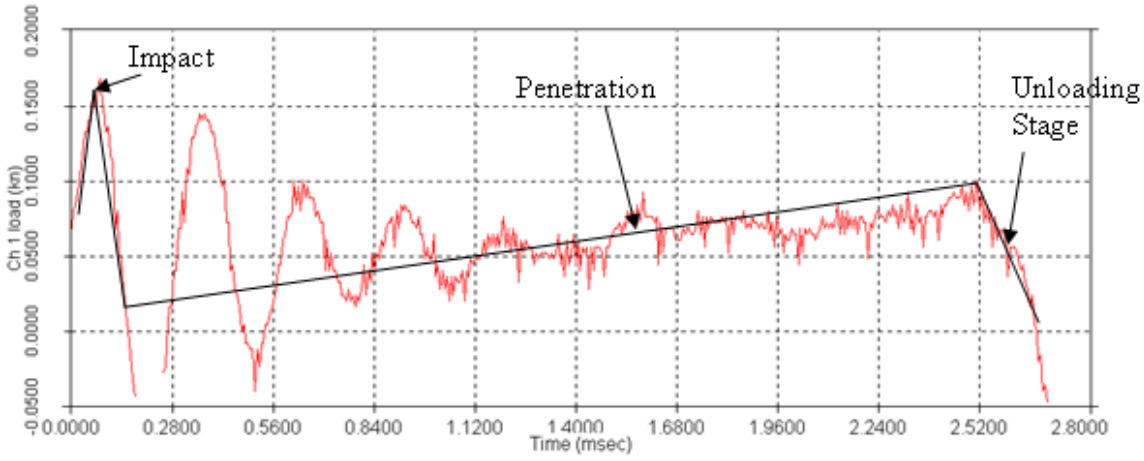

Figure 57: Load-time curve for 400 Plank 25 Nails trial

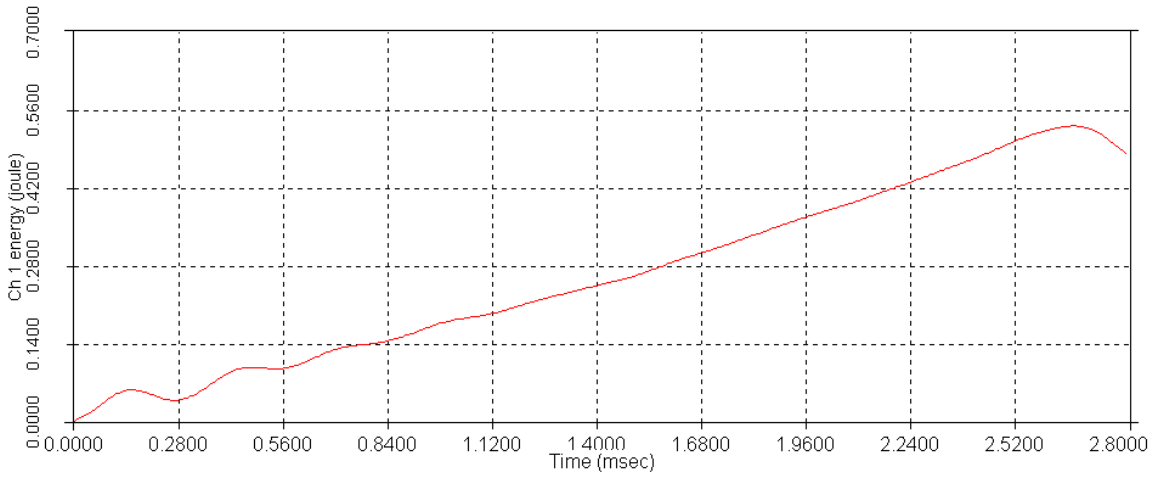

Figure 58: Energy-time curve for 400 Plank 25 Nails trial

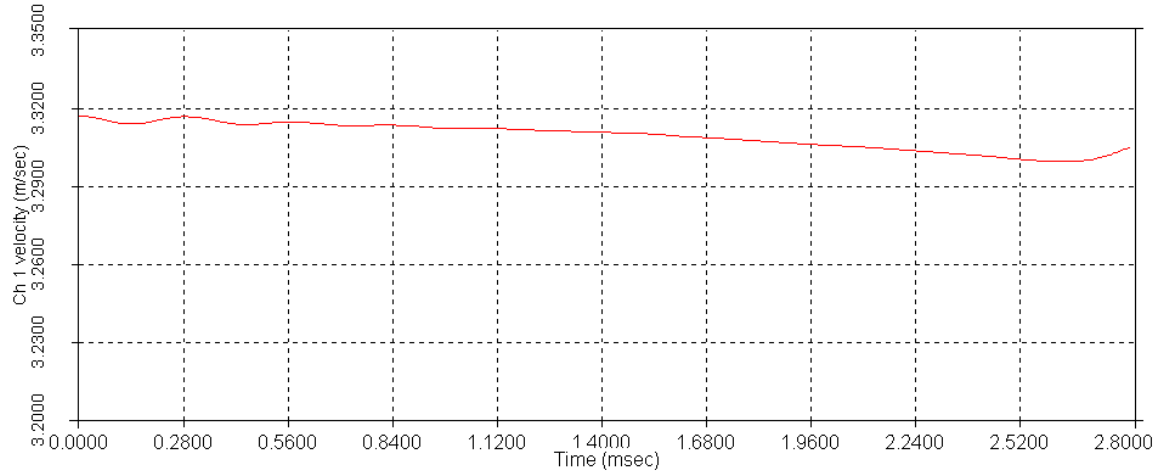

Figure 59: Velocity-time curve for 400 Plank 25 Nails trial

4.4.11 400 Plank 30 Nails Trial

The 400 Plank 30 Nails tests show similar results to the previous 400 Plank Nail trials. The obvious difference in the trials is that a larger load is initiated upon impact of the 30 Nails than the smaller nail quantities. The increase of total energy throughout the experiment is attributed to the larger force. The graphs for the 30 Nails trial can be found in the Appendix.

4.4.12 Polyethylene Results Discussion

The 900 CelluPlank® trials all show profiles similar to the polyurethane tests. The 600 and 400 CelluPlank® trials, however, show a stark contrast in load profiles compared to the 900 CelluPlank®. While the 900 CelluPlank® penetration force rises through penetration, the 400 and 600 penetration loads decrease after impact and only diminutively increase during penetration. An explanation can be given for the drastic change in profiles. The CelluPlank® foams all differ in densities with the 900 having the highest density range and the 400 having the lowest range. An increase in cell size corresponds to the decrease in densities. The nails have a diameter of 0.72 mm. The cell size of the 600 and 400 foam is 0.7 mm and 0.8 mm, respectively. As the cell sizes are either proportional in size or larger than the diameter of the nails, then the penetrating nail is actually encountering more air than foam resistance as compared to the 900 foam (cell size = 0.6 mm). Due to the large cell sizes, the friction forces recorded for the 400 and 600 foams increase less than the 900 foam. Instead, the resistance is an arbitrary combination of friction due to contact at some points along the nail and no contact at other points during penetration. This would explain why a lower force is required to penetrate through the 400 and 600 CelluPlank® foams and why there is a shallow increase in force. Also, the difference between the amplitudes of the 400 foam's impact wave and final wave is greater than that of the 600 foam. The 400 foam should have a larger difference in wave amplitude because the increased cell size provides less contact and corresponds to less damping.

The frequency of the waves present in the penetration load curves is due to the instrumentation and not the materials tested. The frequency of the waves is a result of the natural frequency of the impact tester being indirectly measured. The forces for the

polyethylene foam can be determined by averaging the forces present and dividing by the number of nails. Tables 10, 11, and 12 show the impact results for the polyethylene foam. The increase in penetration forces for the 400 and 600 is less than the increase in force for the 900. The CelluPlank® 900 average penetration force is between 7.38 N and 8.46 N for all trials. The CelluPlank® 600 average force for all trials is between 4.83 N and 5.51 N for a single nail. The CelluPlank® 400 average force for all trials is between 3.64 N and 4.53 N. The force per nail values for each respective CelluPlank® foams are similar, but still vary slightly from each other. Again, this is most likely due to the density and cell size of the foams.

Table 10: PE CelluPlank® 900 impact test data

PE CelluPlank 900 Trials	12 Nails	18 Nails	25 Nails	30 Nails
Quantity of tests	10	10	10	10
Mean Resistive Energy	0.500 J	0.823 J	1.178 J	1.401 J
Resistive Energy Standard Deviation	0.067 J	0.116 J	0.097 J	0.085 J
Resistive Energy Range (95% C.I.)	0.347 J - 0.653 J	0.558 J - 1.087 J	0.957 J - 1.399 J	1.207 J - 1.595 J
Mean Penetration Force/Nail	8.33 N	8.46 N	8.08 N	7.38 N
Penetration Force Standard Deviation	1.24 N	1.07 N	0.56 N	1.79 N
Penetration Force Range (95% C.I.)	5.50 N - 11.16 N	6.02 N - 10.89 N	6.80 N - 9.36 N	3.29 N - 11.46 N
Average Penetration Time	2.62 ms	2.75 ms	2.70 ms	2.4 ms
Average Penetration Depth	9.47 mm	9.47 mm	9.55 mm	9.53 mm

Table 11: PE CelluPlank® 600 impact test data

PE CelluPlank 600 Trials	12 Nails	18 Nails	25 Nails	30 Nails
Quantity of tests	10	10	10	10
Mean Resistive Energy	0.331 J	0.584 J	0.760 J	0.886 J
Resistive Energy Standard Deviation	0.053 J	0.053 J	0.092 J	0.059 J
Resistive Energy Range (95% C.I.)	0.210 J - 0.452 J	0.463 J - 0.705 J	0.550 J - 0.969 J	0.751 J - 1.02 J
Mean Penetration Force/Nail	4.83 N	5.51 N	5.08 N	5.06 N
Penetration Force Standard Deviation	0.95 N	1.09 N	1.07 N	1.38 N
Penetration Force Range (95% C.I.)	2.66 N - 6.99 N	3.02 N - 7.99 N	2.45 N - 7.33 N	1.91 N - 8.21 N
Average Penetration Time	2.77 ms	2.77 ms	2.77 ms	2.77 ms
Average Penetration Depth	9.56 mm	9.55 mm	9.55 mm	9.55 mm

Table 12: PE CelluPlank® 400 impact test data

PE CelluPlank 400 Trials	18 Nails	25 Nails	30 Nails
Quantity of tests	10	10	10
Mean Resistive Energy	0.369 J	0.490 J	0.676 J
Resistive Energy Standard Deviation	0.043 J	0.031 J	0.038 J
Resistive Energy Range (95% C.I.)	0.271 J - 0.467 J	0.419 J - 0.561 J	0.589 J - 0.763 J
Mean Penetration Force/Nail	4.25 N	3.64 N	4.53 N
Penetration Force Standard Deviation	0.76 N	0.35 N	0.28 N
Penetration Force Range (95% C.I.)	2.51 N - 5.99 N	2.84 N - 4.44 N	3.89 N - 5.17 N
Average Penetration Time	2.70 ms	2.70 ms	2.70 ms
Average Penetration Depth	9.52 mm	9.54 mm	9.55 mm

The standard deviation of the penetration energy data increases as the density of the PE foam decreases. Plank 900 shows a small standard deviation 0.067 J, 0.116 J, 0.097 J, and 0.038 J for all trials. Plank 600 show standard deviations of 0.053 J, 0.092 J, and 0.059 J for all trials. Plank 400 show standard deviations of 0.043 J, 0.031 J, and 0.038 J for all trials. The Plank 600 and 400 standard deviations seem as low as the Plank 900, but when compared to their respective sample means their standard deviations are actually higher than the Plank 900. It is expected that Plank 600 and 400 would have higher standard deviations than the 900 Plank. This is once again due to the contact interaction during penetration of these foams. It is obvious from these standard deviations that the cell diameters play an important role in penetration. As a result of the large diameter cells present in the low density PE foam, the nail is not always in complete contact with the foam. At arbitrary points during penetration the nail penetrates the foam's cells and establishes contact with both cell walls and air. The high standard deviations shown in Tables 10, 11, and 12 are a direct result of the contact not only being made between the nail and cell walls, but also between the nail and air. The CelluPlank® 900, on the other hand, consists of cells with diameters smaller than the nail diameter, so the nail is always in contact with more cell walls and the energies stay fairly consistent.

4.5 Polyurethane-Polyethylene Impact Analysis

The polyurethane tests are all represented by a similar load profile. The load profile can be divided into three stages of penetration. The first stage is impact and is shown as an increasing slope from the initial time, 0.00 ms, to a maximum point located on the first wave. The second stage is the penetration phase. The first discernable wave decreases to a point where the second stage begins. The second stage is an increasing slope and ends at the maximum point of the final wave. The second stage is distinguished by several peaks and valleys. These waves are present due to the contact and loss of contact between the nail and impact striker. The waves are also affected by the occurrence of foam densification as a result of the foam crushing. The third stage is a decreasing slope at the end of stage two and signals the end of contact between the striker and nail. The nail will continue to penetrate until contact is fully lost.

The polyethylene tests do not differ greatly from the polyurethane tests. The load profiles are almost identical, with a few exceptions, however. The second stage found for the polyethylene tests has higher wave amplitudes than the polyurethane tests, indicating less resistance by the polyethylene foam. The foam is so easily crushed because of its low density that densification is less prevalent than in the polyurethane foam. For the 400 and 600 CelluPlank® foam the second stage actually increases a very low amount. This is due to the small amount of friction force made between the nail and foam. The 400 and 600 CelluPlank® foams consist of cells with diameters equal to or larger than the 21 gauge nails. The large cell size means a large volume of air is penetrated by the nails, not only foam. As such, the air retards the expected increase of contact area between the foam and nail during penetration. As friction force depends upon contact area, and the contact only slightly increases, then the friction force produced in the 400

and 600 CelluPlank® foam can only increase a modest amount. The other difference between the foams is the force required to penetrate. The nail meets a greater resistance in the polyurethane foam than the polyethylene foam. This is evident in the polyurethane tests where the load and energy values are higher than in the polyethylene tests.

With respect to the polyurethane and the Plank 900 nail trials, their average penetration forces per nail show low standard deviations. The Plank 600 and Plank 400 average penetration force for each trial, though close, show higher standard deviations. This is most likely a result of the ratio of cell size to nail diameter.

After comparison of the polyurethane and polyethylene it can be concluded the foams behave similarly under impact and penetration. The only significant difference in the results between the two foams is due to their density and cell size. That is why the forces for the less dense PE foams (CelluPlank® 600 and 400) increase less than the higher density PE (CelluPlank® 900) and PU foams. The penetration forces acting on foam are caused by constant forces (crushing and shearing) and a variable force (friction). A discussion of the theoretical equations and impact tests can be found next, in Chapter 5.

5. DISCUSSION AND ANALYSIS

This chapter provides a detailed discussion and analysis of the theoretical equations and the impact tests. The results of each analysis are assessed, and an interpretation of the data is provided. A comparison of the results from each of the analyses is completed, and an explanation of this data is given.

The theoretical equations were used to solve the force necessary for a nail to penetrate polyurethane to a depth of 9.55 mm. 9.55 mm was chosen because this depth falls within the range of depths recorded from the impact tests. The impact tests impacted the nails with an initial energy (20 J) much greater than the energy absorbed by the foam. Because of the large impact energy, the velocity of the nails should remain constant, and not experience more than a 10%-20% deceleration [8].

5.1 Polyurethane Results Analysis

Tables 13 and 14 below compare the values derived from the theoretical equations and the data recorded from the impact tests for the polyurethane.

Table 13: Forces and energies for polyurethane

	Fcrush	Fshear	Ffriction	Ftotal	Etotal
Equations	6.68 N	3.80 N	31.4 N	41.88 N	0.25 J
% Total Force	15.95%	9.07%	74.98%	100.00%	
Experiments	9.32 N		22.5 N	31.82 N	0.189 J
% Total Force	29.29%		70.71%	100.00%	

Table 14: Difference ratios between force and energy calculations for polyurethane

	Force Ratio	Energy Ratio
Eqns vs. Experiments	1.32	1.32

The force calculated from the theoretical equations was 41.88 N per nail. The calculations correspond to a depth of 9.55 mm, which was approximately the average

depth of the impact tests. These forces are higher than the range of penetration forces recorded during the impact tests for the polyurethane (Table 9) by a factor of 1.32. The mean force for the PU foam trials was 31.82 N. The friction force for both the equations and experiments account for 75% and 70% of the penetration force, respectively. The crushing and shearing force for the equations equals 10.48 N and accounts for 25% of the total force. The crushing and shearing force for the experiments equals 9.32 N and accounts for 30% of the total force. The percentages of total force for the calculated forces yield values comparable to the percentages given by experiment results. Therefore, the percent force distribution shows the equations are capable of predicting the influence each force has on penetration. The calculated friction differs from the experimental friction force by 10 N, which is equivalent to a 30% error. This shows the penetration equation is less capable of calculating the friction force than the crushing and shearing. Friction is affected by the foam's porosity and is neglected in the equations.

The total penetration energy calculated from the theoretical equations was 0.25 J. The mean energy obtained from impact tests for a single nail to penetrate PU was 0.189 J. The calculated energy falls near the range of energies produced by the impact tests. The difference between the theoretical equation's calculated energy, and the impact experiments' energy, is a factor of 1.32.

5.2 Polyethylene Results Analysis

5.2.1 Plank 900 Results Analysis

Tables 15 and 16 present the results for the Plank 900 polyethylene foam for the analytic equations and impact experiments.

Table 15: Forces and energies for Plank 900

	Fcrush	Fshear	Ffriction	Ftotal	Etotal
Equations	0.54 N	0.63 N	2.5 N	3.67 N	0.023 J
% Total Force	14.71%	17.17%	68.12%	100.00%	
Experiments	2.41 N		5.71 N	8.12 N	0.045 J
% Total Force	29.68%		70.32%	100.00%	

Table 16: Difference ratios between force and energy calculations for Plank 900

	Force Ratio	Energy Ratio
Eqns vs. Experiments	2.21	1.96

The force calculated from the theoretical equations was 3.67 N per nail for a depth of 9.55 mm. The mean force for the Plank 900 foam trials was 8.12 N. The analytic forces are lower than the mean penetration force recorded during the impact tests for the polyethylene (Table 10) by a factor of 2.21. The calculated friction force and the experiments' friction force account for 68% and 70% of the total force, respectively. The calculated friction is 2.3 times less than the experiments' friction force. The calculated crushing and shearing forces equal 1.17 N and account for 32% of the total force. The experiments yielded a combined crushing and shearing force of 2.41 N, around 30% of the total force. The close percentages between the equations and experiments show the equations can predict the contribution of each force component during penetration. The percentages are close, but the forces still slightly differ. The equations neglect the porosity of the foam which explains why the forces between the equations and experiments differ. Friction depends on the area in contact, and the porosity limits the amount of foam the nail contacts during penetration.

The energy calculated from the theoretical equations was 0.023 J. The mean energy obtained from impact tests for the Plank 900 was 0.045 J. The calculated energy

is near the range of energies produced by the impact tests. The difference between the theoretical equation's calculated energy, and the impact experiments' energy, is a factor of 1.96.

5.2.2 Plank 600 Results Analysis

Tables 17 and 18 present the Plank 600 polyethylene foam's results for the analytic equations and impact experiments.

Table 17: Forces and energies for Plank 600

	Fcrush	Fshear	Ffriction	Ftotal	Etotal
Equations	0.24 N	0.41 N	1.20 N	1.85 N	0.012 J
% Total Force	12.97%	22.16%	64.86%	100.00%	
Experiments	2.63 N		2.5 N	5.13 N	0.030 J
% Total Force	51.27%		48.73%	100.00%	

Table 18: Difference ratios between force and energy calculations for Plank 600

	Force Ratio	Energy Ratio
Eqns vs. Experiments	2.79	2.5

The force calculated from the theoretical equations was 1.84 N per nail for a depth of 9.55 mm. The mean force for the Plank 600 foam trials was 5.13 N. The analytic forces are lower than the mean penetration force recorded during the impact tests for the polyethylene (Table 11) by a factor of 2.79. The combined crushing and shearing force is 0.65 N and is 35% of the total force calculated from the equations. The experiments yielded a combined force of 2.63 N, a total of 51% of the recorded force. The calculated friction force is 1.20 N and is less than the experiments' friction force of 2.5 N. The calculated friction accounts for 65% of the total force, while the experiments' recorded friction accounts for 49% of the penetration. The percentages given by the equations vary more from the experiments than the higher density foams. The friction contribution is less for than the Plank 600 than the higher density foams. Again, the

porosity affects the calculated forces because the equations assume a solid continuum. The experiments' friction force accounts for only half of the total force, whereas the friction force for the higher density foams accounts for the majority of the total force. The shows the porosity of the foam affects the friction force. The 600 Plank has a greater porosity and larger cells than the higher density foams. The combined effects of porosity and cell sizes lessen the amount of friction. The crushing and shearing forces are affected by the geometry of the nail's tip. This is further discussed in the discussion section of this chapter.

The energy calculated from the theoretical equations was 0.012 J. The mean energy obtained from impact tests for the Plank 600 was 0.030 J. The calculated energy falls around the range of energies produced by the impact tests. The difference between the theoretical equation's calculated energy, and the impact experiments' energy, is a factor of 2.50.

5.2.3 Plank 400 Results Analysis

Tables 19 and 20 present the Plank 400 polyethylene foam's results for the analytic equations and impact experiments.

Table 19: Forces and energies for Plank 400

	Fcrush	Fshear	Ffriction	Ftotal	Etotal
Equations	0.17 N	0.30 N	0.90 N	1.37 N	0.009 J
% Total Force	12.41%	21.90%	65.59%	100.00%	
Experiments	3.26 N		0.88 N	4.14 N	0.021 J
% Total Force	78.74%		21.26%	100.00%	

Table 20: Difference ratios between force and energy calculations for Plank 400

	Force Ratio	Energy Ratio
Eqns vs. Experiments	3.02	2.33

The force calculated from the theoretical equations was 1.37 N per nail for a depth of 9.55 mm and 4.14 N for the Plank 400 impact tests' mean force. The values differ by a factor of 3.02. The calculated crushing force and shearing force is 0.17 N and 0.30 N, respectively and are 34% of the calculated penetration force. The combined crushing and shearing forces determined through the experiments is 3.26 N, and is 79% of the total force. The equations yielded a friction force of 0.90 N, which equals 66% of the total force. As expected, the friction force accounts for a small percentage, 21%, of the total force given by the experiments. The foam's cells' sizes are larger than the nail diameter by 1 mm. This size difference reduces the amount of foam the nail contacts during penetration and increases the amount of air the nail penetrates. The impact figures for the Plank 400 foam show a shallow load curve which indicates the reduction of friction during penetration.

The energy calculated from the theoretical equations was 0.009 J and 0.021 J for the impact tests. The calculated energy falls around the range of energies produced by the impact tests. The values of each differ by a factor of 2.33.

5.3 Chapter Discussion

The analytic equations yielded results that fell within an order of magnitude of the mean penetration forces recorded by the impact tests. The equations can be considered acceptable after a few justifications are made. First, the equations were developed under the assumption that the foams are homogeneous. However, the foams are not homogeneous and the distribution of cells inside the foams is arbitrary. The equations use material properties provided by the foams' manufacturers. The values given by the manufacturers are nominal values. Also, the equations do not account for the size of the

cells, which has already been determined to affect the penetration forces. To increase the accuracy of the equations, factors need to be introduced that account for the heterogeneity of the foam. These factors need to account for the cell sizes and the porosity distribution of the foams into the penetration equations. The equations account for the area in contact, but do not account for the sharpness of the nail's tip. This would affect the overall forces as well.

Tables 21 and 22 present results that show how density and foam porosity affect the penetration forces. Table 21 shows the calculated forces using the analytic equations and their respective contribution as a percentage of the total force. Table 22 shows the actual friction force and its overall contribution to the total penetration (%). As expected, the calculated friction force decreases as the density decreases, but its contribution to the total force remains around 65%-75%. This is because the analytic equations assume the foam to be a homogenous continuum, so 100% contact always exists between the nail and the foam. Table 22 shows the friction force does decrease with density, but so does its percent contribution to the total force. This is due to the increase in porosity as the density decreases. The nail is not in complete contact with the foam during penetration due to the increased porosity. The equations assume there is always contact between the entire surface of the nail and the foam, though. Figure 60 shows the penetration forces increase with the density of the foam. The calculated total force increases from 1.37 N (Plank 400) to 41.88 (PU). The crushing and shearing forces increase from 0.47 N (Plank 400) to 10 N (PU). The calculated friction force increases from 0.90 N (Plank 400) to 31.4 N (PU). The figure also compares the calculated forces to the experiment forces. According to the graph the equations are able to predict if the forces will increases or

decreases with density. This is shown by the closeness of the curves between the equations and experiments. Figure 61 shows the penetration forces decrease as the porosity increases. The curves between the equations and experiments in Figure 61 show the equations are able to predict if the penetration forces increase or decrease with the porosity of the foam.

Table 21: Analytic equations results

	Analytic Equations			
	PU	Plank 900	Plank 600	Plank 400
Density (kg/m^3)	288.00	150.60	97.70	65.70
Closed Cell Content (%)	97.40	15.06	9.77	6.57
Fcrush (N)	6.68	0.54	0.24	0.17
Fshear (N)	3.80	0.63	0.41	0.30
Ffriction (N)	31.40	2.50	1.20	0.90
Fcrush/Ftotal (%)	15.95	14.71	12.97	12.41
Fshear/Ftotal (%)	9.07	17.17	22.16	21.90
Ffriction/Ftotal (%)	74.98	68.12	64.86	65.69
Ftotal (N)	41.88	3.67	1.85	1.37
Etotal (J)	0.250	0.023	0.012	0.009

Table 22: Impact experiment results

	Experiments			
	PU	Plank 900	Plank 600	Plank 400
Density (kg/m^3)	288.00	150.60	97.70	65.70
Closed Cell Content (%)	97.40	15.06	9.77	6.57
Fcrush + F shear (N)	9.32	2.41	2.63	3.26
Ffriction (N)	22.50	5.71	2.50	0.88
Fcrush + Fshear/Ftotal (%)	29.29	29.68	51.27	78.74
Ffriction/Ftotal (%)	70.71	70.32	48.73	21.26
Ftotal (N)	31.82	8.12	5.13	4.14
Etotal (J)	0.189	0.045	0.030	0.021

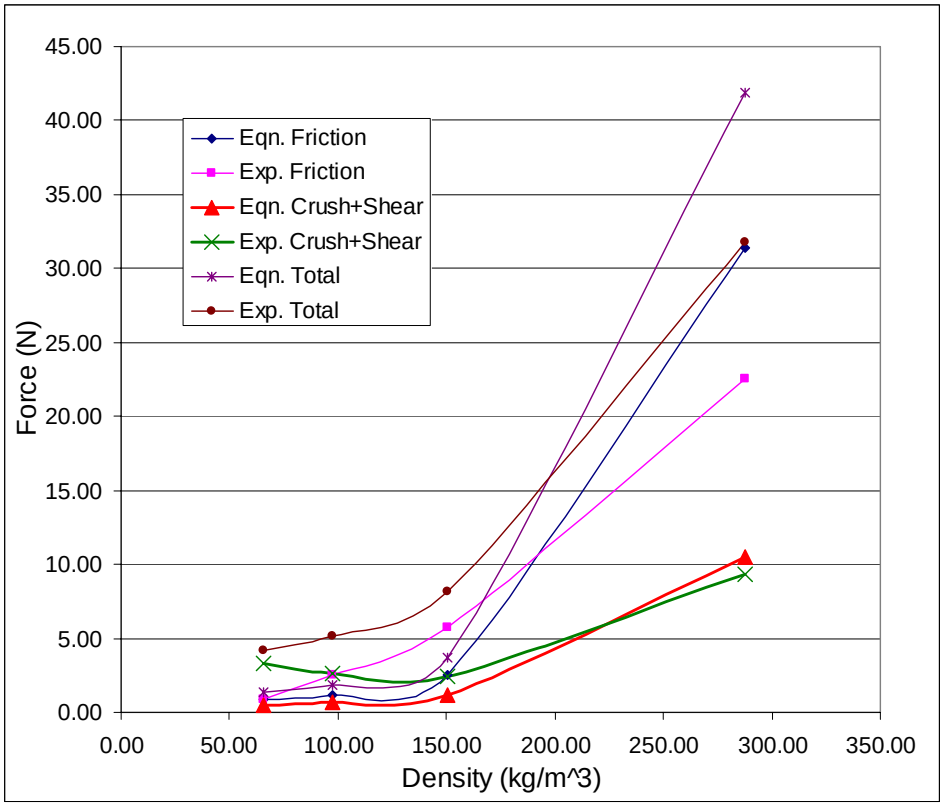

Figure 60: Equations vs. experiments: force results

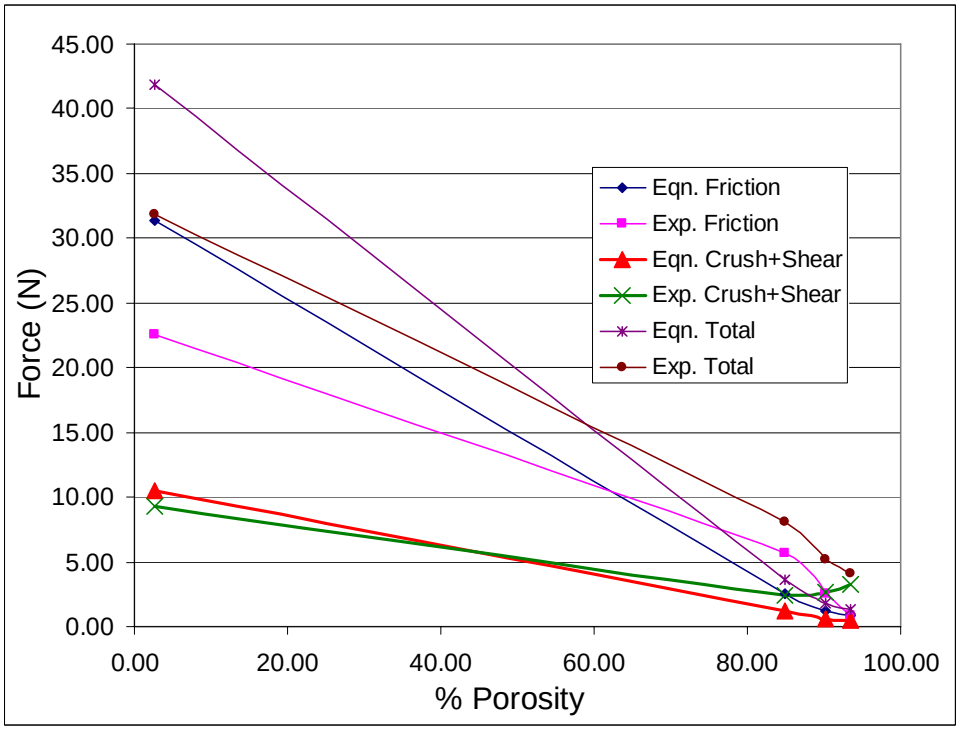

Figure 61: Equations vs. experiments: force % contribution

Figure 62 shows the accuracy of the equations as a function of density. The graph plots the ratio of forces for the equations versus experiments (dependent variable) against the density of the foams (independent variable). According to Figure 62, the force ratios from the Plank 400 (least density) to the polyurethane (greatest density) decrease from 3.02 to 1.32 for the total force. The constant force is the combined crushing and shearing forces for both the equations and experiments. The ratio of the equations to experiments for the constant forces decreases as the density increases from 7.0 to 1.3.

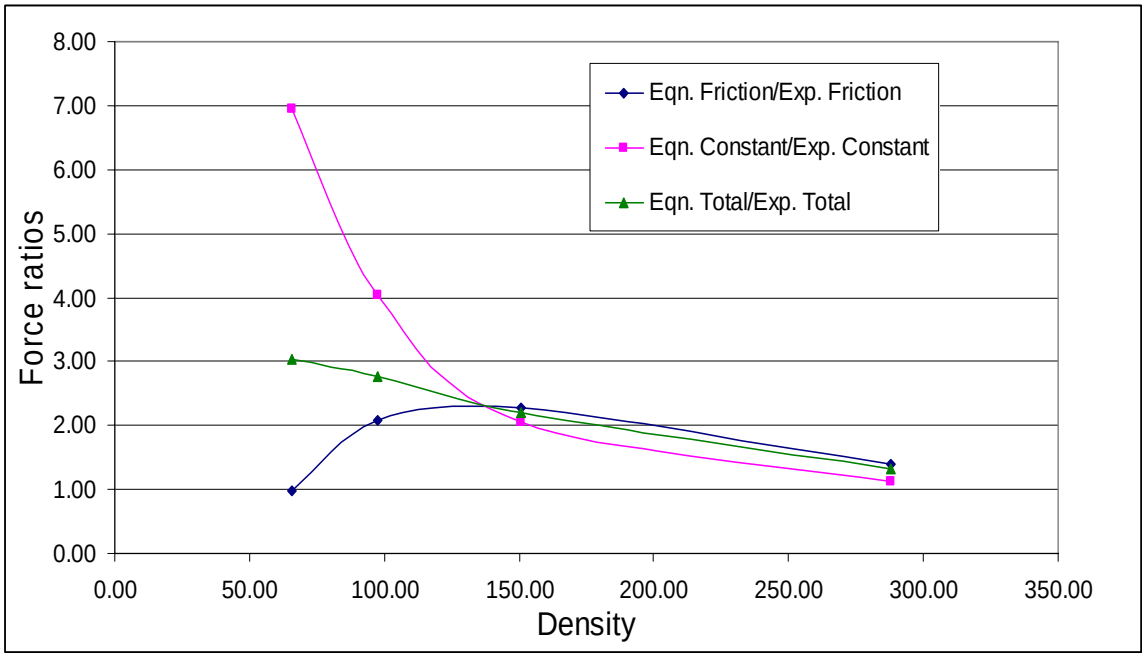

Figure 62: Component force ratios vs. density

Figure 62 shows the equations are more accurate as the density of the foam increases. This is due to the increases in porosity and cell sizes associated with the decreasing density of the foam. As the density of the foam decreases, the penetration through the cells (air voids) increases. The location of these cells is random, so the number of cells penetrated also is random. The cell sizes increase from 0.6 mm for the

dense foam to 0.8 mm for the least dense foam. The nail diameter is 0.7214 mm, so the ratio of the nail diameter to the cell size will decrease with density. Therefore, the values predicted in the equations will be less accurate for the lesser dense foams because they do not account for the random cell distribution and cell sizes. This also is evident in the breakdown of the penetration forces for all foams (Tables 13 through 20) which show the capability of the equations to predict the penetration forces lessens as the density decreases. Several parameters were developed to increase the accuracy of the equations. These parameters included the porosity distribution (A), the density ratio (B), and the ratio of the nail diameter to the foam's cell size (C). The density ratio was calculated as the density of the foam divided by the density of the actual material (i.e., polyurethane and polyethylene). Parameter 'C' calculates the nail diameter over the cell size of the foam. The diameter of the nail is 0.7214 mm while the size of the cells increased from 0.6mm to 0.8mm as the density decreased. This gives smaller ratios for the less dense foams, showing that the nail penetrates through voids larger than its diameter. A table of the different parameter combinations can be seen in Table 23.

Table 23: Parameter combinations

Porosity = A	Density ratio = B	Diameter/cell size = C
Parameter Combinations		
A	B	C
1/A	1/B	1/C
1-A	1-B	1-C
1/(1-A)	1/(1-B)	1/(1-C)
1-(1/A)	1-(1/B)	1-(1/C)
1-(1/(1-A))	1-(1/(1-B))	1-(1/(1-C))

These combinations were multiplied by the equations to determine the affect of each parameter combination on the accuracy of the results. After analyzing the results of each combination, it was concluded the original analytic equations provided more accurate results than the parameterized equations. Tables of the calculated forces can be seen in the Appendix along with graphs of the parameterized results versus the experimental results.

Chapter 5 presented the penetration results for all foams from both the analytic equations and the experiments. These results were compared and analyzed to determine the accuracy of the equations. The equations proved capable of yielding more accurate values for high density foams than low density foams. The equations do not explicitly account for foam porosity or cell size, and these effects were determined to influence the penetration forces. Therefore, it was concluded parameters need to be included in the equations that account for porosity and cell size. Several parameters were developed and tested, but the original equations yielded the most accurate results. The following chapter, Chapter 6, details the experimental setup and operation of the automatic nail gun.

6. AUTOMATIC NAIL GUN: PROOF OF CONCEPT

A pneumatic firing nail gun was designed to insert metal wires into foam for the purpose of manufacturing dielectric antenna spacers. The nail gun is to be mounted to a fixed position in the center of a standard CNC mill. The foam is to be placed beneath the nail gun on the CNC mill. The mill is used to translate the foam in both the x-direction and the y-direction. The mill has a tolerance of 0.001 mm. The desired nailing pattern is designed in a CAD program and is loaded into the mill's hard drive. A controller box is used to detect when the foam is in the correct firing position and to control the firing of the nail gun. Figure 63 is a schematic of the operational setup for the production of antenna spacers.

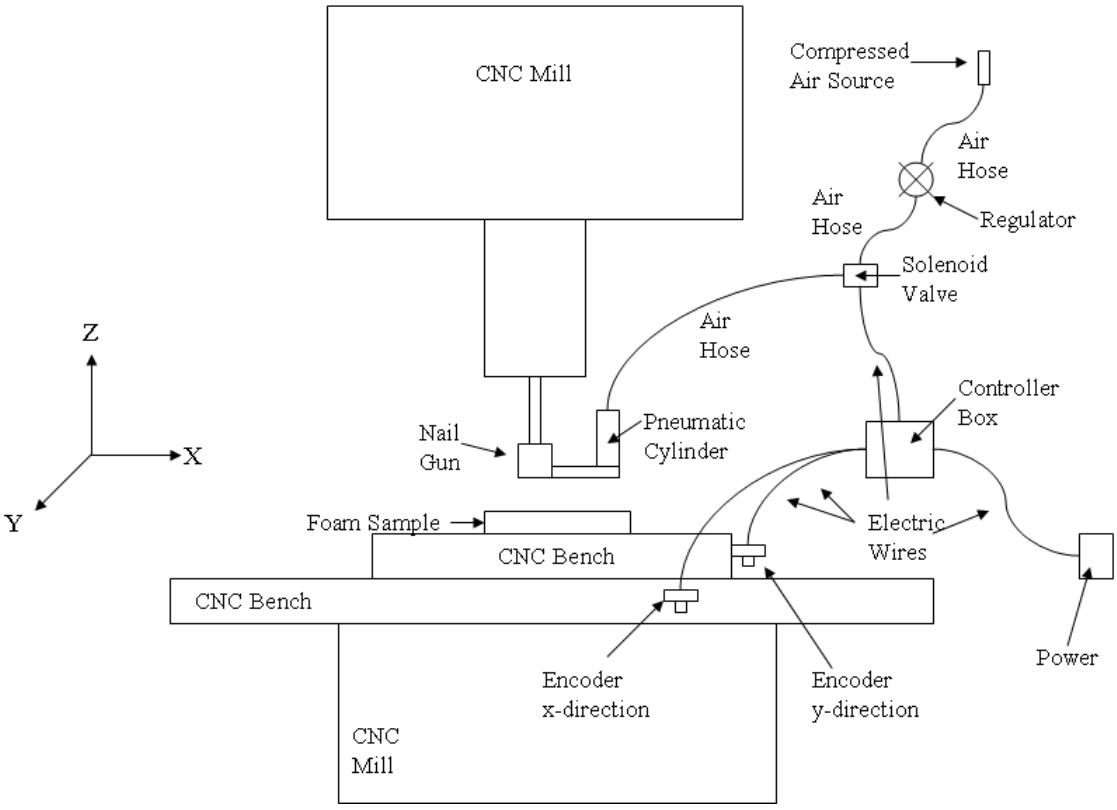

Figure 63: Schematic of complete machine setup

The operational nail gun is composed of both mechanical and electrical components. The section below describes the different parts of the nail gun: the firing mechanism, the frame and material selection, and the nail carriage. It also details how the nail gun receives its firing signal and how the firing mechanism is controlled.

6.1 Components of Nail Gun

The nails are fired using a steel pneumatic cylinder that hammers the nails into the foam. The pneumatic cylinder operates by utilizing compressed air. The compressed air is controlled by a solenoid valve and an air regulator. The solenoid valve manages when the air is released for firing by opening and closing its gate. This is accomplished by applying a voltage to the valve. The valve gates are closed when no electrical power is applied and opened when a voltage of 12 V is introduced. The air regulator is controlled manually by the operator. It allows for the amount of air pressure required by the nail gun for firing to be controlled by manually opening and closing its valve.

The frame of the nail gun was fabricated using common grade structural steel. The purpose of the frame was to encase the firing mechanism and attach the nail gun to any standard machining mill. According to Newton's law the pneumatic should produce a recoil equal in magnitude but opposite in direction to its firing solution (nail ejection). This was one reason steel was chosen as the frame material for the nail gun. Steel increases the weight of the gun, but it was desired to have a device that could resist the recoil effect. The rubbing between the pneumatic and frame as a result of the recoil could cause wear, so introducing steel as the frame also limits any wear effect.

The nail carriage was taken from an existing Arrow ET200™ electric brad nail gun (Arrow Fastener Company, Inc., Saddle Brook, NJ). The carriage allowed for 100

brad wires of lengths of 32 mm, 25 mm, 20 mm, or 15 mm to be loaded within the gun [16]. The nails are spring loaded in the carriage. When one nail is fired into the foam, the remaining nails are pushed forward through the carriage by the spring. Figures 64 and 65 show the assembled nail gun modeled in SolidWorks. Figure 66 shows the actual fabricated nail gun attached to a CNC mill.

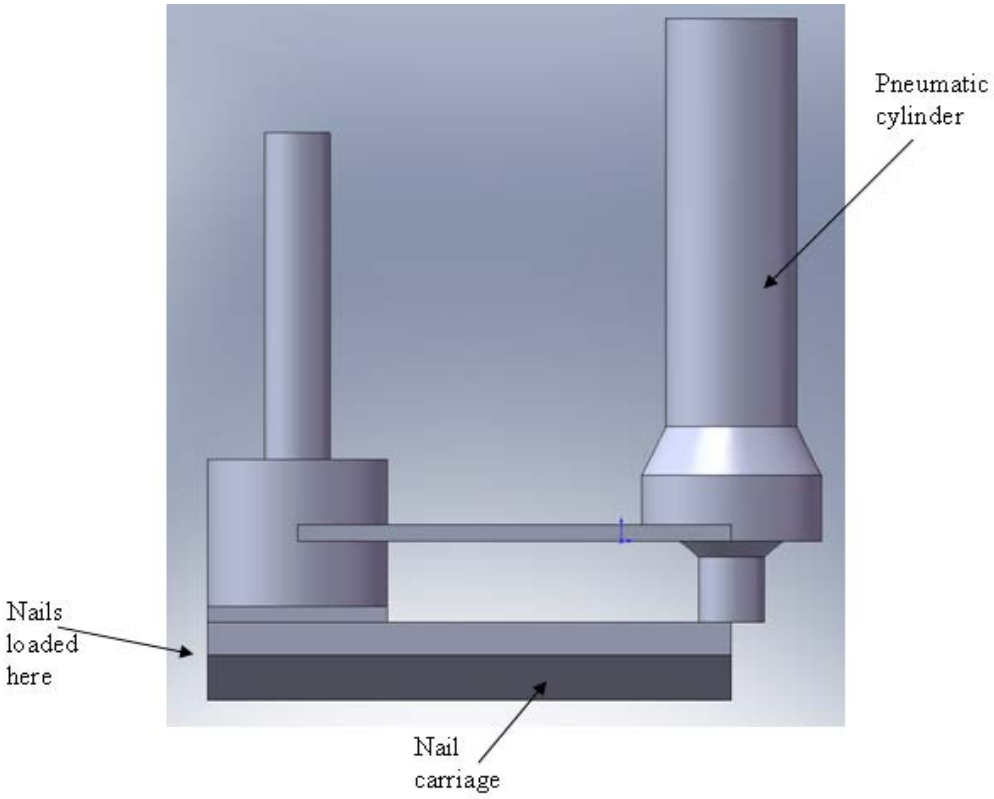

Figure 64: Side profile of computer modeled nail gun

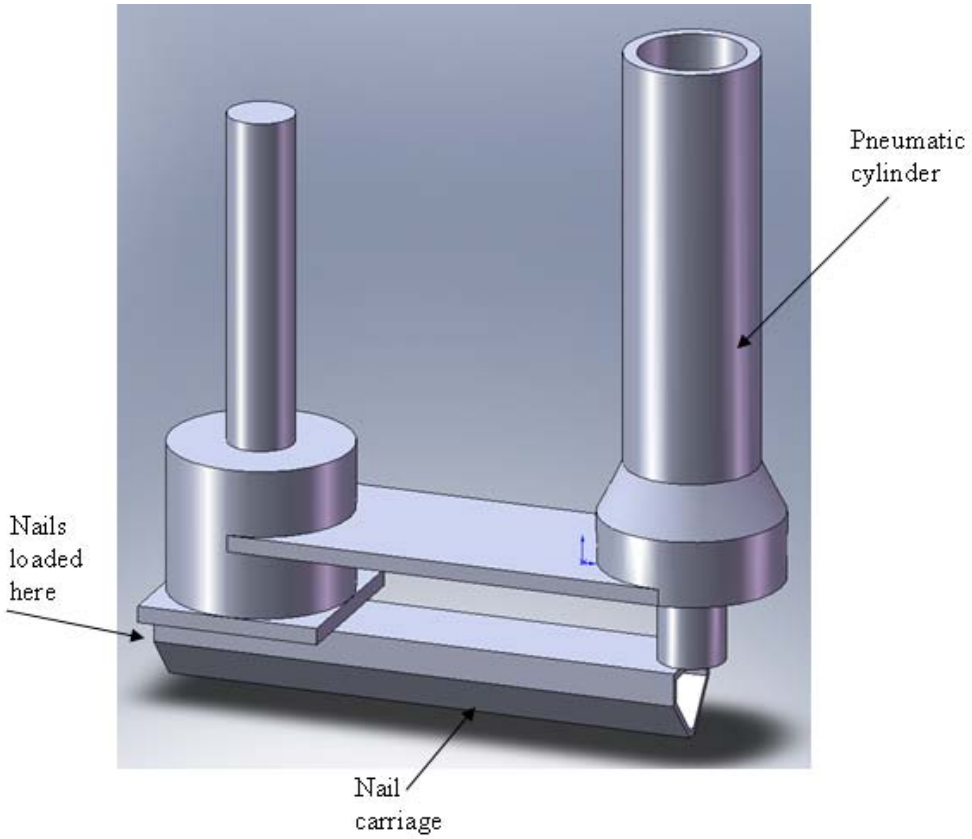

Figure 65: Isometric view of computer modeled nail gun

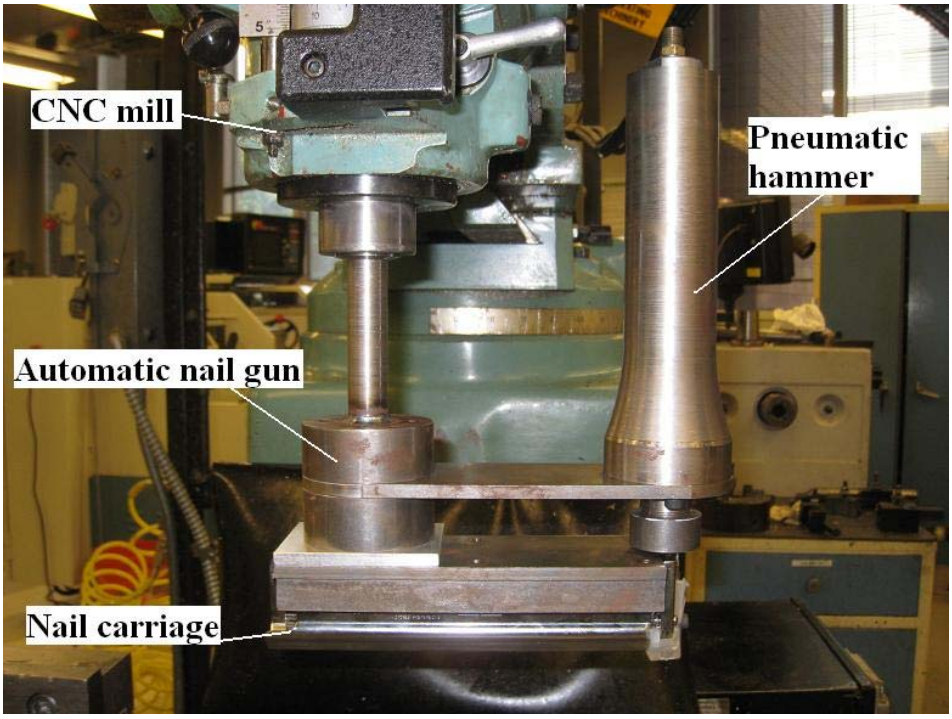

Figure 66: Automatic nail gun fixed to CNC mill

The nail gun code is programmed to detect whether the foam is in motion or is stationary, and when to fire. This is performed through the use of its electrical components. The electrical components consist of a controller box and two rotary encoders.

Two Clarostat optical rotary encoders 600EN-128-CBL with a 128 pulses/revolution resolution are implemented to detect the x and y translation of the foam [17]. The encoders are attached to the mill: one for movement in the x-direction and one for movement in the y-direction. As the mill translates the foam the encoders rotate, sending a signal to the control box that the foam is in motion. When the foam is completely stationary, the encoders remain motionless and no signal is sent. An image of one of the encoders is shown in Figure 67.

Figure 67: Clarostat optical rotary encoder

The controller box is a 76.2 mm x 127 mm aluminum box that houses the circuitry and the code used for firing the nail gun. It is powered through a standard 12 volt A/C wall adapter. The control box is programmed to recognize whether or not at least one of the encoders is rotating. As long as a single encoder rotates, the controller box will read the foam as moving. When the foam is stationary, neither encoder will rotate, and the controller box will assume the foam is in the correct firing position. At this time the controller box sends a voltage output to the valve to open the gate and release the air. After a set time the controller box terminates the voltage output. The controller box is programmed to constantly check for signals from the encoders. A schematic of the wiring diagram can be seen in Figure 68.

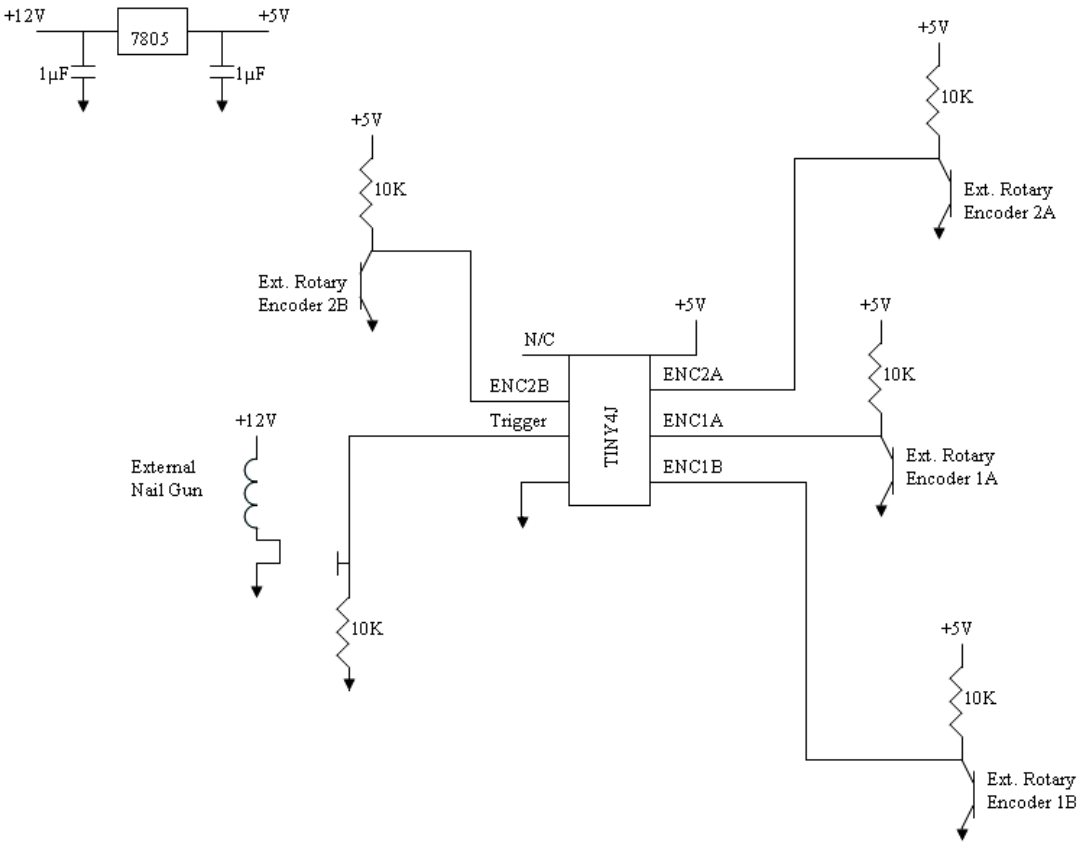

Figure 68: Electric circuit diagram

6.2 Process of Operation

Figure 69 shows the process flow for the production of the antenna spacers.

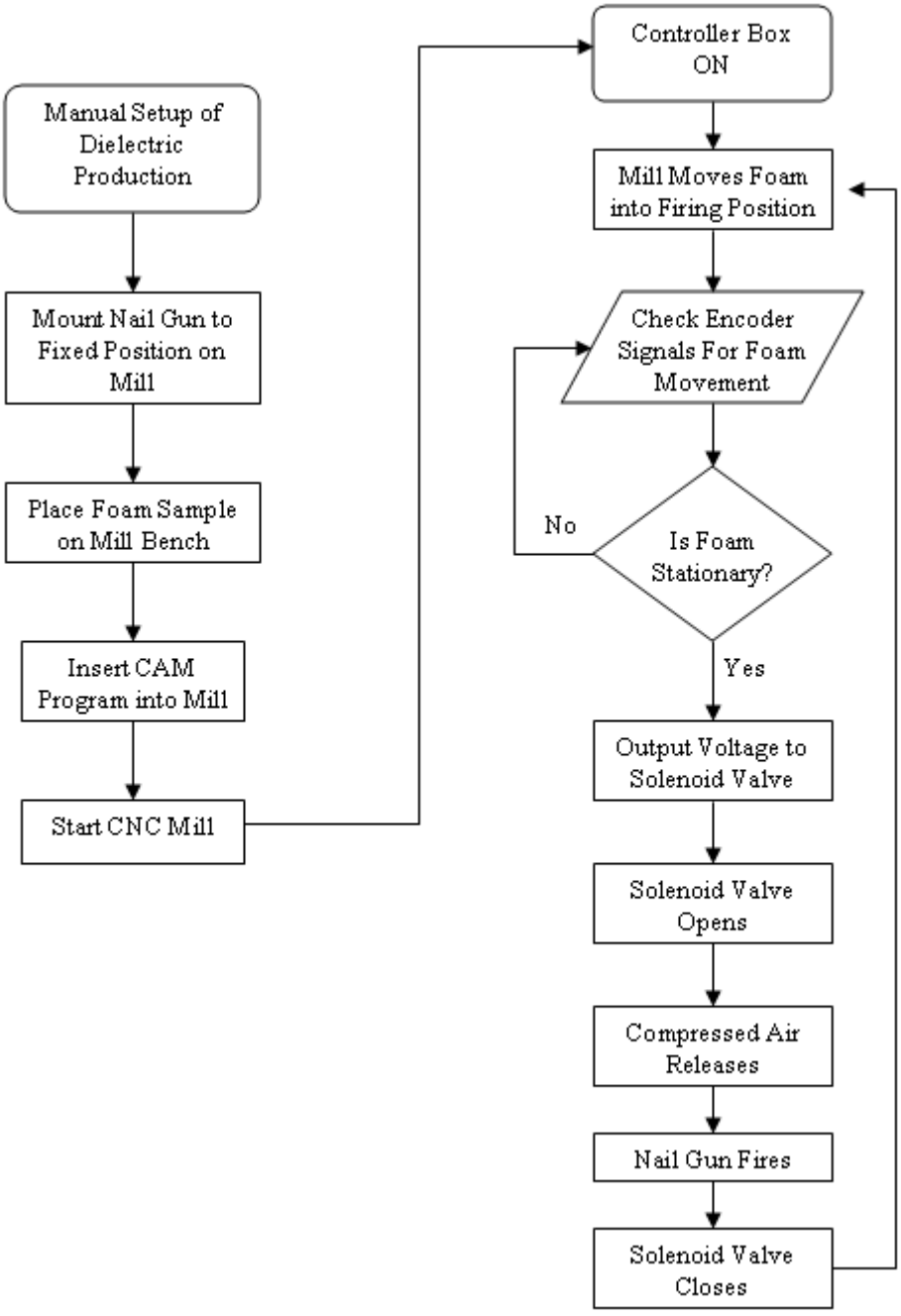

Figure 69: Operational flow chart

Initially, the operator must attach the nail gun to the CNC mill, and secure the foam on the mill bench. The nail pattern is programmed into the mill, and the controller box is powered on before starting the CNC. The mill bench translates the foam in the x- and y- directions to each firing position (based on the nail pattern loaded in the mill). As the foam is translated, the encoders rotate and transmit a signal to the controller box. One encoder detects translation in the x-direction and one encoder detects translation in the y-direction. The controller box continuously checks for signals sent by the encoders to determine whether they are rotating or stationary. When no signal is received, the controller box assumes the foam is stationary (in the correct position) and outputs a voltage to the solenoid valve. The valve receives the voltage and opens its gate. The compressed air flows through the regulator at a set pressure, and is released through the valve. The air enters the pneumatic cylinder, and the nail gun fires the nails into the foam sample. After a short delay the valve closes, and the mill translates the foam to the next position. The process is repeated until the sample is complete and the program is stopped.

6.3 Proof of Concept

Current tests show the analytic equations provide accurate force values for the nail penetration into foam. The nail gun's program code proved to be successful as well. The controller box successfully detected the foam's movement and correctly fired when the foam was stationary. Table 24 gives the parameters and results from the first test run of the automatic nail gun. Eight nails were fired using a pressure of 517 kPa. This pressure corresponds to a force of 36.83 N over a circular area (hammer's head) of diameter 8.89 mm. The final depth for each trial was a consistent 11 mm.

Table 24: Proof of concept trials for automatic nail gun

Number of Trials	Pressure	Force	Diamater of Hammer	Penetration Depth	Force/depth
8	517106.8 Pa	36.83 N	8.89 mm	11 mm	3.35 N/mm

6.4 Chapter Discussion

Overall, the nail gun was fabricated and the electronics were programmed successfully. The proof of concept tests show a force of 36.83 N can penetrate a nail into polyurethane a depth of 11 mm. This force is similar to the average force recorded from the impact tests to drive a nail 9.55 mm. This depth is the average depth of penetration by the nails recorded during the impact tests. The average depth of the impact tests was recorded to be approximately 9.55 mm. The nail gun's mean force per depth was 3.35 N/mm. The force measured by the impact tests, to penetrate a nail into polyurethane a depth of 9.55 mm, was 31.82 N. The impact tests mean force per depth was 3.45 N/mm. This shows the research provided in this thesis can be used to control the settings of the nail gun. Chapter 7 reveals the conclusions made from this research and future recommendations.

7. CONCLUSIONS AND RECOMMENDATIONS

7.1 Summary and Conclusions

Theoretical equations for penetration of nails into foam were developed. The mechanics of the foam penetration were investigated and were found to consist of crushing, shearing, and friction. The theoretical equations quantified the penetration mechanics into equations of force and energy. Impact tests were performed to determine the validity of the theoretical equations. The empirical impact tests revealed the actual penetration forces and energies necessary for a nail to penetrate polyurethane and polyethylene foam a certain depth. When compared to the impact results, the values calculated from the theoretical equations returned excellent results, falling within a factor of 1.2 to 3.0 for the forces. The minimum energy found through the equations falls inside the range of energies yielded from the impact tests. The maximum energy calculated from the equations exceeds the impact tests energy only by a factor of 2.5. As such, it can be concluded the proposed theoretical equations are reasonably accurate in predicting penetration forces and energies. Therefore, penetration into foam is influenced by the mechanics of crushing, shearing, and friction. The equations of penetration can be used to determine the forces or energies required for penetration into foam at any depth.

Overall, the theoretical equations can be applied to determine the appropriate settings (air pressure) of the nail gun necessary for firing the nails into foam a desired depth. The settings and controller box were, in fact, accurate. Nails were successfully placed in foam using the forces determined from this research. The setup of the nail gun is not appropriate for making antenna spacer samples and needs to be addressed. Recommendations were made for the nail gun setup in the following section.

7.2 Recommendations of Future Work

Future work can be conducted on increasing the accuracy of the penetration equations. The equations were created after neglecting the interaction between the nail and hammer. The removal of the hammer disregards the following effects: varying stress distribution through the entire volume of the nail due to impact loading, and possible linear elastic and plastic deformations [11-19]. Further analysis can be performed to determine the extent these behaviors have on the nail-foam penetration. Also, the equations modeled the penetration into homogeneous foams. In actuality, the foams are heterogeneous due to their variable cell sizes and random distribution of cells. Research should be made to determine how these variables affect the penetration into foam, and how to factor these effects into the equations of penetration. Research should also be made to determine the affects of tip geometries on penetration. The nails have a relatively sharp geometry, and this should be accounted for in the equations.

Further impact tests should be performed to include a wider variety of densities and foams. This would help to better validate the penetration equations and the necessary control settings for the nail gun. Future tests should also include varying the shapes of the nail tips and examining the effect of larger diameters on penetration.

The nail gun is currently machined of steel. Future work could be performed to fabricate the nail gun from different materials. It is recommended to look into 2024 and 7075 aluminum as they both are easy to machine and have better corrosion resistance than plain steel. 7075 also has a high strength for aluminum and is still lightweight. 303 and 416 stainless steels are easy to machine, and 303 has a good resistance to corrosion. 316 stainless steel excels at both ease of machinability and corrosion resistance. Stainless steels are expensive, though, so the cost would have to be evaluated [19]. A few factors

should be reviewed when selecting new materials. The pneumatic cylinder used for pushing out the nails produces a mild recoil effect. The pneumatic is a steel cylinder, and the recoil initiates a friction contact between the pneumatic and nail gun frame due to rubbing. If other materials are to be considered for the frame then lubricants may need to be introduced to decrease the friction and wear caused by the recoil. Paraffin or microcrystalline petroleum waxes could be useful as they are often employed as friction reducers. Shock absorbing materials such as rubber or foam could be used as a boundary layer between the frame and the pneumatic to reduce the frictional wear.

The nail gun settings were accurate, but the setup for the nail gun needs to be improved before it can be employed to make dielectric antenna spacer samples. There were problems that need to be addressed involving air leaking through the connectors and the solenoid valve. New connectors should be provided and the valve should be properly sealed or replaced. Also, the controller box needs to be mounted on the mill so as to not get in the way of the foam and nail gun. Currently the controller rests on the mill bench. As a result, its wires are constantly crossing and getting tangled when the mill translates the foam in the x- and y-directions. Correcting these issues would yield a nail gun capable of producing antenna spacer samples.

APPENDIX A

Impact Tests Results

Polyurethane

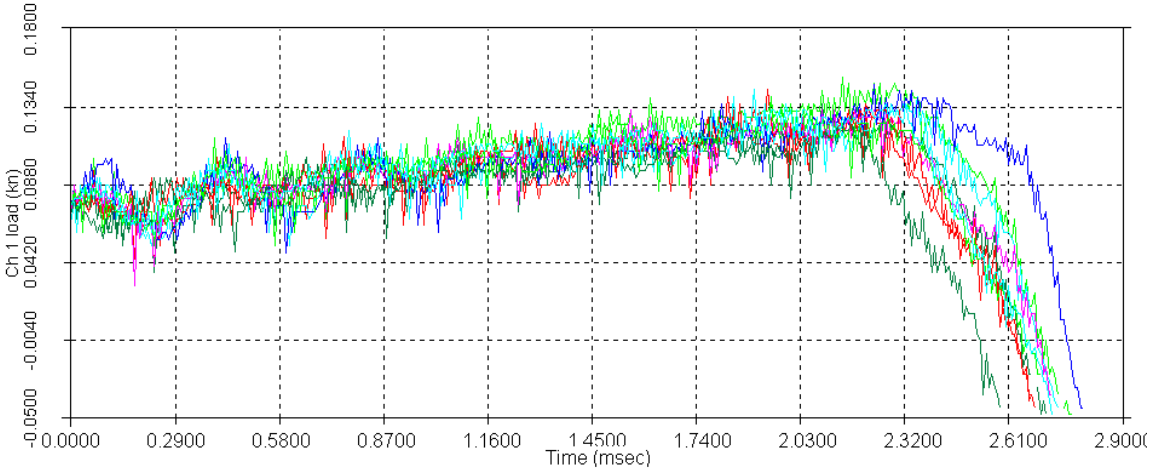

Figure 70: PU 4 Nails trials load curves

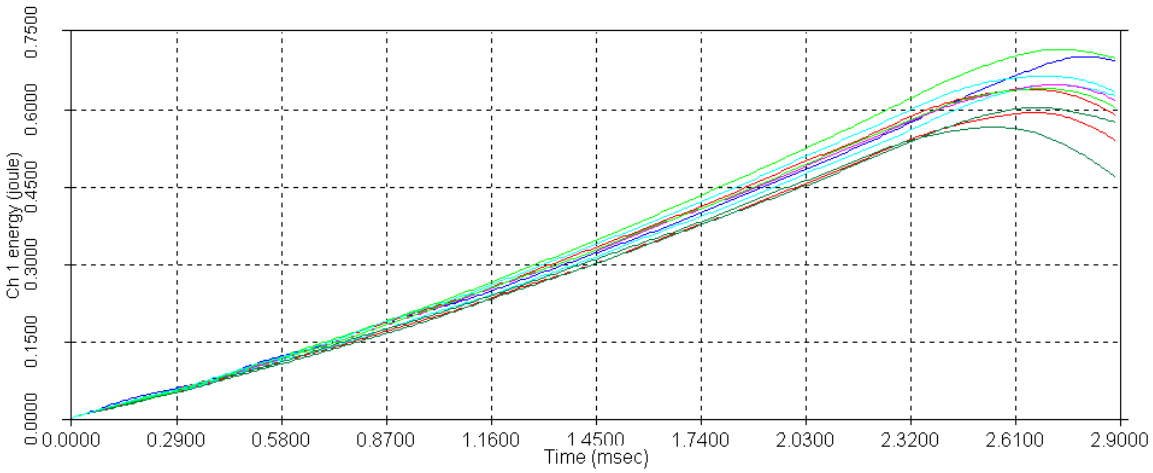

Figure 71: PU 4 Nails trials energy curves

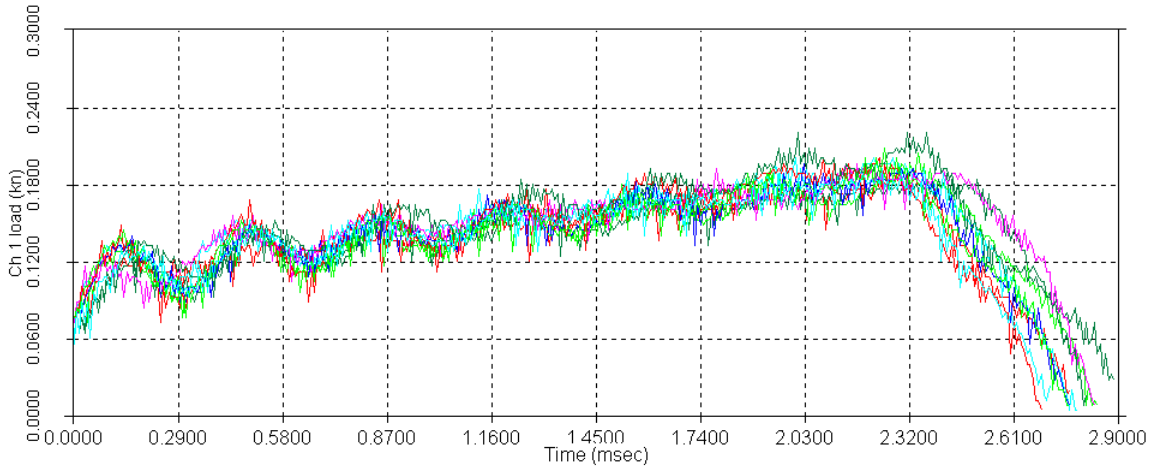

Figure 72: PU 6 Nails trials load curves

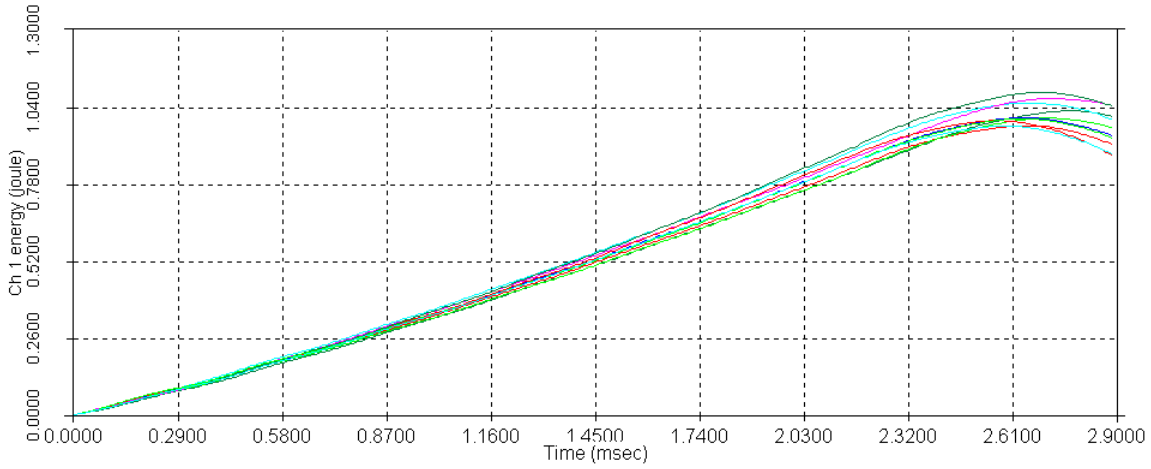

Figure 73: PU 6 Nails trials energy curves

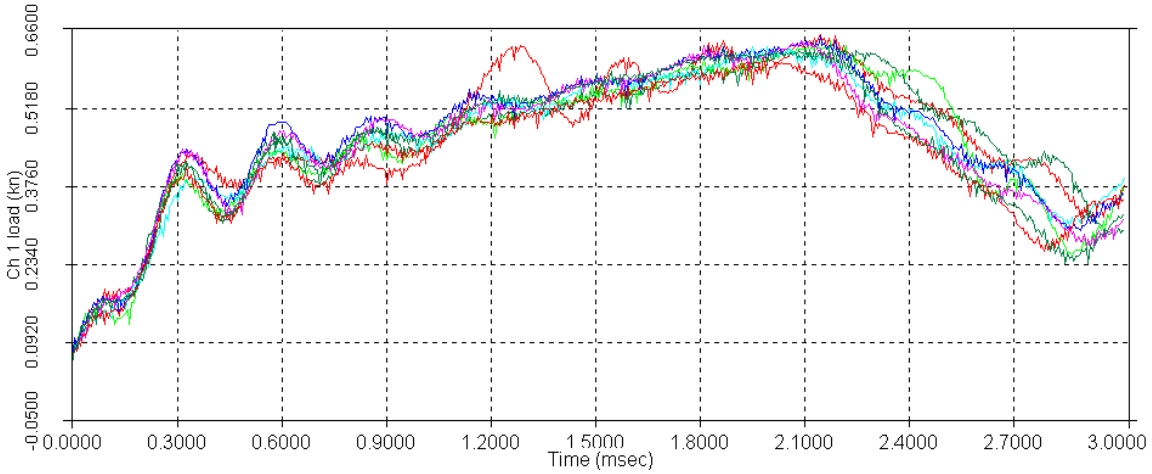

Figure 74: PU 20 Nails trials load curves

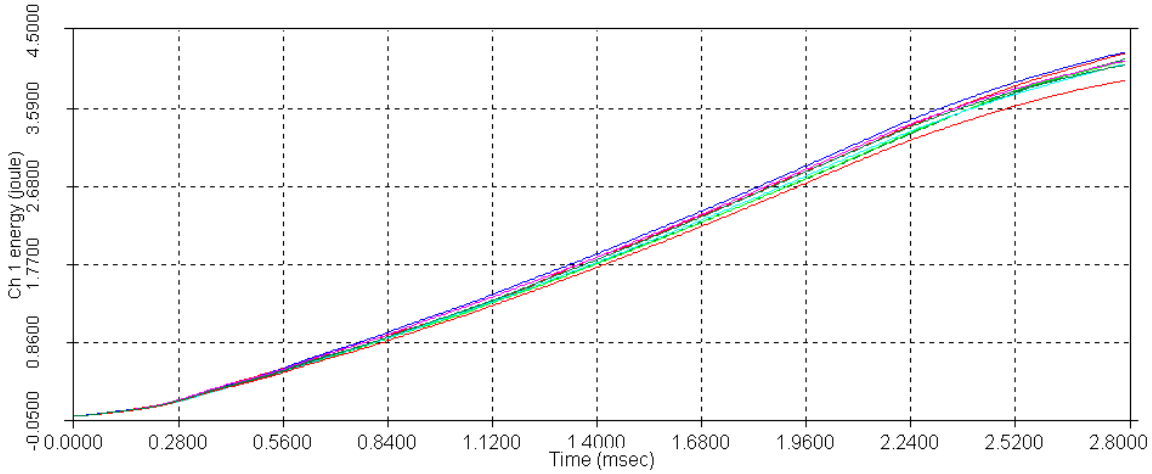

Figure 75: PU 20 Nails trials energy curves

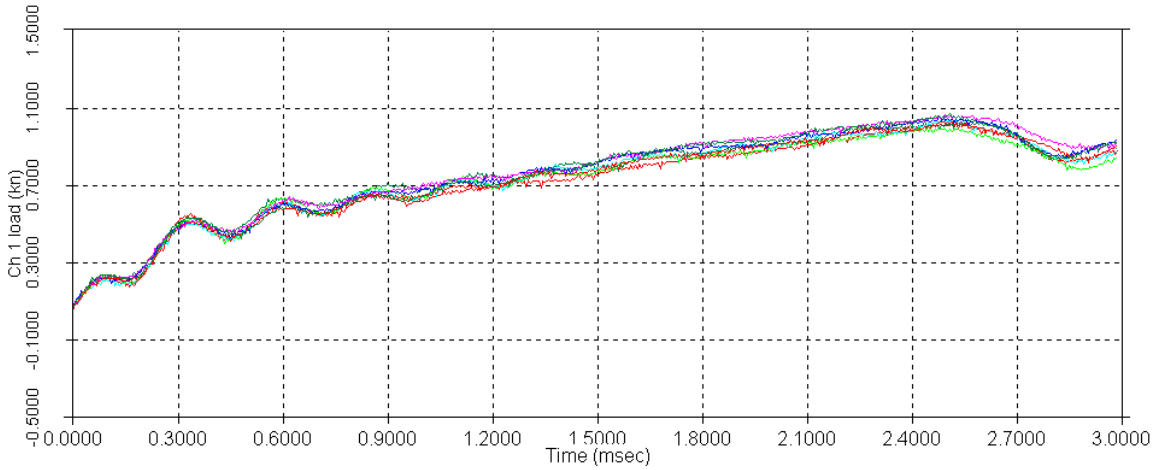

Figure 76: PU 30 Nails trials load curves

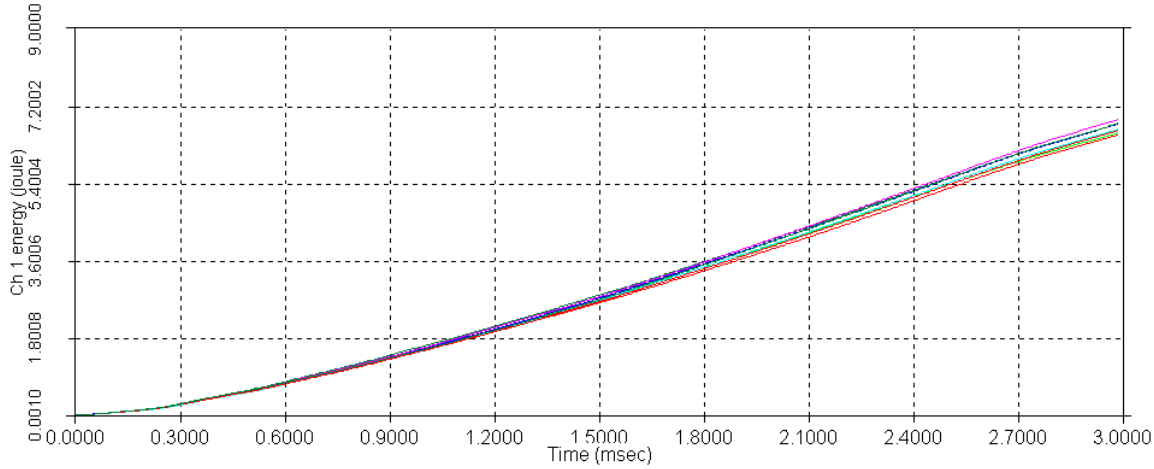

Figure 77: PU 30 Nails trials energy curves

Plank900

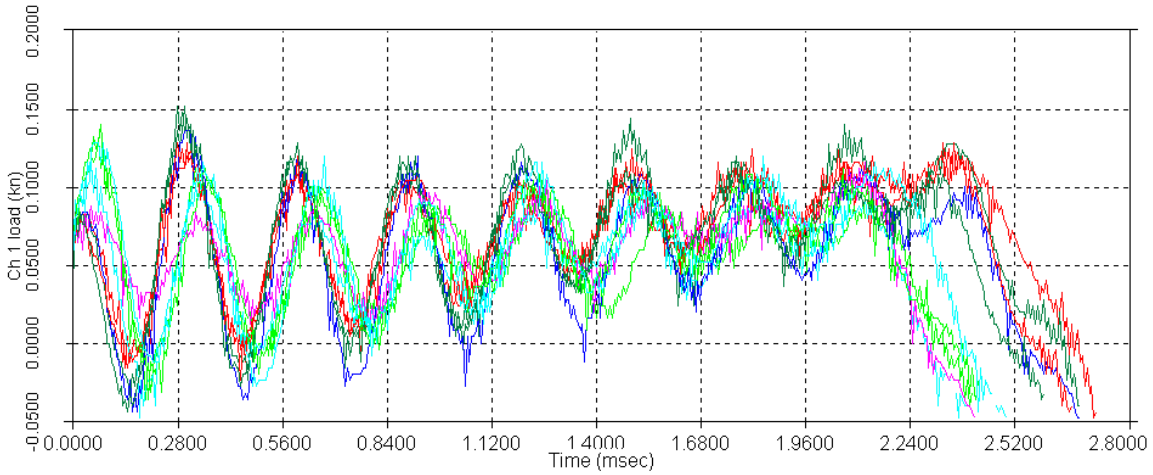

Figure 78: Plank 900 12 Nails trials load curves

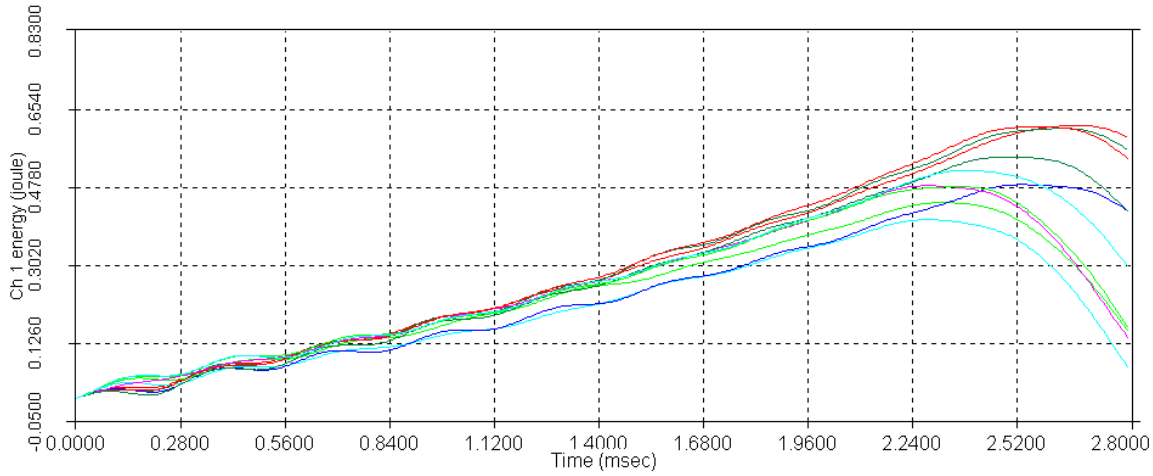

Figure 79: Plank 900 12 Nails trials energy curves

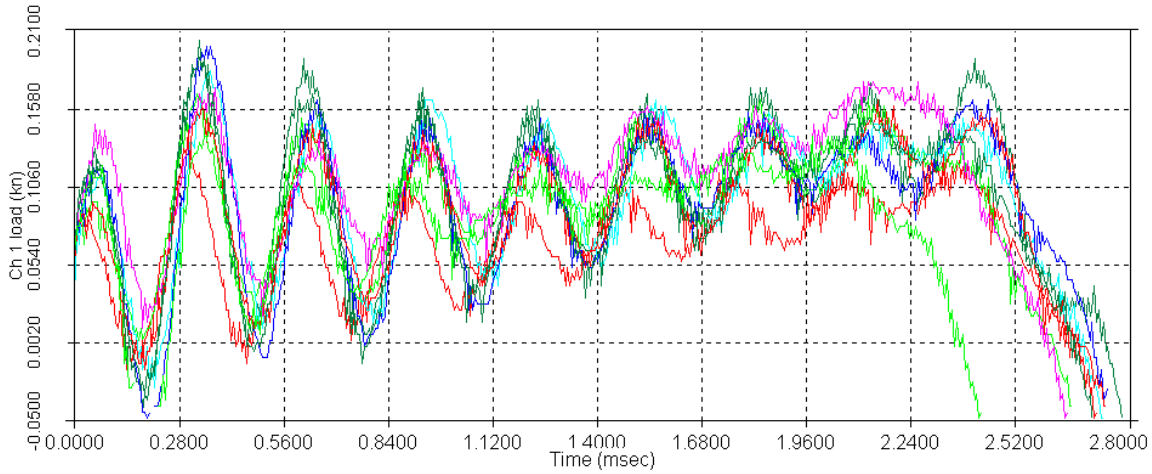

Figure 80: Plank 900 18 Nails trials load curves

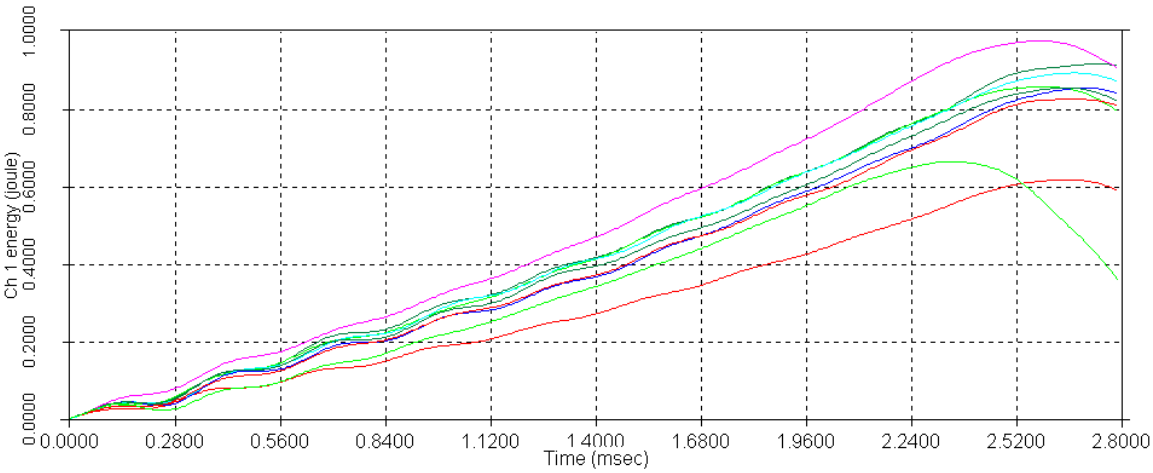

Figure 81: Plank 900 18 Nails trials energy curves

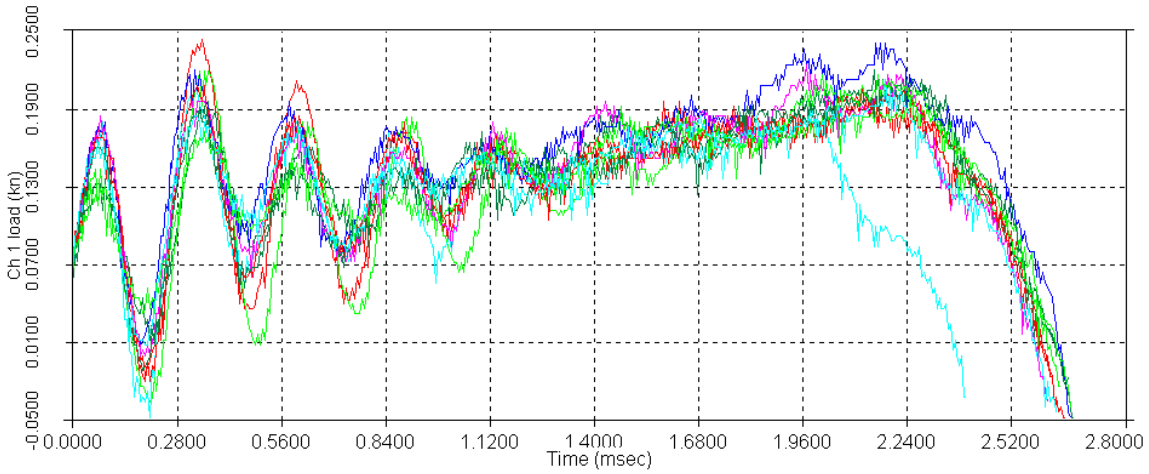

Figure 82: Plank 900 25 Nails trials load curves

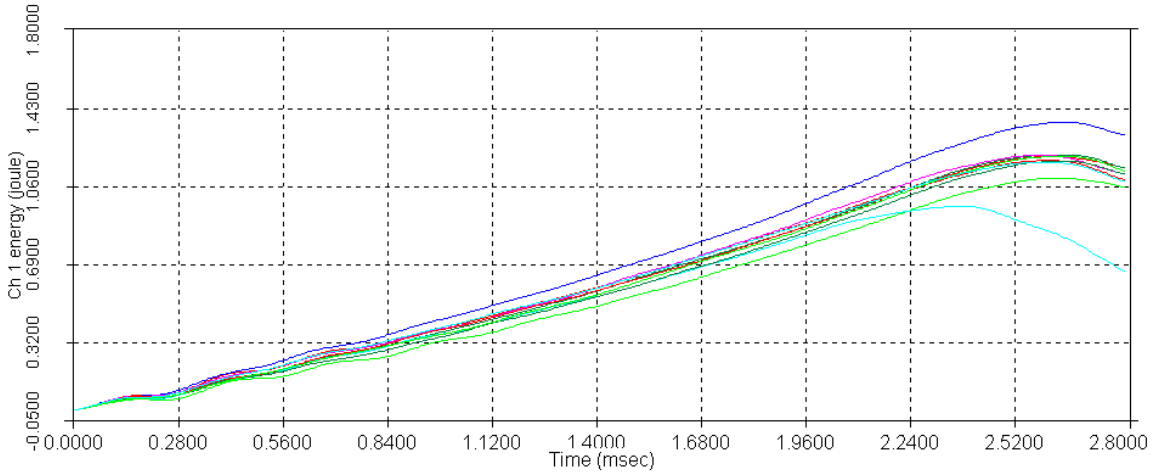

Figure 83: Plank 900 25 Nails trials energy curves

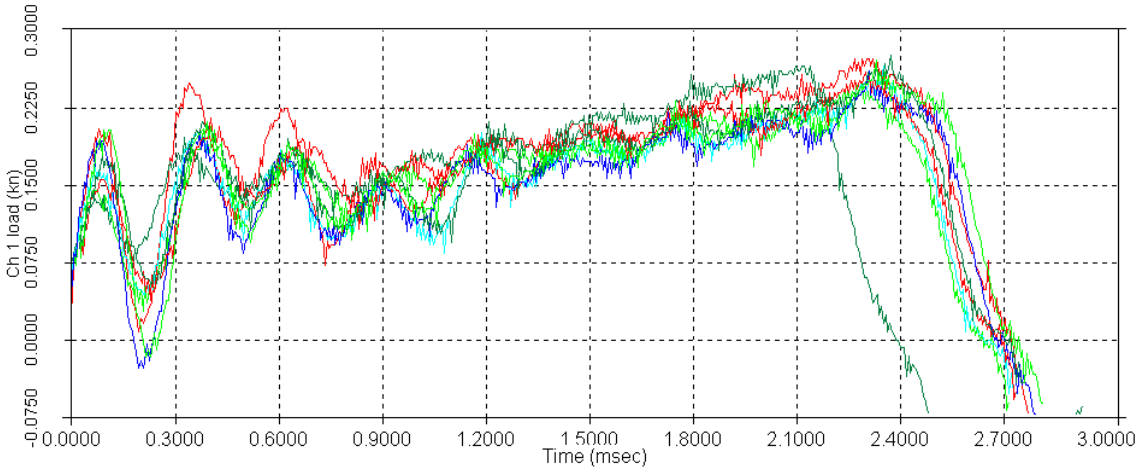

Figure 84: Plank 900 30 Nails trials load curves

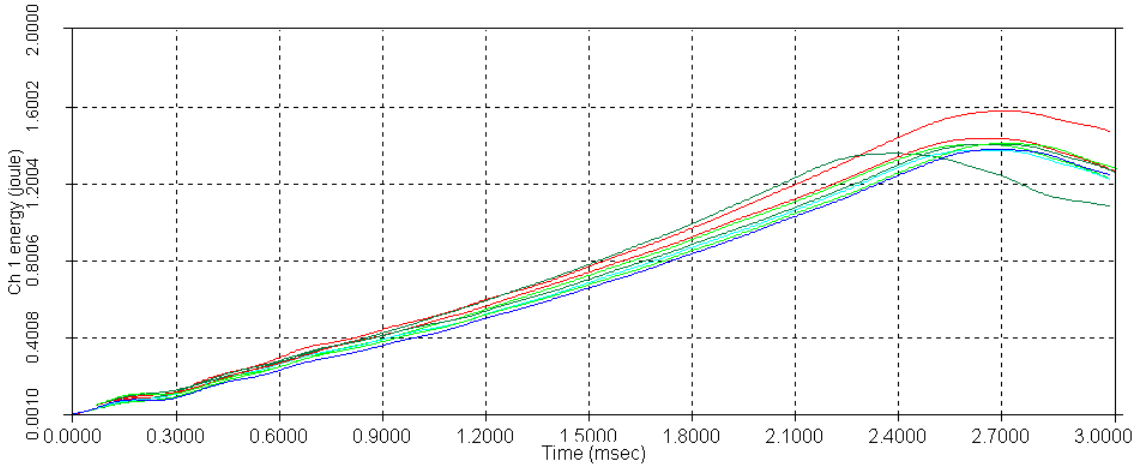

Figure 85: Plank 900 30 Nails trials energy curves

Plank 600

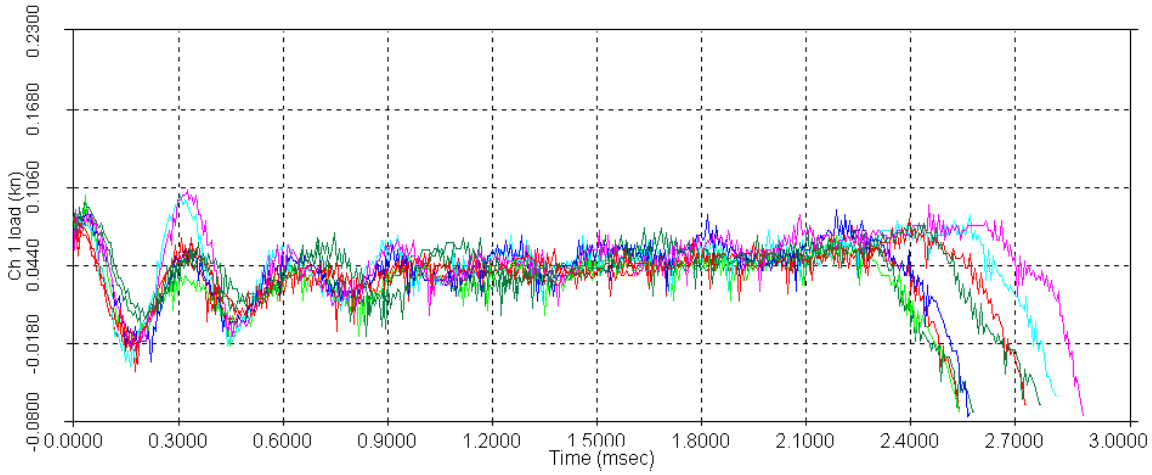

Figure 86: Plank 600 12 Nails trials load curves

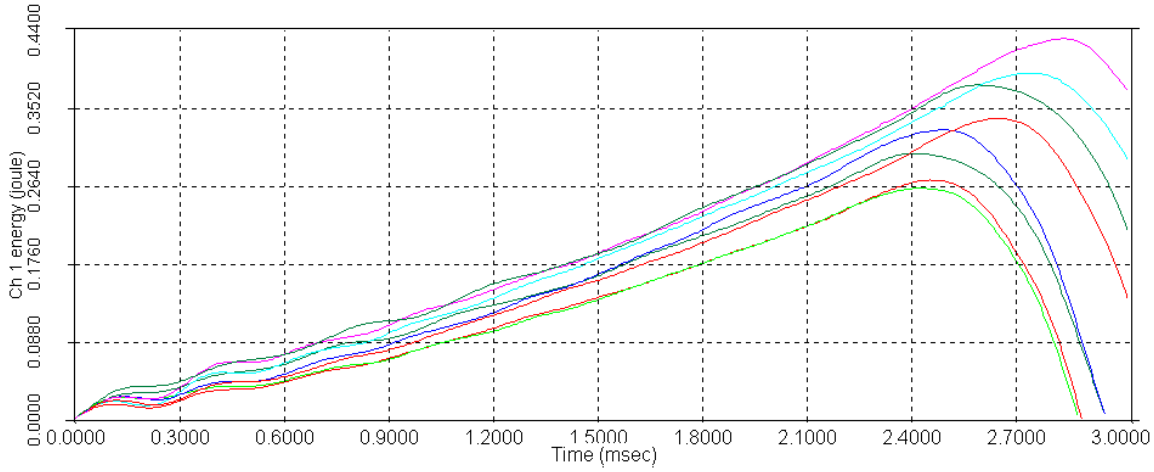

Figure 87: Plank 600 12 Nails trials energy curves

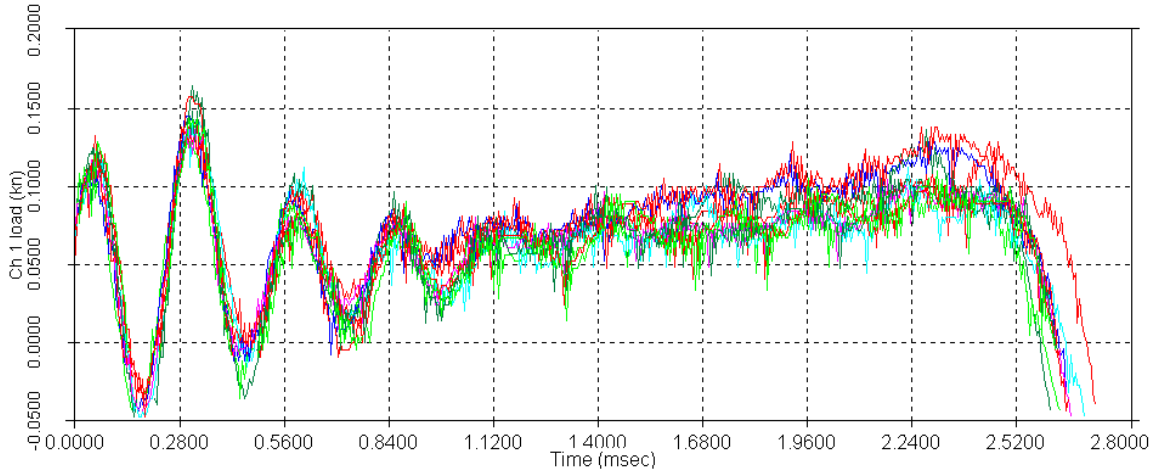

Figure 88: Plank 600 18 Nails trials load curves

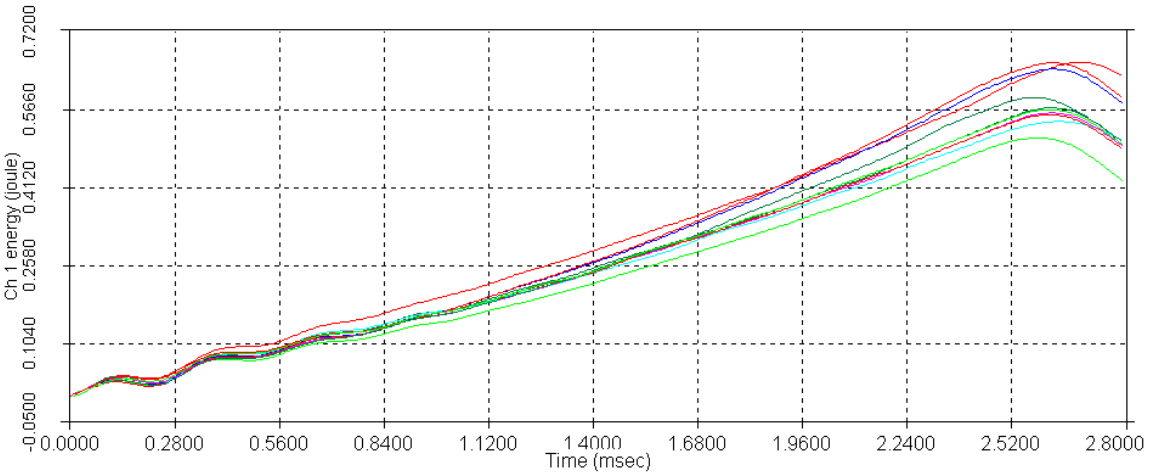

Figure 89: Plank 600 18 Nails trials energy curves

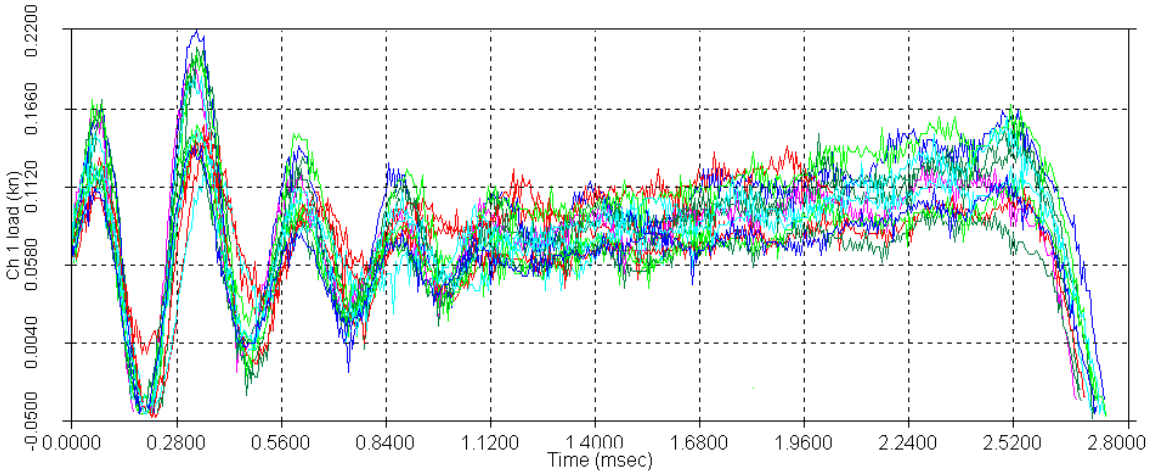

Figure 90: Plank 600 25 Nails trials load curves

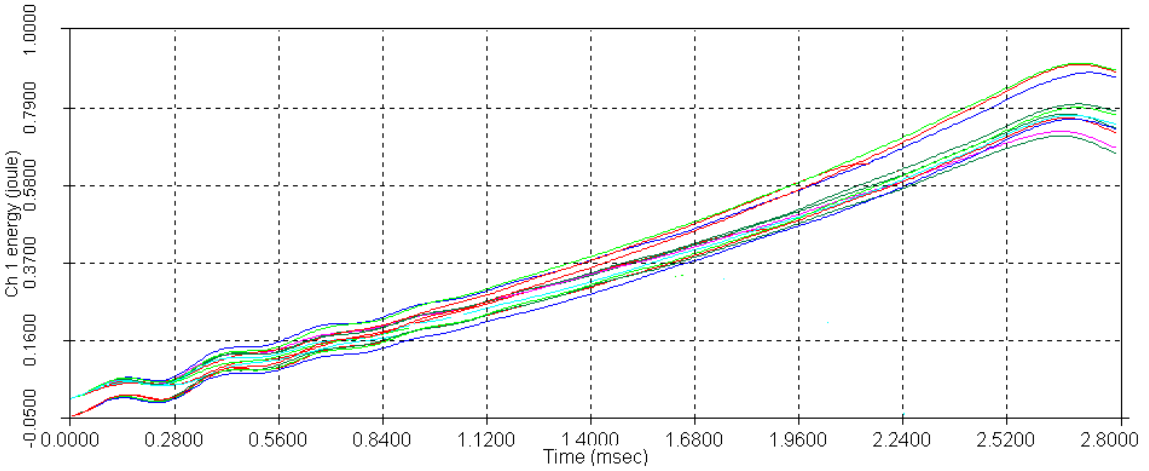

Figure 91: Plank 600 25 Nails trials energy curves

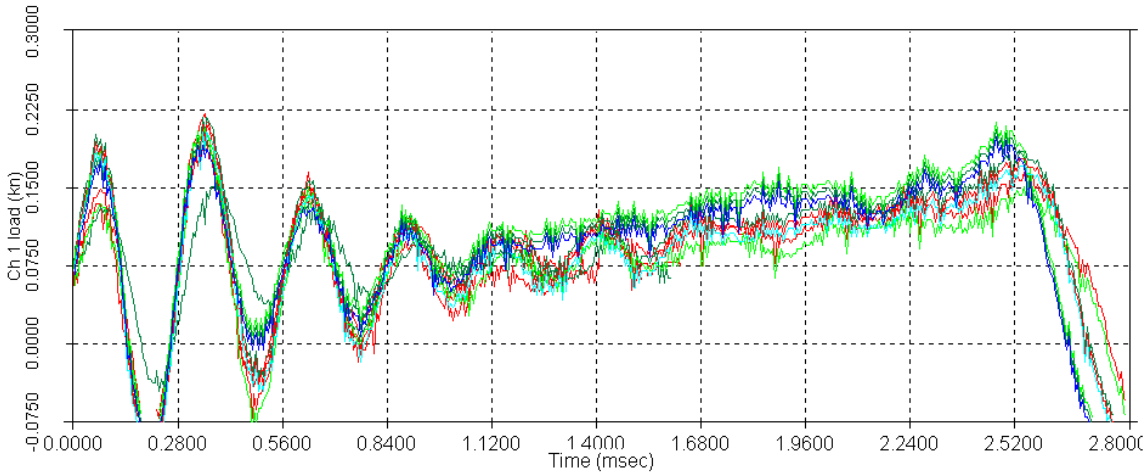

Figure 92: Plank 600 30 Nails trials load curves

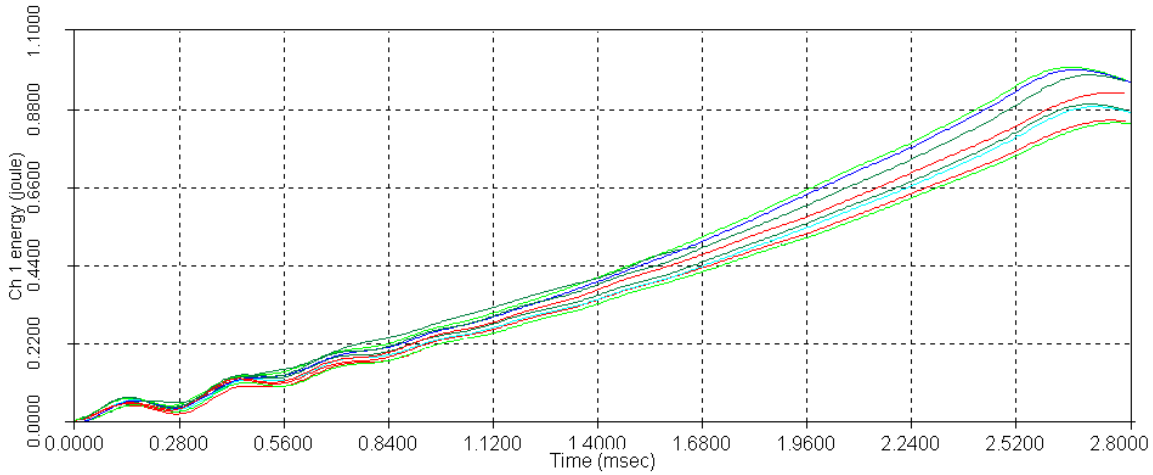

Figure 93: Plank 600 30 Nails trials energy curves

Plank 400

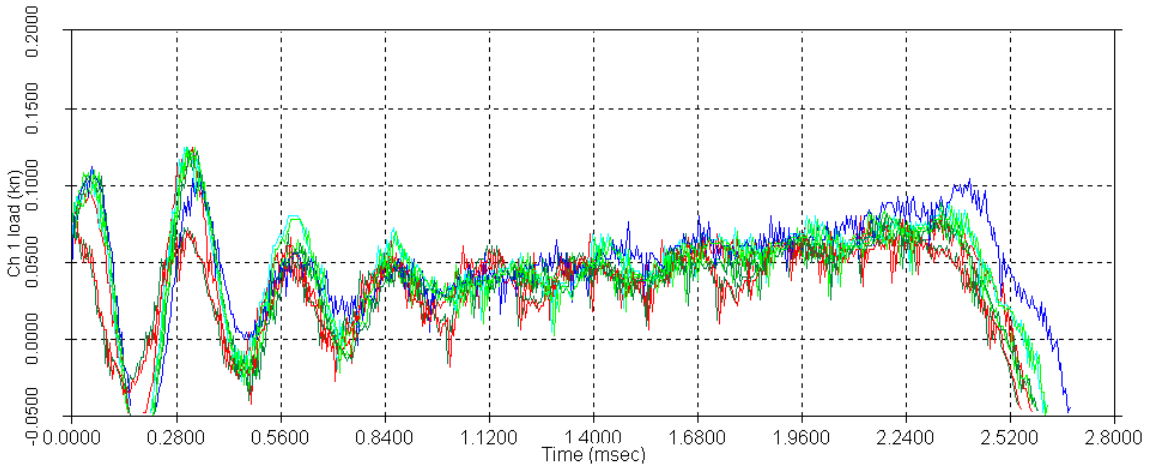

Figure 94: Plank 400 18 Nails trials load curves

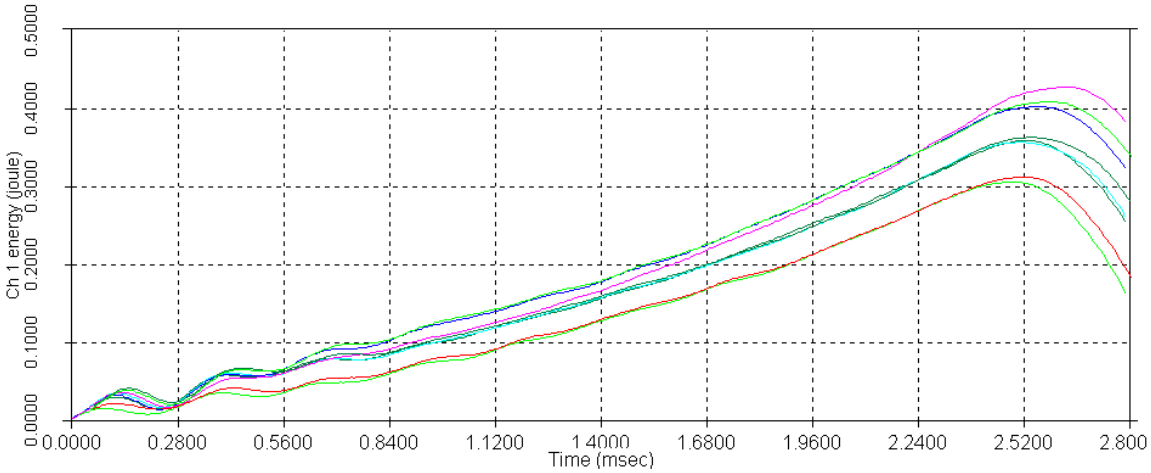

Figure 95: Plank 400 18 Nails trials energy curves

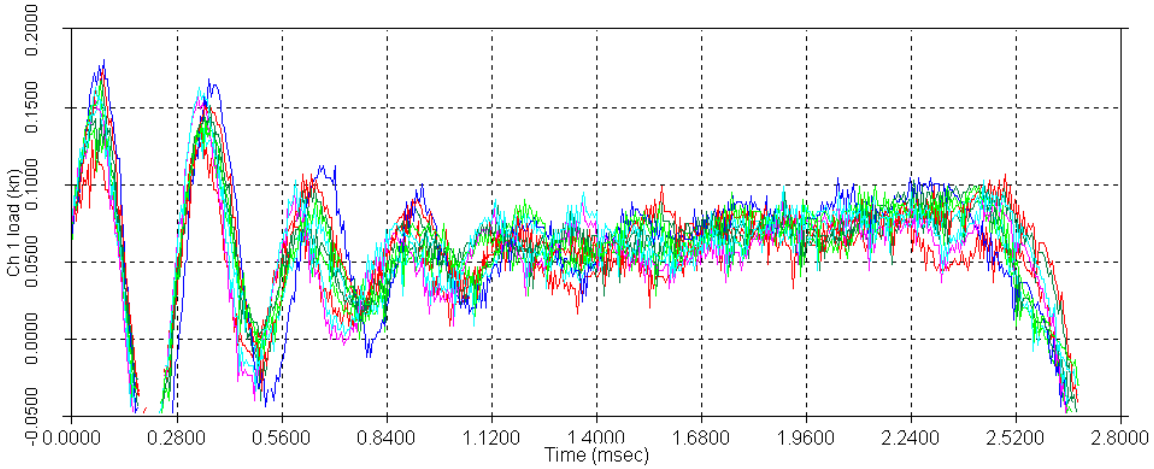

Figure 96: Plank 400 25 Nails trials load curves

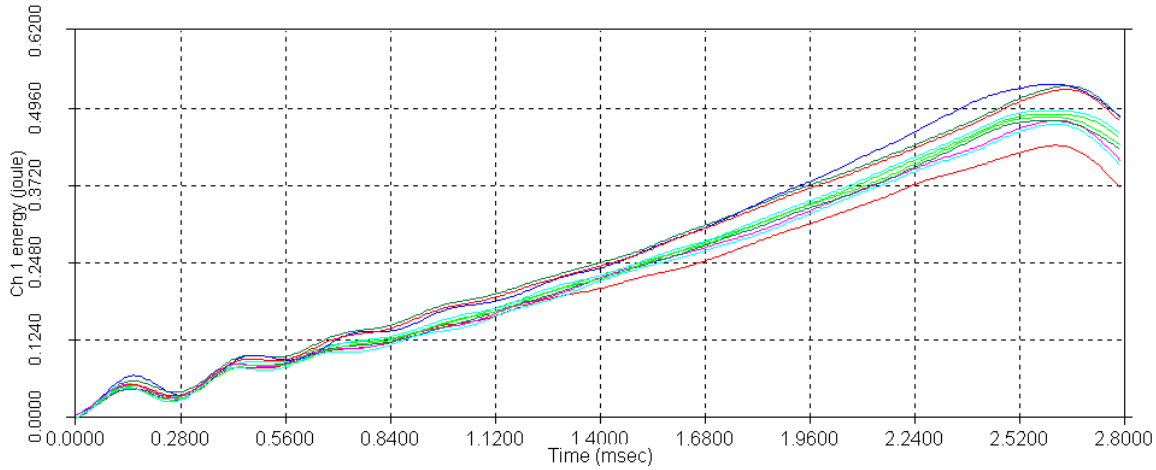

Figure 97: Plank 400 25 Nails trials energy curves

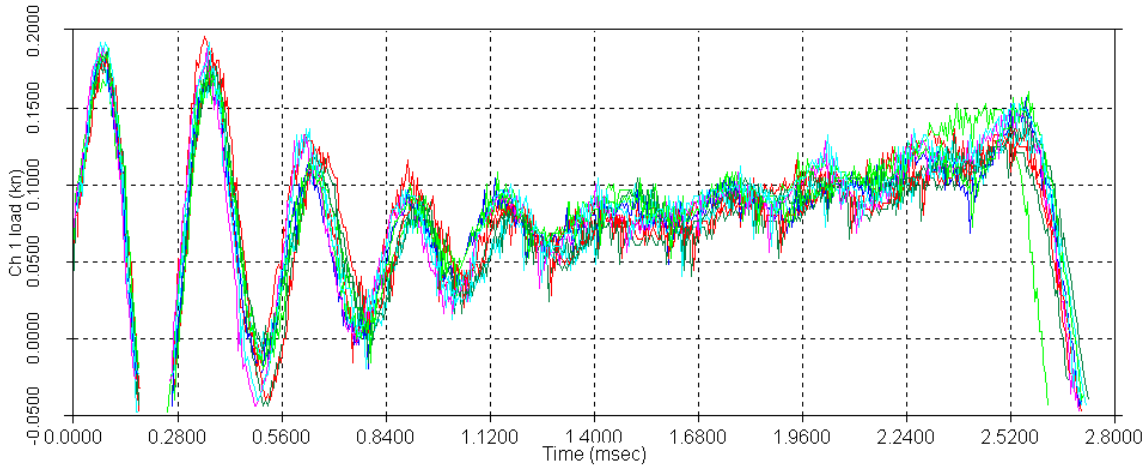

Figure 98: Plank 400 30 Nails trials load curves

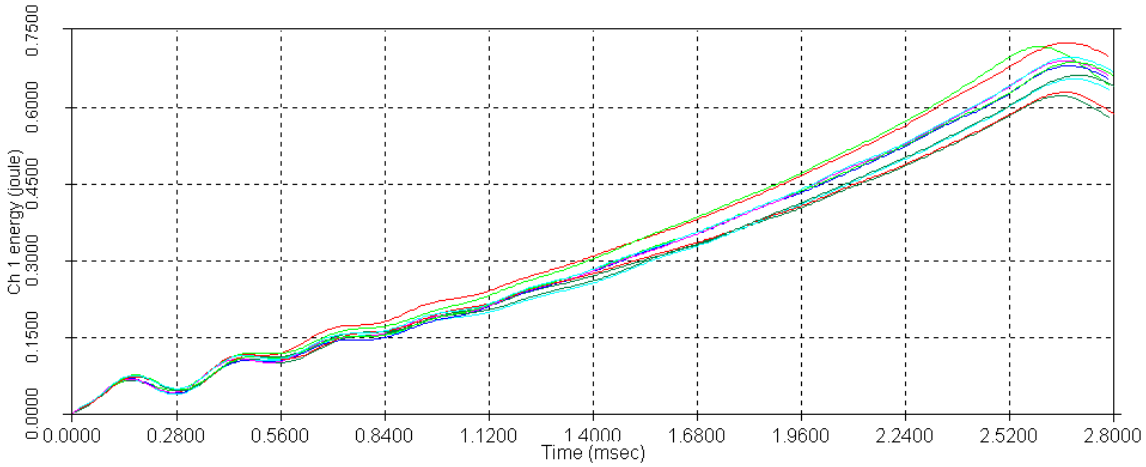

Figure 99: Plank 400 30 Nails trials load curves

APPENDIX B

Table 25: Parameter combinations

	PU	Plank 900	Plank 600	Plank 400
A = porosity	0.03	0.85	0.90	0.93
1/A	38.46	1.18	1.11	1.07
1-A	0.97	0.15	0.10	0.07
1/(1-A)	1.03	6.64	10.24	15.22
1-(1/A)	37.46	0.18	0.11	0.07
1-(1/(1-A))	0.03	5.64	9.24	14.22
B = density ratio	0.96	0.15	0.10	0.07
1/B	1.04	6.64	10.24	15.24
1-B	0.04	0.85	0.90	0.93
1/(1-B)	25.00	1.18	1.11	1.07
1-(1/B)	0.04	5.64	9.24	14.24
1-(1/(1-B))	24.00	0.18	0.11	0.07
C = diameter/cell size		1.20	1.03	0.90
1/C		0.83	0.97	1.11
1-C		0.20	0.03	0.10
1/(1-C)		4.94	32.71	10.18
1-(1/C)		0.17	0.03	0.11
1-(1/(1-C))		5.94	33.71	9.18

The highlighted parameterized forces yielded the best results from all combinations. The highlighted combinations are presented below in the figures.

Table 26: Total force times 'A' combinations

Ftotal*A	PU	Plank 900	Plank 600	Plank 400
A = porosity	1.09	3.12	1.67	1.28
1/A	1610.77	4.32	2.05	1.47
1-A	40.79	0.55	0.18	0.09
1/(1-A)	43.00	24.37	18.94	20.85
1-(1/A)	1568.89	0.65	0.20	0.10
1-(1/(1-A))	1.12	20.70	17.09	19.48

Table 27: Friction force times 'A' combinations

Ffrict*A	PU	Plank 900	Plank 600	Plank 400
A = porosity	0.82	2.12	1.08	0.84
1/A	1207.69	2.94	1.33	0.96
1-A	30.58	0.38	0.12	0.06
1/(1-A)	32.24	16.60	12.28	13.70
1-(1/A)	1176.29	0.44	0.13	0.06
1-(1/(1-A))	0.84	14.10	11.08	12.80

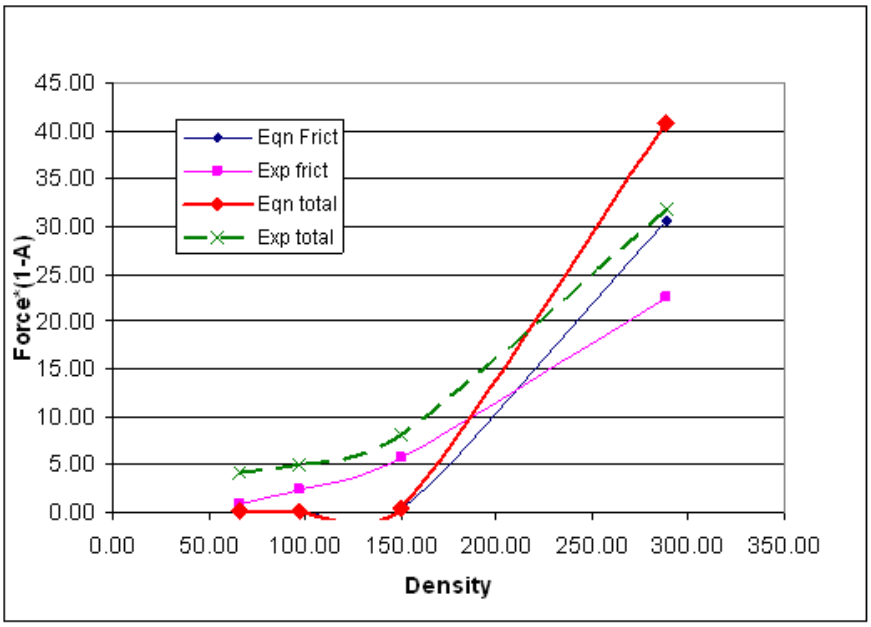

Figure 100: Combination '1-A' vs. density

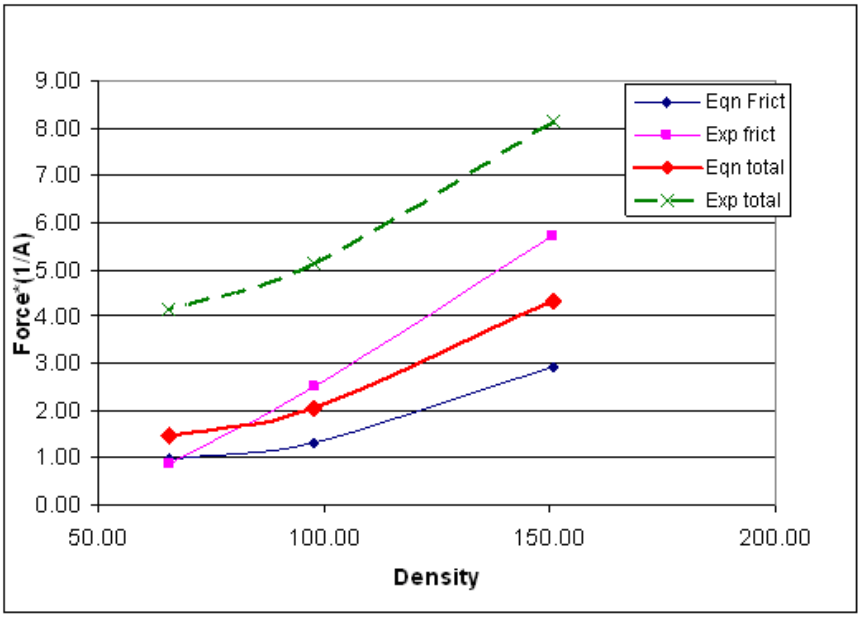

Figure 101: Combination '1/A' vs. density

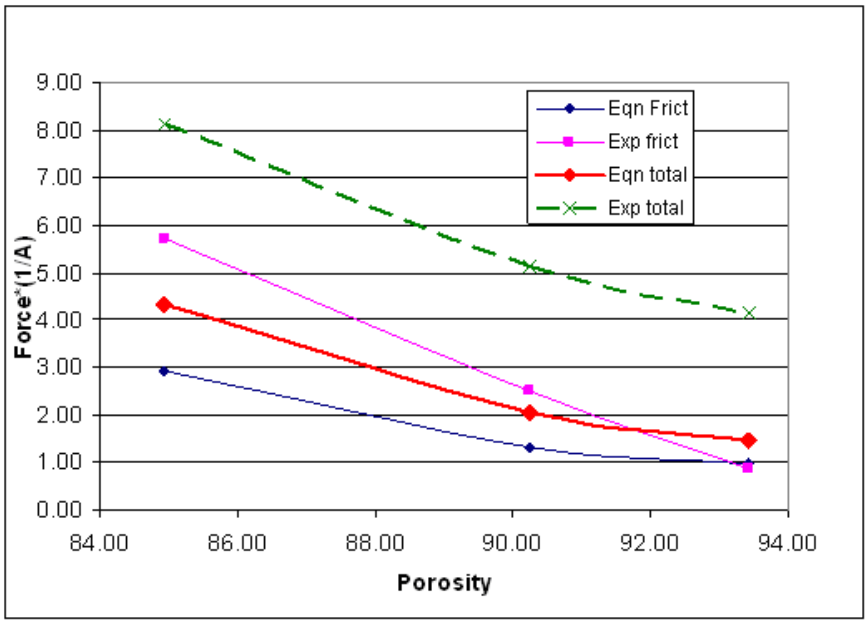

Figure 102: Combination '1/A' vs. porosity

Table 28: Total force times 'B' combinations

Ftotal*B	PU	Plank 900	Plank 600	Plank 400
B = density ratio	40.20	0.55	0.18	0.09
1/B	43.63	24.37	18.94	20.88
1-B	1.68	3.12	1.67	1.28
1/(1-B)	1047.00	4.32	2.05	1.47
1-(1/B)	1.75	20.70	17.09	19.51
1-(1/(1-B))	1005.12	0.65	0.20	0.10

Table 29: Friction force times 'B' combinations

Ffrict*B	PU	Plank 900	Plank 600	Plank 400
B = density ratio	30.14	0.38	0.12	0.06
1/B	32.71	16.60	12.28	13.72
1-B	1.26	2.12	1.08	0.84
1/(1-B)	785.00	2.94	1.33	0.96
1-(1/B)	1.31	14.10	11.08	12.82
1-(1/(1-B))	753.60	0.44	0.13	0.06

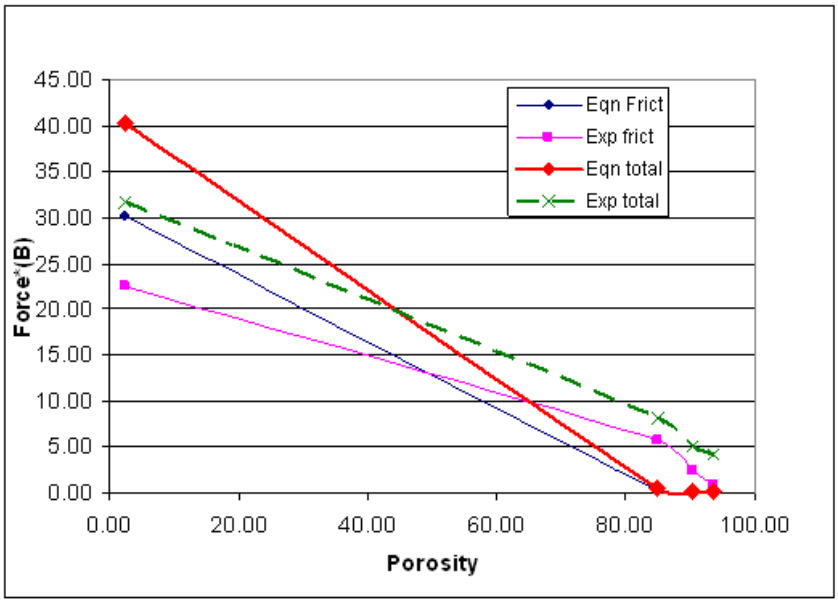

Figure 103: Combination 'B' vs. porosity

Table 30: Total force times 'C' combinations

Ftotal*C	PU	Plank 900	Plank 600	Plank 400
C = diameter/cell size		4.41	1.91	1.24
1/C		3.05	1.80	1.52
1-C		0.74	0.06	0.13
1/(1-C)		18.14	60.51	13.94
1-(1/C)		0.62	0.05	0.15
1-(1/(1-C))		21.81	62.36	12.57

Table 31: Friction force times 'C' combinations

Ffrict*C	PU	Plank 900	Plank 600	Plank 400
C = diameter/cell size		3.01	1.24	0.81
1/C		2.08	1.16	1.00
1-C		0.51	0.04	0.09
1/(1-C)		12.36	39.25	9.16
1-(1/C)		0.42	0.04	0.10
1-(1/(1-C))		14.86	40.45	8.26

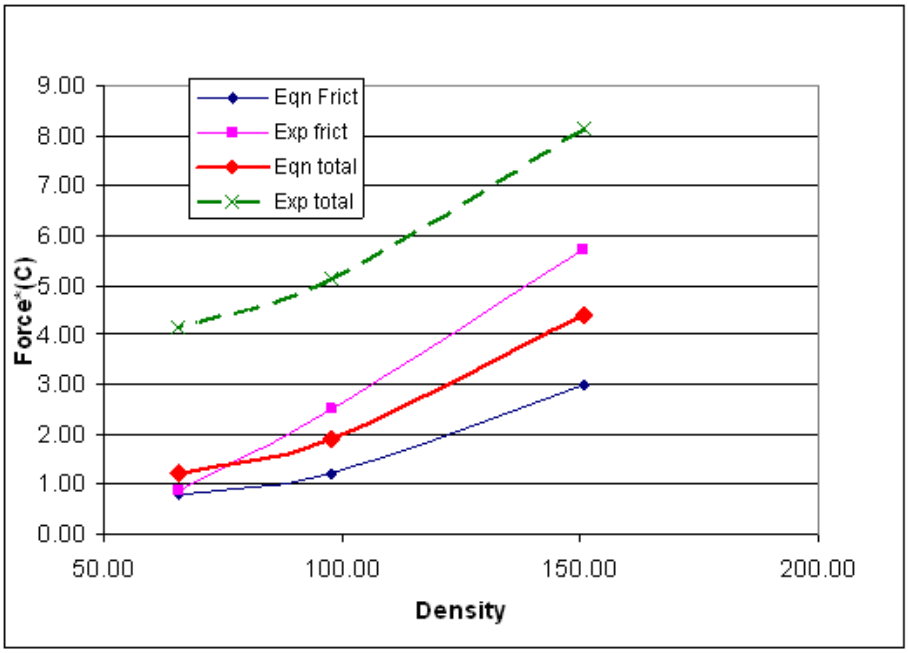

Figure 104: Combination 'C' vs. density

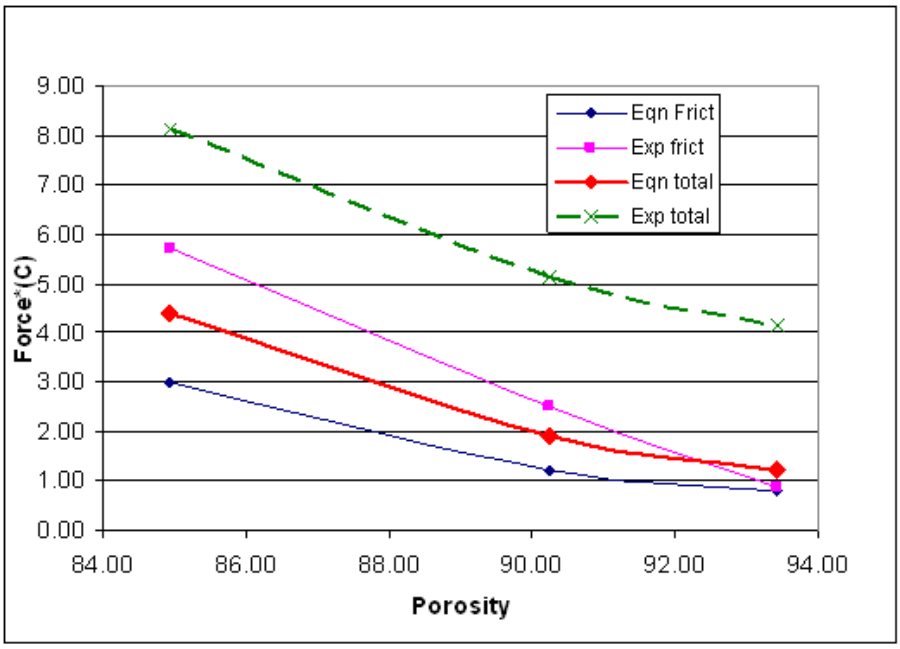

Figure 105: Combination 'C' vs. porosity

APPENDIX C

Nail Gun Program Code

```
.include "tn45def2.inc"


; CONSTANTS:
; Change these to change the timing of the program.
.equ    OnTime                  = 5             ;Time the trigger signal stays high
(1/5 sec)
.equ    WaitTime        = 5             ;Time waited after stop condition before
                                                ;       triggering (1/5 sec
increments)



;*****************************************************************
***
;       This code was written by RAVIKANTH DEVIREDDY and KEVIN JOHNSON
;               of the Georgia Tech ME Electronics Lab
;
;*****************************************************************
***
;*
;*      HARDWARE connection:
;*      PB0 - Encoder1, CH.A.
;*      PB1 - Encoder1, CH.B.
;*      PB2 - Encoder2, CH.A.
;*      PB3 - Encoder2, CH.B.
;*      PB4 - Trigger Output
;*
;*****************************************************************
***
;*
;*      Program description:
;*      This program is designed to detect a still condition on a moving stage.
;*      Two quadrature encoders are used to monitor orthogonal axes.
;*      When no movement is detected on the encoders for a given time interval,
;*              the output will trigger for a given time.
;*
;*****************************************************************
***
;*
;*      Theory:
```

```
;*      As long as the stage is still, at least one channel in each encoder
;*              must be stable.  To find this pair of inputs, the program monitors
;*              one channel from each encoder until a change is detected.  Once
;*              change is detected, the pair of monitored inputs is changed.  This
;*              cycle continues until a stable condition is detected.
;*      While inputs are changing, a timer is continually counting down.  Each
;*              time movement is detected, this timer is reset.  If the timer
;*              reaches zero, the stage is assumed still, and the output is set.
;*
;*************************************************************************
***


.def    counter1        = r16   ;Outermost timer variable
.def    counter2        = r17   ;Middle timer variable
.def    counter3        = r18   ;Innermost timer variable
.def    temp            = r21   ;Temp. register
.def    switcher        = r23   ;Register for switching the masks
.def    temp_pcmsk      = r24   ;temp register that holds PCMSK
.def    addendum        = r25   ;contains the value to adjust PC mask


;*************************************************************************
***
;*
;*      PROGRAM START - EXECUTION STARTS HERE
;*
;*************************************************************************
***
        .cseg

        .org $0000
        rjmp    start                           ;Reset handler

        .org INT0addr
        reti                                            ;External interrupt handler

        .org $0002
        rjmp    pc_int0                         ;Pin Change interrupt handler

        .org OVF0addr
        reti                                            ;Timer0 overflow handler

        .org ACIaddr
```

```
        reti                                    ;Analog comparator handler
(Not Used)


;*******
;* pc_int0 (pin change interrupt)
;* This function resets the timer to delay the trigger.
;* As long as this gets called faster than the timer time, the
;*  output will not trigger.
;*******
pc_int0:
        rcall   timer_reset                     ; Reset the timer
        pop             temp                            ; Pop return address
because
        pop             temp                            ;       we won't be
returning to it
        sei                                             ; Manually
enable interrupts
        rjmp    Loop                            ; Begin the loop


;*******
;* start (intital code, run on reset)
;* This function initializes various variables and configures interrupts.
;*******
start:
        clr             counter1                        ; Clear all timer
variable
        clr             counter2                        ;  (esentially for no
reason)
        clr             counter3

        ldi             switcher, 0x01

        ldi             temp,           0x20
        out             GIMSK,temp                      ;Enable external
interrupt PCIE
        ldi             temp_pcmsk,  0x05
        out             PCMSK,temp_pcmsk        ;Enable external interrupts
PCINT2 and PCINT0

        ldi             temp, 0b00110000
        out             DDRB,temp                       ;Set PB4 as output

;       rcall   trigger                         ; Trigger the trigger (why?)
```

```
        sei                                                     ;Enable
interrupts

;*******
;* Loop (main loop)
;* Each time the timer gets reset, the program is redirected here.
;* This function calls the timer, and if the timer runs out, calls
;*       the function to trigger the output, then suspends program flow.
;*******
Loop:
        rcall   delay                                   ; Call waiting routine
        cli                                                     ; disable
interrupts during trigger
        rcall   trigger                                 ; trigger the trigger
        sei                                                     ; enable
interrupts again
Here:
        rjmp    Here                                    ; wait to start again.


;*******
;* delay (main timing function)
;* This function and its sub functions wait for some time.
;* delay1, with counter2 loaded with 0xFF, is appx 1/5 sec.
;* Thus delay, with counter1 loaded with 05, will wait appx 1 sec.
;*******
delay:
        ldi             counter2, 0xFF
delay0i:
        rcall   delay1
        dec             counter1
        brne    delay0i
        ret

delay1:
        ldi             counter3, 0xFF
delay1i:
        rcall   delay2
        dec             counter2
        brne    delay1i
        ret

delay2:
        dec             counter3
        brne    delay2
        ret
```

```
;*******
;* timer_reset (timer reset)
;* This function resets the timer as well as adjusts the PC interrupts.
;* The PC interrupt mask is cycled through the four combinations of possible
;*       stable locations, attempting to find a stable situation.
;******* (note: mostly written by Ravi.  Elegant but obfuscated.  Apparently working.)
timer_reset:

        mov             addendum,     switcher
        sbrc    temp_pcmsk,  3                          ; skip if bit 3 in the mask
register is 0
        neg             addendum                                ; 2's complement of
switcher for subtracting
        add             temp_pcmsk,  addendum
        clc

        ldi             temp, 0x05
        EOR             switcher,       temp            ; to skip between 0000 0001
and 0000 0100

        out             PCMSK,          temp_pcmsk      ;Enable external
interrupts PCINT2 and PCINT0

        ldi             counter1,       WaitTime                ; main timer value
        clr             counter2                                ; reset sub-timer value
        clr             counter3                                ; reset sub-timer value

        ret


;*******
;* trigger (Trigger output)
;* This function turns on the output and waits for some time, then turns it off.
;*******
trigger:
        sbi             PORTB,          PB4                             ; Turn on PB4

        ldi             counter1,       OnTime                  ; delay
        rcall   delay

        cbi             PORTB,          PB4                             ; Turn off PB4


        ret
```

REFERENCES

[1] Shim, V.P.W., Z.H. Tu, and C.T. Lim. Two-dimensional response of crushable polyurethane foam to low velocity impact. *International Journal of Impact Engineering*, 2000. 24, 703-731.

[2] Gilchrist, A. and N.J. Mills. Impact deformation of rigid polymeric foams: experiments and FEA modeling. *International Journal of Impact Engineering*, 2001. 25, 767-786

[3] McIntyre, A. and G.E. Anderton. Fracture properties of rigid polyurethane foam over a range of densities. *Polymer*, 1979. 20, 247-253.

[4] Ravid, M. and S.R. Bodner. Dynamic Perforation of Viscoplastic Plates by Rigid Projectiles. *International Journal of Engineering Science*, 1983. 21, 577-591.

[5] Sharma, S.C., H.N. Narasimha Murthy, and M. Krishna. Low-Velocity Impact Response of Polyurethane Foam Composite Sandwich Structures. *Journal of Reinforced Plastics and Composites*, 2004. 23, 1869-1882.

[6] Reis, Rui, and Daniel Cohn. Polymer Based Systems on Tissue Engineering, Replacement and Regeneration. Boston: Kluwer Academic Publishers, 2001. 321.

[7] Shigley, Joseph and Larry Mitchell. Mechanical Engineering Design. 5th ed. New York: McGraw-Hill Book Company, 1989. 62-63.

[8] Instron Reference Manual

[9] Moseley, Henry and Dennis Mahan. The Mechanical Principles of Engineering and Architecture. New York: Wiley and Halsted. 2004. 559-560.

[10] Bovey, Henry. Theory of Structures and Strength of Materials. 4th ed. London: John Wiley and Sons, 2007. 174-176.

[11] Juvinall, Robert and Kurt Marshek, Fundamentals of Component Design. 3rd ed. USA: John Wiley and Sons, 2000. Appendix C-1, C-2, C-4a. 840-841, 845-846.

[12] FR-6718 Nominal Physical Property Data. General Plastics Manufacturing Company. 2008. <http://www.generalplastics.com/products/idatapopup.php?density=18&pfoamname=FR-6700&>. 15 Aug 2008.

[13] Specialty Materials - CelluPlank® data sheet. Sealed Air. PPD-T-224, 2005.

[14] Dynatup® 9200 Series Impact Test Machines. Impact test machine image. http://www.instron.us/wa/products/impact/series_9200.aspx. 15 Aug 2008.

[15] Spiegel, Murray. Theory and Probability of Statistics. *Schaum's Outline Series In Mathematics*. New York: McGraw-Hill Book Company, 1961. 156-170.

[16] Arrow Fastener ET200 Product Information. Arrow Fastener Company. <http://www.arrowfastener.com/FMPro?-db=web.fp5&-format=product.html&-lay=Entry&-Op=Equals&itemnumber=ET200&-find=>. 15 Aug 2008.

[17] Optical rotary encoder data sheet and image. <http://dkc3.digikey.com/PDF/T081/P2026.pdf>. 15 Aug 2008.

[18] Gere, James M. Mechanics of Materials. 5th ed. USA: Brooks/Cole, 2001. 128-133.

[19] McMaster-Carr Supply Company. Material properties and specifications for Al, steel, and stainless steel. <http://www.mcmaster.com>. 15 Aug 2008.